INVESTIGATION OF *LIX1* AND ITS ROLE IN FELINE SPINAL MUSCULAR ATROPHY PATHOGENESIS

By

Erin Wakeling

A DISSERTATION

Submitted to
Michigan State University
in partial fulfillment of the requirements
for the degree of

DOCTOR OF PHILOSOPHY

GENETICS

2010

ABSTRACT

INVESTIGATION OF *LIX1* AND ITS ROLE IN FELINE SPINAL MUSCULAR ATROPHY PATHOGENESIS

By

Erin Wakeling

The spinal muscular atrophies (SMA) are a group of inherited disorders distinguished by proximal muscle weakness and atrophy due to spinal cord lower motor neuron degeneration. Autosomal recessive SMA is the leading genetic cause of infant mortality and divided into four subtypes based on severity, age of onset and survival time. In humans, at least 97% of autosomal recessive SMA is due to a mutation in the *survival of motor neuron* gene. Despite intensive research, the molecular mechanism by which SMN depletion results in motor neuron death remains poorly defined. Feline SMA is an autosomal recessive, juvenile onset lower motor neuron disease that resembles Type 3 human SMA. Molecular analysis identified a 140 kb deletion on feline chromosome A1q that eliminated exons 4-6 of *limb expression 1* (*LIX1)* and nearly all of *leucyl/cystinyl aminopeptidase* (*LNPEP)*. Little is currently known about LIX1, except that it is highly expressed in the spinal cord. *LNPEP* is an ubiquitously expressed aminopeptidase and a *Lnpep* knockout mouse has been generated and did not demonstrate any overt neuromuscular phenotype. The aim of my research was to characterize feline SMA onset and progression and to identify molecular functions of *LIX1*.

Motor neurons and muscles of SMA affected cats developed normally until 8 weeks. At this age, motor axons in affected cats failed to undergo radial expansion to generate the bimodal distribution of axon diameters found in normal animals. Significant ventral root axon loss and atrophic muscle fibers were observed at 12 weeks. No cell body loss was detected at 21 weeks, although chromatolytic cells and acentric nuclei were observed. Thus the first pathological change in feline SMA detected in this study was a failure of axon radial outgrowth. In order to confirm that *LIX1* is the feline SMA disease gene and facilitate future investigation of

LIX1 function, a *Lix1* knockout mouse was ordered from Lexicon Genetics, Inc. Homozygous *Lix1* knockout mice did not demonstrate any neuromuscular phenotype even at two years of age, as assessed by motor function tests and spinal cord and muscle histology. However, expression of a *Lix1* alternative transcript (*Lix1alt*) with an independent promoter was maintained in *Lix1*$^{-/-}$ mice and may compensate for the loss of *Lix1*.

A yeast two-hybrid screen of a human fetal brain cDNA library was conducted to identify putative LIX1 interacting partners. This screen of 2 x 10^7 clones identified twelve unique preys, some of which were identified multiple times. Confirmation of the protein interactions was accomplished by *in vitro* co-immunoprecipitation and band shift assays. The cytoplasmic domain of DACHSOUS1 (DCHS1) was identified 20 times in the yeast two-hybrid screen and was the only prey that had a confirmed interaction with LIX1 *in vitro*. GFP tagged Lix1 and Lix1alt co-localized with DsRed tagged Dchs1 in cultured Cos7 and NSC34 cells. Although the co-localization in cultured cells supports an *in vivo* interaction between Lix1 or Lix1alt and Dchs1, no such interaction could be detected by *in vivo* co-immunoprecipitation.

Computational analysis of LIX1 predicted amino acids 22-99 to fold into a double stranded RNA binding domain. To test this prediction I conducted gel mobility shift assays with single and double stranded RNA and purified, recombinant LIX1. No interaction with RNA was observed *in vitro*. Furthermore, GFP-tagged Lix1 did not co-localize with Poly A Binding Protein 1 (Pabp1) a marker of ribonucleoprotein complexes in cultured NSC34 cells. Therefore, this does not support the predicted RNA binding activity of LIX1. More work is necessary to confirm that LIX1 is the feline SMA disease gene and whether the interaction of LIX1 and DCHS1 is directly involved or completely unrelated to feline SMA pathogenesis.

ACKNOWLEDGMENTS

First and foremost I would like to thank Dr. John Fyfe for his unwavering support and guidance during my graduate career. I could not have chosen a better mentor to provide the right amount of oversight and independence necessary for my success as a student and researcher. I would also like to thank my committee members, Dr. William Atchison, Dr. Karen Friderici, Dr. Cynthia Jordan, and Dr. Ronald Patterson. Their expertise and thoughtful critiques were instrumental in the development and progression of this research project. I would also like to acknowledge Dr. Donna Koslowsky for her guidance and assistance with the RNA and protein gel mobility shift assays and Ralph Common, Amy Porter, Kathy Joseph and Rick Rosebury for their excellent histology work.

I must acknowledge previous members of the Fyfe lab, Brittany Gregory, Megan Barry, Stacie Dodgson, Kyle Snowden, Nicole Messenger, Lisa St. Charles, and Brian Farber for their assistance with various aspects of this research. I would also like to acknowledge Jessica LeBoeuf for her technical assistance with spinal cord dissection, cryostat sectioning and acetylcholine receptor staining. I would like to specifically recognize my good friend and lab mate, Dr. Rabeah Al-Temaimi. Her support in and out of the lab was encouraging and her kindness was truly appreciated.

I must thank my 5th floor neighbors, the members of the Friderici and Schutte lab for their camaraderie. To Meghan, Kathy, Soumya, Ellen, Mei, Eric, Ayo, Arianna, Paula, Walid, Youssef and Dan, whose friendship made coming to lab everyday enjoyable. I must also recognize Gabriele Meyer and Rachel Spurbeck who kept me sane and made life outside of the lab great fun. To all my other friends here and elsewhere, sincere thanks for your love and support. Finally, to my family, Mom, Dad, Kate and Colin, thank you for your love and support

despite my knack for enrolling in distant universities in colder climates. I could not nor would I have wanted to undertake this without you.

TABLE OF CONTENTS

LIST OF TABLES

LIST OF FIGURES

KEY TO ABBREVIATIONS

A	affected
A6U	ATPase subunit 6
Actb1	β-actin
Actg1	γ-actin
APRT	adenine phosphoribosyltransferase
AR	androgen receptor
ASO	antisense oligonucleotides
BiFC	bimolecular fluorescence complementation
CMAP	compound motor action potential
CNS	central nervous system
Co-IP	co-immunoprecipitation
Cyb	cytochrome b
Cyp	cyclophilin
DAPI	4',6-diamidino-2-phenylindole
DCHS1	Dachous1
DMD	Duchenne muscular dystrophy
D-MEM	Dubelcco's Modified Eagle Medium
dNTPs	deoxynucleotide triphosphate
Ds	Dachsous
EC	extracellular cadherin
ECD	extracellular domain
ECL	enhanced chemiluminescence
EDL	extensor digitorum longus
EMG	electromyography

ESE	exonic splicing enhancer
Fj	four jointed
Ft	Fat
FVT1	3-ketodihydrosphingosine reductase
Gems	Gemini of Cajal bodies
GFP	green fluorescent protein
HCSMA	hereditary canine spinal muscular atrophy
HDAC	histone de-acetylase
H&E	hematoxylin and eosin
HPRT	hypoxanthine-guanine phosphoribosyltransferase
IGHMBP2	immunoglobulin μ-binding protein 2
kb	kilobase
kDa	kilo-Dalton
KO	knockout
LHS	Lesch-Nyhan syndrome
LIX1	limb expression 1
Lix1alt	limb expression 1 alternative transcript
LNPEP	leucyl/cystinyl aminopeptidase
LTR	long terminal repeat
MBP2	maltose binding protein
MHFMS	Modified Hammersmith Functional Motor Scale
N	normal
NA	numerical aperture
NAIP	neuronal apoptosis inhibitory protein
N-CAM	neural cell adhesion molecule

NCV	nerve conduction velocities
Nmd	neuromuscular degeneration
NF	neurofilament
NMJ	neuromuscular junction
PABP	poly A binding protein
PBA	phenylbutyrate
PCP	planar cell polarity
PBS	phosphate buffered saline
PBST	phosphate buffered saline with Tween20
PCR	polymerase chain reaction
PLS3	PLASTIN3
PNS	peripheral nervous system
Pmn	progressive motor neuropathy
PrP	prion promoter
PVDF	polyvinylidene fluoride
RT-PCR	reverse transcriptase polymerase chain reaction
RT-qPCR	reverse transcriptase quantitative polymerase chain reaction
s	seconds
SAHA	suberoylanilide hydroxamic acid
SBMA	spinal bulbar muscular atrophy
S.D.	standard deviation
SDS	sodium dodecyl sulfate
SDS-PAGE	sodium dodecyl sulfate polyacrylamide gel electrophoresis
SMA	spinal muscular atrophy
SMARD	spinal muscular atrophy with respiratory distress
SMN	survival of motor neuron

snRNP	small nuclear ribonucleoprotein
SOD1	Cu, Zn superoxide dismutase
TA	anterior tibialis
Tbce	tubulin-specific chaperone E
TBS	Tris buffered saline
TBST	Tris buffered saline with Tween 20
UTR	untranslated region
VPA	valproic acid
Vsp54	vacuolar-vesicular protein sorting factor 54
Wr	wobbler

CHAPTER 1: Literature Review

Motor neuron diseases are characterized by degeneration of upper motor neurons, lower motor neurons or both, without sensory neuron involvement (1). The cell bodies of upper motor neurons lie in the motor cortex and their axons synapse either directly, or via interneurons, with lower motor neurons in the brainstem and spinal cord. Lower motor neurons innervate skeletal muscle fibers and spindles. Upper motor neuron degeneration results in spasticity and hyperreflexia, as seen in hereditary spastic paraplegia and primary lateral sclerosis. Lower motor neuron diseases are characterized by muscle weakness and atrophy. The spinal muscular atrophies (SMA) are a heterogeneous group of lower motor diseases that vary in onset, severity and genetic basis and are the focus of this review.

Proximal SMA – Clinical classification

Proximal SMA is characterized by weakness and atrophy of proximal limb and trunk muscles, with muscles of lower limbs being more affected than those of upper limb muscles (2). Guido Werdnig and Johann Hoffmann first described the disease in 1891 and 1893, respectively (3). In the century that followed, clinical variability made it difficult to determine whether proximal SMA was a single entity. Today, proximal SMA is divided into 4 clinical types, based on age of onset, severity and survival time. Type I SMA, or Werdnig-Hoffmann disease (also infantile SMA, or acute SMA), is the most severe form of the disease, with onset prior to 6 months of age. In one-third of cases, onset occurs prior to or at birth (4, 5). In another third of cases, onset occurs prior to two months (5). Affected individuals never gain the ability to sit up and death ensues by 2 years of age. Muscle atrophy is often not apparent due to increased adiposity; instead infants appear hypotonic and weak. Affected infants often have difficulty feeding and breathing is rapid and diaphragmatic. Atrophy of the intercostal muscles give the trunk a distinct

bell shape (6). Recurrent respiratory infections are common and lead to respiratory insufficiency and eventually death.

Clinical onset in Type 2 SMA (intermediate form) occurs after 6 months, but prior to 18 months of age (2). Type 2 patients are able to sit up unaided, but never gain the ability to walk (6-8). Scoliosis is common, and as in Type 1, intercostal weakness gives the trunk a bell shape. Fasciculations of the tongue and hands are often observed. Approximately 25% of Type 2 cases have difficulty chewing and swallowing (9). Death occurs due to respiratory insufficiency, but in the childhood to early adolescent years.

Type 3, or Kugelberg-Welander disease, is the least severe, juvenile onset form of the disease (2). Onset occurs after 18 months of age and patients are able to stand and walk (10, 11). Type 3 is often divided into sub-types based on age of onset; Type 3a onset occurs prior to 3 years and Type 3b onset occurs after 3 years (12). As the disease progresses, the ability to walk may be lost and scoliosis is prevalent in patients that are wheelchair-dependent. Unlike Type 1 and Type 2 there is not a significant decrease in lifespan. Type 4 is the rare adult-onset, comparatively mild form of proximal SMA and does not result in shortened life span.

Electrophysiology

Electromyography results are dependent on the severity and duration of SMA. Both severe and mild SMA patients demonstrate loss of motor units (10, 13-15). Abnormal fibrillation potentials are present in severe SMA patients, but not in Type 3 patients (6, 10, 13). In later stages of severe SMA and in mildly affected individuals, motor action potentials are increased due to collateral sprouting of surviving motor axons (11, 13). Nerve conduction velocity is not typically affected, although there have been some reports of reduced motor nerve conduction velocity in Type 1 cases (16, 17, 18).

Pathology

Histology of muscle biopsy specimens from all types of proximal SMA, identified groups of atrophic fibers, rounded hypertrophic fibers and normal fibers (6, 8, 11, 17). Both slow and fast twitch fibers types are affected in severe SMA, but fast twitch fibers are predominately atrophic in Type 3 SMA (2, 19). The degree of atrophy increases with disease severity and duration, as does the amount of connective tissue and fat (13, 15). Immunohistochemistry against neural cell adhesion molecule (N-CAM), a marker of denervation, was found to be elevated in biopsied muscles from Type 1 and Type 3 patients (19).

In all types of SMA, loss of large motor neurons in the anterior horn is the most striking neuropathology (6, 20-22). The remaining motor neurons are often chromatolytic with accentric nuclei. The perikarya of chromatolytic cells are positive for phosphorylated neurofilaments, suggesting a defect in anterograde axonal transport (18, 22, 23). In Type I SMA, swollen achromatic motor neurons, called ballooned neurons, are often observed. These ballooned neurons contain phosphorylated neurofilaments in the peripheral perikarya and ubiquitinated epitopes accumulate in the central perikarya. Increases in astrocytes and microglia in the spinal cord are also observed (6, 20-22). Ventral roots are atrophic with decreased numbers of myelinated axons and increased amounts of connective tissue. Sensory neurons are not usually affected; however, there have been a few reports of Type 1 cases in which degeneration in Clarke's column and dorsal root ganglia were observed (24, 25).

Inheritance and Incidence

Prior to genetic mapping, the clinical heterogeneity of SMA made it difficult to determine whether it was a single entity. Pedigree analysis determined that all types of proximal SMA are inherited in an autosomal recessive manner (4, 6, 10, 15, 26-28). Siblings are usually affected to the same severity (29); however, there are reports of siblings affected to different degrees (8, 30-32). In these cases, males were more severely affected than their female siblings. Rare

cases of autosomal dominant or X-linked recessive proximal SMA have been documented, demonstrating some genetic heterogeneity (11, 15, 33). Proximal SMA is the second most common genetic disorder after cystic fibrosis with a frequency of 1/6,000 live births (34). Type 1 SMA is the most common form of the disease with an incidence of 1/10,000 to 1/25,000 live births (15, 26, 28, 35, 36). Type 2 and Type 3 occur together at a similar frequency to Type 1.

Mapping of the SMA locus

Through linkage analysis, Type 2 and Type 3 SMA were mapped to chromosome 5q11.2-q13.3 in early 1990 (37-39). The lack of large, multiply affected Type 1 SMA families made mapping by linkage analysis difficult. Instead, Type 1 SMA was mapped by a homozygosity mapping in consanguineous pedigrees and linkage analysis in a large number of small pedigrees to 5q11.2-q13.3 (38, 40). Thus all three types mapped to an interval between markers D5S6 and D5639, providing strong evidence that proximal SMA is due to mutations in a single gene. Genotyping of more families with highly polymorphic microsatellite markers further refined the SMA locus to a ~ 2 cM region (41-48). Several yeast artificial chromosome and radiation-hybrid based physical maps of the SMA critical region were constructed (49-51), but no consensus map could be generated due to the variability of the region (51-53). Inherited and *de novo* deletions in Type 1 SMA families were critical to indentifying the minimum SMA region.

Two candidate genes were identified at the SMA locus (Figure 1.1). These genes are present in multiple copies on chromosome 5q because of a 500 kilobase (kb), inverted duplication (54, 55). One gene was named *neuronal apoptosis inhibitory protein* (*NAIP*) due to its homology with baculoviral genes that prevent apoptosis within the insect cell it infects. Over-expression of *NAIP* significantly decreased apoptosis in serum deprived or free radical induced mammalian cell culture (56). *NAIP* spans 70 kb of genomic DNA and consists of sixteen exons (55). The 3796 nucleotide long open reading frame encodes an 140 kDa protein with two

Figure 1.1. Schematic of 500 kb inverted duplication on chromosome 5q that contains the SMA critical region. Thin black arrows represent 500 kb duplicated fragments. Red and blue arrows depict the direction of transcription of genes within the duplicated region. Positions of microsatellite markers (red) used in linkage analysis are also shown. Image from Lunn and Wang, 2008 (57). For interpretation of the references to color in this and all other figures, the reader is referred to the electronic version of this dissertation.

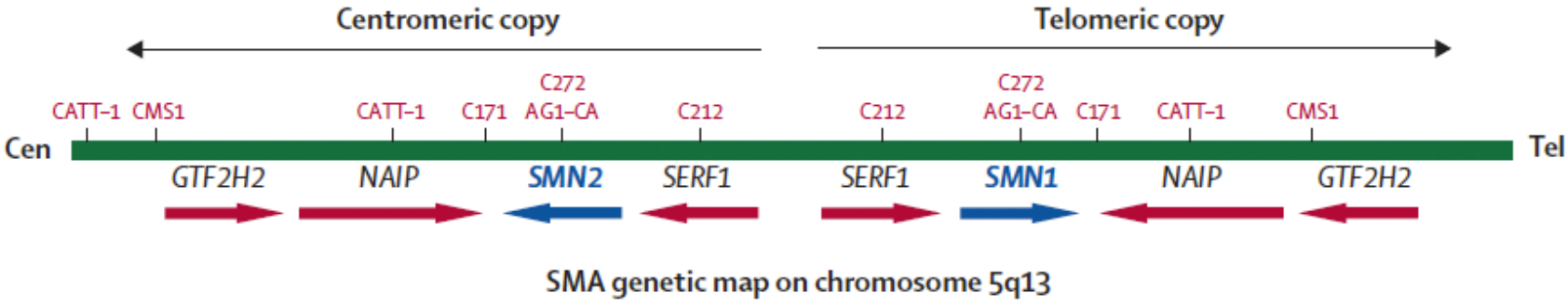

predicted transmembrane domains and a ATP/GTP binding site. *NAIP* expression was detected in liver and placenta by Northern blots and by reverse transcriptase coupled polymerase chain reaction (RT-PCR) in spinal cord. Homozygous deletion of *NAIP* exons 5 and 6 was detected in 45% and 18% of Type 1 and Type 2/3 SMA patients, respectively. However, homozygous loss of *NAIP* was also detected in three unaffected parents of SMA children.

The other candidate gene, named the *survival of motor neuron* (*SMN*) gene, is present in two nearly identical copies (54). Exons 7 and 8 of the telomeric *SMN* gene (*SMN1*) are deleted in ~93% of SMA patients. An additional 5% of patients show loss of exon 7 alone (58). Deletions in the centromeric *SMN* copy (*SMN2*) alone were only found in normal controls. The identification of subtle *SMN1* mutations in SMA patients, including missense, splicing and frameshift mutations, provided evidence that *SMN1* is the proximal SMA disease gene (54, 59-61). Homozygous deletion of *SMN1* exons 7 and 8 were also identified in 0.3% of normal parents with SMA affected children, suggesting that other genes may be involved in SMA pathogenesis (62).

SMN1 Structure and Function

SMN1 spans 20 kb of genomic DNA and contains 9 exons (63). The 1.5 kb transcript encodes a ~38 kDa protein of 294 amino acids that is ubiquitously expressed (64). Strong expression is seen in lower motor neurons of mammalian spinal cord and brainstem with higher expression in neonatal tissues than in adult tissues. SMN protein localizes to the cytoplasm and nuclear Gemini of Cajal bodies (Gems) (65). SMN protein contains several domains that are important for SMN interactions with itself and other proteins (Figure 1.2). Exons 1 and 2b encode residues critical for binding of GEMIN2 (66, 67). A Tudor domain, named for its homology to the *Drosophila melanogaster* tudor protein, is encoded by exon 3 (68). This domain

Figure 1.2. SMN transcript and protein structure. Coding regions are depicted in teal and untranslated regions are shown in purple. Poly-proline motifs are depicted in green and the Y/G box is indicated in orange. The exon 7 cytoplasmic targeting motif, QNQKE, is indicated in black. Missense mutations identified in SMA patients are labeled below the protein schematic. Figure from Rossoll and Bassell, 2009 (69).

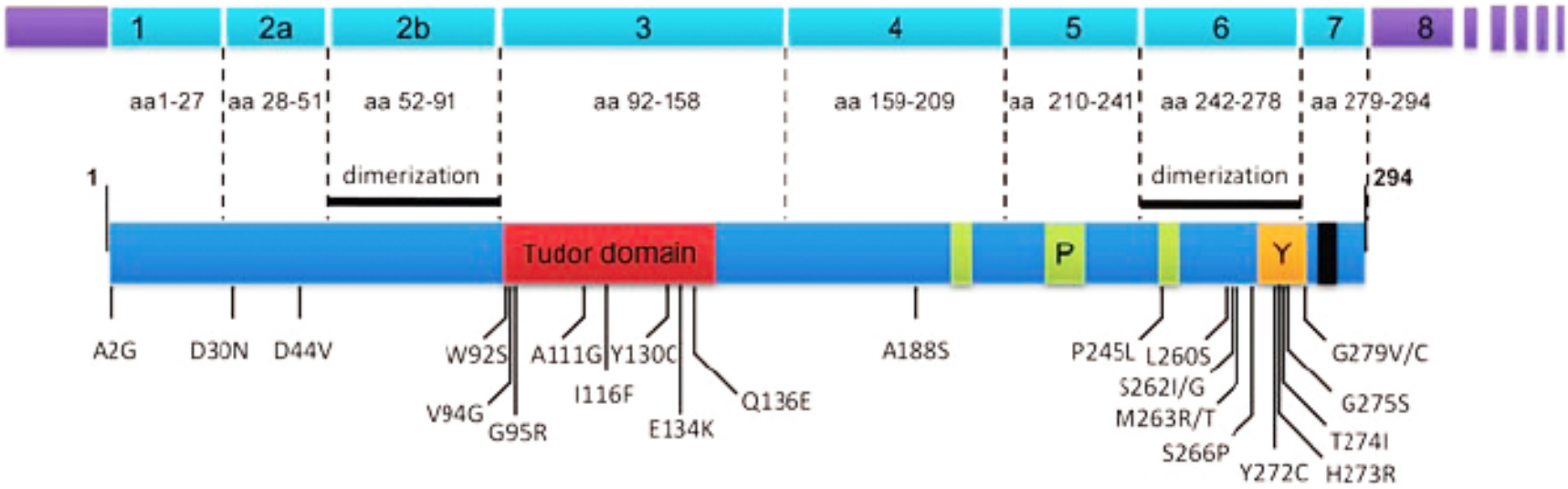

mediates interactions between SMN and proteins containing methylated arginine and lysine residues, such as the Sm proteins. SMN also contains three poly-proline tracts in exons 4-6 that are bound by PROFILIN. Exons 2b and 6 encode for amino acid residues that are required for self-oligomerization (67, 70). Missense mutations identified in non-*SMN1* deleted patients cluster around the Tudor domain and Y/G box. The most frequent missense mutation in SMA patients, Y272C, decreased self-association four-fold *in vitro* when compared with wild-type SMN. Thus the Tudor domain and Y/G box are required for SMN function.

The best characterized function for SMN is in spliceosomal small nuclear ribonucleoprotein (snRNP) synthesis (Figure 1.3). The SMN complex contains nine proteins, SMN, GEMINS 2-8, and UNRIP at an unknown stoichiometry (66, 71-81). This complex loads the heptameric ring of Sm proteins onto the stem loops of U snRNAs in an ATP-dependent manner. After loading of Sm proteins, the 7-methylguanosine cap of the snRNA is hypermethylated and the entire complex is imported to the nucleus. The snRNPs and SMN complex then localize to Cajal bodies, where the snRNPs are further modified before participating in pre-mRNA splicing. In 2008, Zhang *et al*. reported that SMN deficiency in a SMA Type 2 mouse model resulted in significant reduction of U11, U12, and U4atac snRNAs in spinal cord, at P11, or ~3 days before death due to disease (82). RNA isolated from spinal cord was analyzed with an Affymetrix mouse exon microarray and splicing pattern changes were detected in 259 genes. However, it was unclear at what ages and thus disease stage these splicing changes were detected. These results were repudiated by Bäumer *et al*. (2009), who detected significant changes in splicing only in spinal cord from end-stage SMA mice (83). These data suggests that splicing defects are secondary to motor neuron dysfunction and thus not involved in the primary pathogenesis of SMA.

Further evidence for a motor neuron-specific function of SMN came from work in zebrafish from Christine Beattie's laboratory. Knockdown of SMN with morpholinos results in

Figure 1.3. The snRNP biogenesis pathway. SMN and its associated proteins load the Sm proteins on U snRNAs. Figure from Burghes and Beattie, 2009 (86).

Figure 1.3 continued.

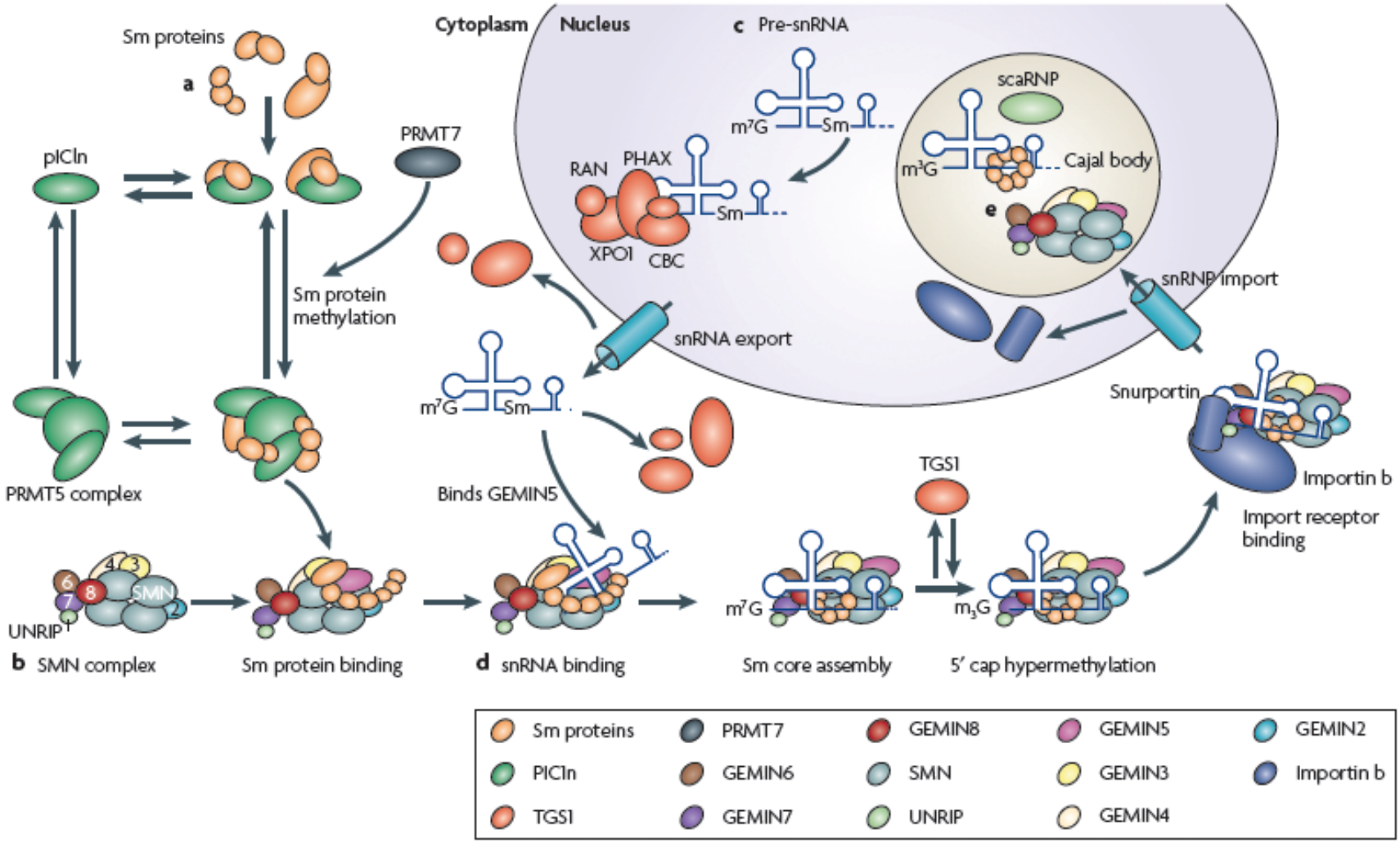

motor-axon path-finding defects that can be rescued by human SMN expression (84, 85). Expression of mutant, human SMN that was able to oligomerize and bind Sm proteins could not rescue motor-axon defects. Furthermore, knockdown of GEMIN2 had no effect on motor-axon outgrowth (87).

SMN localizes within granules in axons and growth cones of neurons in culture (88). These granules co-localize with mRNA and ribosomes and are trafficked along microtubules. Some of these granules contain Gemins 2 and 3, but Sm proteins were largely absent (89). The identities of mRNAs within SMN granules remain largely unknown. However, SMN deficient-motor neurons have reduced *β-actin* mRNA in axons and β-Actin protein in growth cones (90). Furthermore, SMN interacts with heterogeneous nuclear ribonucleoprotein R (hnRNP R), which binds the 3' UTR of *β-actin* mRNA (91). Knockdown of hnRNP R in zebrafish and cultured mouse motor neurons results in reduced axon outgrowth of motor neurons and reduced amounts of distal *β-actin* mRNA (92). Recently, SMN, GEMIN2 and GEMIN3 were found to co-localize and co-immunoprecipitate with *β-actin* mRNA in human SHSY5Y neuroblastoma cells (93). Further evidence of SMN's role in actin metabolism came from yeast-two hybrid assays and co-localization studies in motor neurons and PC12 cells that identified Profilin I and II as a SMN binding protein (94, 95). *In vitro* actin polymerization assays demonstrated that SMN has an inhibitory effect on Profilin's actin monomer sequestering ability. *In vivo*, increased Profilin IIa immunofluorescence and decreased expression of Plastin3, an actin bundling protein, were detected in spinal cord motor neurons of a SMA mouse model (96). *PLASTIN3* (PLS3) is hypothesized to be a protective modifier of SMA (97). Unaffected females, harboring the same SMN1 deletions as affected siblings, had significantly higher expression of *PLS3* and filamentous actin in lymphoblasts. Furthermore, over-expression of *PLS3* in *SMN* deficient mouse and zebrafish embryos rescued axon outgrowth defects. Thus, deregulation of actin dynamics may be an important factor in SMA pathogenesis. Support for this hypothesis came

from pharmacological inhibition of RhoA kinase, a modulator of actin dynamics that increased the lifespan and neuromuscular function of an intermediate SMA mouse model (98).

Several other functions for SMN have been proposed in the literature based on its interacting partners. SMN interacts with Bcl-2 and p53 (99-101), RNA polymerase II (102), small nucleolar ribonucleoproteins (103), and fibroblast growth factor-2 (104), to name a few. These interactions suggest SMN functions in diverse cellular pathways such as apoptosis, transcription, and ribosomal RNA processing. However it remains unclear, which, if any of these identified SMN functions is important for SMA pathogenesis.

SMN2

In humans, SMN is duplicated on chromosome 5q. The centromeric copy, *SMN2*, differs from SMN1 by five nucleotides (Figure 1.4) (54, 63). Three of these changes are located in introns and one change is located in the 3'UTR. The only exonic nucleotide change, a C to T transition in exon 7, is translationally silent. This C to T transition disrupts an exonic splicing enhancer element that is normally recognized by splicing factor SF2/A2F (105-108). As a result, approximately 90% of *SMN2* transcripts lack exon 7 (*SMN2Δ7*). The correct splicing of the remaining SMN2 transcripts is probably due to binding of an exonic splicing enhancer in the middle of exon 7 by Htra2-β1, over-expression of which restores exon 7 in 80% of *SMN2* transcripts (109, 110). Protein translated from full-length *SMN2* transcripts is identical to SMN1 protein. Protein produced from *SMN2Δ7* transcripts is truncated by twelve amino acids. SMNΔ7 is less stable and has a reduced ability to self-oligomerize (70, 111, 112). Furthermore, SMNΔ7 lacks a critical cytoplasmic targeting motif (QNQKE) that is required for localization within axons (88, 113). Expression of SMNΔ7 in *SMN* deficient zebrafish is not sufficient to rescue axon

Figure 1.4. Comparison of *SMN1* and *SMN2* transcripts. Only 5 nucleotides distinguish *SMN1* from *SMN2*. The C to T transition in exon 7 of *SMN2* results in exon 7 skipping in 90% of *SMN2* transcripts. Figure from Wirth, Brichta and Hahnen, 2006 (119).

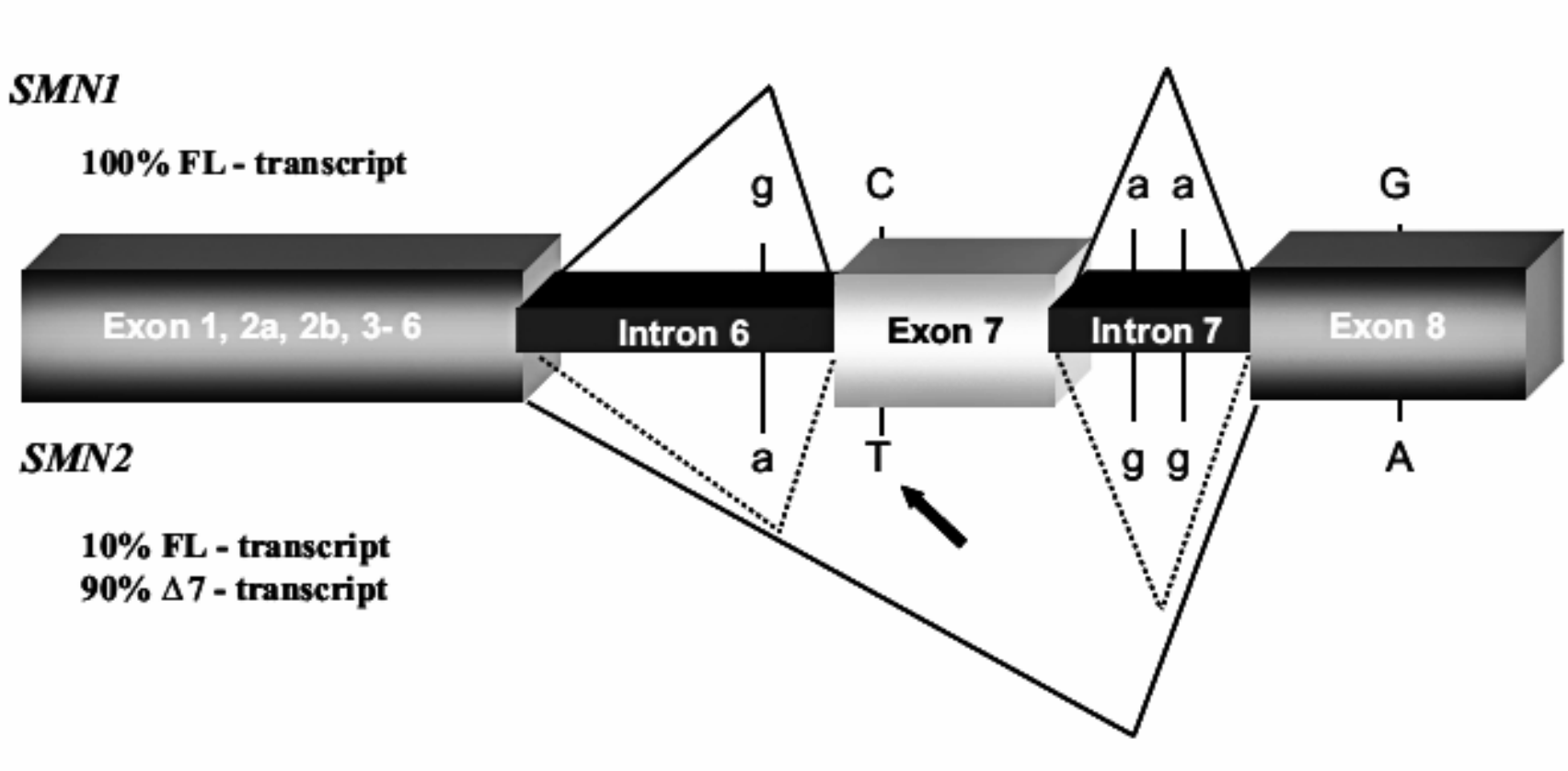

outgrowth defects (85). Thus SMNΔ7 is not able to compensate for loss of *SMN1*. The variation in clinical severity of proximal SMA correlates with full-length *SMN* expression and thus, *SMN2* copy number (115-117). *SMN2* is typically present in 1 to 4 copies, with gene conversion being the most likely mechanism for increased *SMN2* and decreased *SMN1* copy number (118, 119). Type 1 patients typically have 2 *SMN2* copies; Type 2 patients have 3 *SMN2* copies; Type 3 patients have 3 to 4 *SMN2* copies and Type 4 patients have 4 to 6 copies (120). A rare variant in *SMN2* exon 7 (c.859G>C) increases the inclusion of exon 7 in *SMN2* transcripts, resulting in Type III SMA despite the presence of only 2 *SMN2* copies (121). The modulation of SMA severity by *SMN2* copy number has been recapitulated in mouse models of SMA (see below).

SMA variants

There are several motor neuron diseases whose clinical phenotype is similar to 5q proximal SMA. These diseases can either be inherited or sporadic. A small subset of lower motor neurons diseases with a known genetic basis is discussed below.

SMA with respiratory distress (SMARD)

SMARD is a severe infantile onset (prior to six months), distal spinal muscular atrophy (122). Patients with SMARD typically show decreased fetal movements and intrauterine growth retardation. Unlike 5q-linked SMA, patients most often demonstrate respiratory complications due to diaphragmatic weakness prior to the onset of skeletal muscle weakness. Muscle weakness first occurs in the distal, lower limbs with eventual paralysis of the limbs and trunk. Histologic examination of muscle biopsies reveal atrophic and hypertrophied fibers, which is consistent with neurogenic atrophy. In contrast with proximal SMA, SMARD involves the sensory neurons as well as anterior horn cells. SMARD is an autosomal recessive disease caused by mutations in the immunoglobulin μ-binding protein 2 gene (*IGHMBP2*) on

chromosome 11q13 (123). Missense mutations are the most common type of mutation in *IGHMBP2* and these mutations cluster at a DEAD box helicase domain that is often found in RNA helicases. Similar to SMN, IGHMBP2 in found in the nucleus, in the cytoplasm and in the axons of motor neurons. IGHMBP2 is ubiquitously expressed and as in 5q SMA, it remains unclear why mutations in this gene result in motor neuron loss.

Spinal bulbar muscular atrophy (SBMA, Kennedy's disease)

SBMA is an adult onset, slowly progressing, X-linked recessive lower motor neuron disease (124). In comparison to 5q SMA, SBMA is rare with an incidence of ~3/100,000. Onset typically occurs between 20 and 40 years of age and the disease does not result in decreased lifespan. Affected males most often present with proximal lower limb weakness, difficulty swallowing, and fasciculations. Approximately 50% of affected males also have gynecomastia. Female carriers are very rarely symptomatic and these cases are usually attributed to skewed inactivation of the mutant X chromosome (125). Affected female carriers typically demonstrate very mild muscle weakness, fasciculations, or muscle cramps. SBMA is caused by a CAG repeat expansion in the *androgen receptor* gene (126). This repeat expansion results in an enlarged poly-glutamine tract in the androgen receptor (AR). Normal individuals have 20 or less repeats, whereas affected males have greater than 40 repeats. As is seen in other triplet repeat diseases, repeat length is negatively correlated with age of onset and disease severity (127, 128). In addition to the loss of motor neurons and neurogenic atrophy, SBMA pathology is characterized by aggregates of mutant AR in the nucleus and cytoplasm. Mutant AR is hypothesized to cause motor neuron degeneration through a gain of function or toxicity of the AR aggregates.

Animal models of SMA

Several animal models, either engineered or naturally occurring, of SMA are in existence. As humans are the only animals with two *SMN* genes, homozygous deletion of *SMN* in other species is lethal. Mammalian models of spinal muscular atrophy are discussed below.

Engineered mouse models

Homozygous disruption of *Smn* by *lacZ* reporter gene insertion resulted in early embryonic death prior to uterine implantation (129). At six months of age, heterozygous mice have 40% fewer spinal cord motor neurons, although no overt phenotype was reported (130). There was no decrease in nuclear Gems and lifespan was normal.

Expression of human *SMN2* is sufficient to rescue the embryonic lethality of *Smn* absence (131, 132). Furthermore, the copy number of *SMN2* transgenes modulated the phenotype severity. Fifteen percent of mice carrying one or two *SMN2* transgenes died within the first six hours of birth. The remainder appeared normal for the first 48 hours after birth, but deteriorated rapidly in the next few days. *Smn-/-; SMN2* mice became less mobile and were smaller than their normal littermates. Labored breathing and muscle tremors were apparent by P3 and mice died by P6. Spinal cord lower motor neurons were normal at birth, but decreased by ~35% at P5. Primary motor neurons cultured from these mice showed normal survival, but axon outgrowth was significantly reduced (90). However, this effect was not seen in *Smn-/-; SMN2* mice carrying a *HB9:GFP* transgene to label motor neurons (133). Axonal swellings containing neurofilaments in these mice were observed, as were unoccupied acetylcholine receptor clusters during embryonic and postnatal development. Long living mice exhibited digital necrosis, which has been reported in some severe Type 1 SMA cases (134, 135). Recently, heart defects including a thinner inter-ventricular septum and left ventricle wall were identified in

these severe SMA mice (136). This finding supports a role for SMN in cardiogenesis that has been suggested by several case reports of Type I SMA patients with cardiac defects (137, 138).

The addition of a *SMNΔ7* transgene onto the *Smn-/-; SMN2* background extended survival to thirteen days (139). At P5, mice carrying the *SMNΔ7* transgene were significantly smaller than normal littermates and had difficulty righting themselves. Gait abnormalities and hindlimb tremors were apparent at 10 days. A significant reduction in spinal cord motor neurons was observed at 9 days and grip strength was significantly decreased at 11 days (140). Loss of pre-synaptic terminals at neuromuscular junctions and accumulation of neurofilaments were observed early in the disease course (141). Thus it appears that neuromuscular junctions form normally in SMA, but that pre-synaptic pathology occurs early in the disease course.

Alternatively, expression of a mutant *SMN* transgene with the human A2G mutation, extends survival in *Smn-/-;SMN2* mice to approximately 8 months (142). Expression of SMN A2G failed to complement embryonic lethality in *Smn-/-* mice, thus low levels of wild-type SMN are required for the formation of functional SMN complexes. *Smn-/-;SMN2 ;SMNA2G* mice become less active, displayed labored breathing and lose weight towards the end of their life. Muscle weakness and neurogenic atrophy is evident by one month of age by hindlimb clasping and muscle histology. A 25% reduction in the number of L4 ventral root axons is seen in five month old mild SMA animals, and the surviving axons are smaller. Presence of the SMN A2G transgene in two copies extended survival and prevented the development of a neuromuscular phenotype even at 15 months of age.

Near complete rescue of the *Smn-/-;SMN2* phenotype was accomplished by transgenic expression of SMN under the prion promoter (PrP) (143). *Smn* null mice with two copies of *SMN2* and *PrP-SMN*, survived for an average of 210 days. L4 ventral root axon numbers were normal in these mice; however muscle fiber size was smaller than in *Smn+/-;SMN2* controls. Expression of SMN under the control of the human skeletal actin promoter was not sufficient to

improve the SMA phenotype of *SMN-/-;SMN2 mice*. Thus, restoration of SMN expression in the central nervous system of human patients will be necessary to treat 5q SMA.

Conditional *Smn* knockout mice have also been generated (144). These mice carry an *Smn* allele with LoxP sites flanking exon 7, allowing for tissue specific disruption of *Smn* when crossed with different Cre recombinase expressing mice. Loss of full-length Smn in neurons resulted in mean survival of only 25 days. By two weeks of age, muscle tremor and hypotonia were evident. Muscle histology revealed neurogenic atrophy at two weeks. L4 ventral root axon numbers were decreased by 49% at 15 days and 78% at 30 days of age (145, 146). In comparison, only a 30% reduction in L4 motor neuron cells bodies was observed at day 30. Abnormal neurofilament accumulation was observed in neuromuscular junctions of 15 day old mutant mice. Thus, SMA occurs through a dying back process in this mouse model. Deletion of *Smn* exon 7 in skeletal muscle resulted in muscular dystrophy (147). Limb paralysis occurred at 4 weeks of age. At the same age, there was great variability in muscle fiber size, centralized nuclei and increased connective tissue observed in muscle specimens. Furthermore, decreased expression of Dystrophin was detected in transverse muscle sections. There was no motor neuron loss or acetylcholine receptor abnormalities noted. Therefore full length Smn expression is critical for skeletal muscle, but loss of SMN in muscle is not responsible for motor neuron degeneration in SMA.

The most recently developed model of SMA, is a knock-in mouse in which the endogenous *Smn* gene has been replaced with a copy that contains the C to T transition found in *SMN2* (148). Homozygous knock-in mice had reduced levels of full-length *SMN* mRNA and protein, but survival was unaffected. Beginning at 60 days of age, knock-in mice were less likely to rear onto their hindlimbs and grip strength was reduced. Examination of muscle fiber morphology identified hypertrophied muscle fibers. No motor neuron axon or cell body counts were reported. This mouse model of SMA is comparable to Type 3 SMA and will assist in the identification of SMA modifiers.

Spontaneous mouse models of SMA

There are multiple naturally occurring mouse models in which motor neurons are affected, three of which are discussed below. The wobbler (wr) mouse was first identified as a spontaneous mutation in a breeding colony of C57 Bl/Fa mice (149). This mutation results in an autosomal recessive lower motor neuron disease with clinical signs visible at 4 weeks. These mice have an abnormal gait with progressive muscle weakness and atrophy that is most obvious in forelimbs. Progression of the disease continues until 5 months of age and mice survive until a year of age. Histology of spinal cord and brain revealed motor neuron degeneration prior to the onset of clinical signs. A striking feature of wobbler motor neurons was the presence of numerous vesicles in the perikarya. Atrophic fibers were not observed in transverse muscle sections until after clinical onset. Sensory neurons are unaffected. The wobbler phenotype is due to a missense mutation (L967Q) in the vacuolar-vesicular protein sorting factor 54 (*Vsp54*) gene (150). This mutation is thought to disrupt vesicular trafficking along motor neurons axons.

The progressive motor neuropathy (pmn) mouse has an autosomal recessive lower motor neuron disease (151). HIndlimb paralysis develops by the third week and mice die by seven weeks. The degeneration appears to proceed in a “dying back” manner as distal motor axons have almost disappeared by 6 weeks, but there is no reduction in ventral root axons number. However, axon diameter is reduced in affected mice and some mild chromatolysis of ventral horn motor soma was noted. This phenotype is due to a missense mutation (G524W) in the *tubulin-specific chaperone E* (*Tbce*) gene on mouse chromosome 13 (152). Tbce is essential for the assembly of α-tubulin and β-tubulin heterodimers. Primary motor neurons

cultured from these mice had shorter axons with axon swellings containing β-tubulin. Thus, this mutation provides evidence that tubulin dysfunction can result in motor neuron degeneration.

The neuromuscular degeneration (nmd) mouse model develops progressive hindlimb muscle weakness at 3 weeks of age with paralysis occurring at 5 weeks (153). Mice typically survive for 14 weeks. Significant loss of spinal cord motor neuron cell bodies was detected as early as 10 days. By 12 weeks of age, only 30% of lumbar motor neurons remained. Loss of pre-synaptic terminals was observed at 10 days in the gastrocnemius and quadriceps muscles. Neuromuscular junctions of the diaphragm were spared even at 14 weeks of age. The nmd mouse has a 4 base pair insertion in intron 4 of *Ighmbp2* creating a cryptic splice site, which results in aberrant splicing in 80% of transcripts. Thus, the nmd mouse is a naturally occurring model of human SMARD. However, there are some discrepancies between the human and mouse disease. Mice do not develop respiratory distress until late in the disease, due to sparing of the diaphragm motor neurons. Furthermore, there is no involvement of sensory neurons in the mouse model. Despite these differences the nmd mouse model will provide valuable insight into the human disease and allow for testing of therapeutic compounds.

Spontaneous large animal models of SMA

Naturally occurring motor neuron disease has been described in three large animals species; cow, dog and cat. Bovine and canine SMA are described below. For discussion of feline SMA please refer to Chapter 2. Bovine SMA was first described in 1989 in Brown-Swiss cattle (154). It is an autosomal recessive disease with onset around 3 weeks of age. Muscle weakness and atrophy presented in the hindlimbs and progressed to the forelimb. Calves typically developed bronchopneumonia in later stages of the disease. In addition to the degeneration of ventral horn motor neurons there is also degeneration in the upper motor neurons of the motor cortex (155). Due to the involvement of upper motor neurons, bovine SMA is a better model of amyotrophic lateral sclerosis than SMA. Bovine SMA is caused by a

missense mutation (A175T) in the *3-ketodihydrosphingosine reductase* (*FVT1*) gene (156). *FVT1* is a housekeeping gene involved in sphingolipid synthesis. As in human SMA, it is unknown how a mutation in a housekeeping gene results in a motor neuron specific disease.

Hereditary canine SMA (HCSMA) is an autosomal dominant lower motor neuron disease in Brittany spaniels (157). The disease is divided into 3 clinical forms based on age of onset and severity. The accelerated disease presents at 6 weeks with weakness and a fine tremor of the head. By 13 to 16 weeks affected dogs are unable to stand or lift their heads. In the intermediate form, the first clinical signs occur at a year of age with pronounced gait abnormalities. Weakness progresses from proximal to distal and posterior to anterior. By two to three years of age, dogs are unable to walk. The chronic form is characterized by onset after 6 months, with very slow progressive muscle weakness that is compatible with life beyond 6 years. The numbers of spinal cord and brain stem motor neurons do not appear to be decreased in HCSMA. However, small-caliber axons are predominant in ventral roots from the accelerated and intermediate types. Swollen axons were observed in ventral horn gray matter. The molecular basis of HCSMA remains unidentified; however, the canine *SMN* and *SOD1* genes have been excluded (158, 159).

These large and small animal models of SMA are critical to our understanding of SMA pathogenesis. Thus far, animal models have implicated RNA metabolism, cytoskeleton dynamics, vesicle trafficking, and lipid synthesis as being critical to motor neuron maintenance. Animal models of SMA will be instrumental in safety and efficacy testing of therapeutic agents as well the identification of new therapeutic targets (see below).

Genetic testing and therapy

The gold standard in SMA diagnosis is confirmation of *SMN1* homozygous absence by DNA testing. Carrier testing and pre-natal diagnosis are available to families in which an affected child has been born. Carrier testing is not 100% sensitive because 2% of SMA cases

are caused by *de novo* deletions or gene conversions and 3% of SMA cases are unlinked to chromosome 5q (61, 117, 160). Furthermore, 4% of SMA patients are compound heterozygotes with *SMN1* deletion on one chromosome and a subtle *SMN1* mutation on the other chromosome. Carriers of subtle *SMN1* mutations are not detected by current SMA genetic tests, which measure copy number of *SMN1* exon 7. *SMN2* copy number analysis is predictive of SMA severity; however it is not absolute (161). Although rare, there are reports of siblings with identical *SMN1* deletions and *SMN2* copy number that are affected to varying degrees. Despite a carrier frequency of 1:35, no neonatal screening program has been established due to the lack of effective SMA therapy (162). Neonatal screening will become necessary once an effective treatment is available, so that the therapeutic regimen can be instituted prior to the onset of pathological changes.

The current treatment for SMA is mainly supportive care (163). Respiratory insufficiency in Type 1 and Type 2 patients is treated with non-invasive or invasive ventilation and antibiotics to combat respiratory infections. Proactive care, especially ventilation, has increased the average life span of Type I patients (164). Infants with Type I SMA born between 1980 and 1994 survived for 7.5 months; whereas, those born between 1995 and 2006 survived for 24 months on average. Special diets and feeding tubes overcome nutritional deficits that result from feeding difficulties. Surgery is often required to correct scoliosis in non-ambulatory patients. Finally, wheelchairs, walkers and motorized scooters increase mobility and quality of life.

As the majority of SMA cases are due to a decrease in SMN protein, researchers have sought to increase SMN protein expression from the *SMN2* locus or exogenously. Several histone de-acetylase (HDAC) inhibitors have been found to increase transcription of *SMN2* and thus levels of full-length SMN in SMA patient-derived cell lines and/or SMA mouse models. Of these valproic acid and phenylbutyrate have reached clinical trials. Valproic acid (VPA) is a Food and Drug Administration (FDA) approved drug that has been used to treat epilepsy and

has been shown to increase SMN protein levels in SMA patient cell cultures (165, 166). In a small clinical trial, Britcha et al, 2006 treated 10 SMA carriers and 20 SMA patients with VPA (167). Seven of ten carriers had increased *SMN2* transcript levels in blood. However, *SMN2* transcript levels were only increased in 7 patients. Thus, some SMA patients are non-VPA responders. This finding was supported by a larger, phase II clinical trial of VPA in 2 SMA Type 1 patients, 29 Type 2 and 11 Type 3 patients (168). Changes in *SMN2* transcript levels in blood were highly variable between patients and in the same patient at different office visits. However, 27 of the 29 SMA Type 2 patients did demonstrate improvement in motor function as assessed by the Modified Hammersmith Functional Motor Scale (MHFMS). The most common side effect of VPA treatment was carnitine depletion, and VPA treatment was supplemented with L-carnitine in a second phase II trial to avoid negative effects of carnitine insufficiency (169). This trial, known as the SMA CARNI-VAL trials, was a double blind placebo controlled study. Sixty-one non-ambulatory SMA patients aged 2-8 years were treated with either VPA or placebo for six-months followed by VPA treatment for another six months. There was no improvement in MHFMS scores at six months. However, there was significant improvement in MHFMS scores after twelve months of treatment in SMA patients aged two to three years. The results of the SMA CARNI-VAL trial in ambulatory patients have yet to be reported.

Phenylbutyrate (PBA) is a derivative of sodium butyrate, the first HDAC inhibitor to increase expression of SMN in SMA patient cell lines and in a SMA mouse model (170). PBA is FDA approved and has been used to treat urea cycle disorders. PBA treatment in SMA patient fibroblast cell lines resulted in increased SMN levels and nuclear gem number. In a small pilot study of 4 Type 2 SMA patients, and 2 Type 3 patients, PBA treatment increased full-length *SMN2* transcript levels in blood (171). A modest increase in muscle strength was also reported. Several other HDAC inhibitors, including trichostatin A and suberoylanilide hydroxamic acid (SAHA) have shown promise in cell culture and SMA mouse models but have yet to be tested in humans (133, 172).

Another method for increasing endogenous levels of full-length *SMN* transcripts is to correct splicing of *SMN2* exon 7. One way to correct *SMN2* splicing is to use antisense oligonucletides to inhibit binding of negative splicing factors. Antisense oligonucleotides (ASO) directed to introns 6 and 7 or exon 7 splicing silencers have been shown to increase exon 7 inclusion in SMA-patient derived cells and animal models (173-175). Multiple intracerebroventricular injections of an intron 6 antisense oligonucleotide increased body weight and motor function in *Smn-/-; SMN2; SMNΔ7* mice (176). However, the effect of the ASO on survival of SMA mice was not reported. An alternative to ASOs is bi-functional RNA. These RNAs contain two regions, one that is complementary to the target and one that contains exonic splicing enhancer (ESE) elements. The ESE tail acts as a platform to recruit positive splicing factors. Bi-functional RNAs targeted to *SMN2* have successfully corrected exon 7 splicing in patient-derived cell lines and SMA mouse models (177-179). What remains to be determined with RNA based therapies are the appropriate delivery method, duration of a single treatment and thus the number of doses required and potential for adverse immune reactions. Thus identification of pharmaceutical compounds that correct *SMN2* splicing defects may be more practical. Successful *SMN2* exon 7 inclusion has been reported after hydroxyurea treatment in SMA derived cell lines and clinical trials are currently underway (180, 181).

The sixteen amino acids encoded by *SMN* exon 7 are critical for protein stability and cytoplasmic localization. However, work by Christian Lorson *et al*. suggested that SMN stability and localization are not sequence specific (182, 183). Rather, the addition of several different, short peptides to SMN exons 1-6 was able to substitute for exon 7 residues. SMNΔ7 stability and cytoplasmic localization in cultured cells was also achieved by administration of different aminoglycosides known to induce stop codon read-through. Intraperitoneal injection of G418, in five day old *Smn-/-; SMN2; SMNΔ7* mice resulted in increased levels of SMN in spinal cord and increased motor function (184). However, chronic administration of G418 was toxic so the effect

of treatment on survival could not be assessed. Subcutaneous delivery of a novel aminoglycoside, TC007, in SMA mice improved gross motor function but did not extend survival (185). Administration of TC007 directly to the CNS was sufficient to increase SMN levels and ventral horn cell numbers and extend survival 30% (186).

Another method to increase SMN levels is to deliver exogenous copies of *SMN1*. One major hurdle to effective *SMN1* gene therapy is the blood brain barrier. Azzouz *et al.* (2004), were able to achieve efficient transduction of lower motor neurons with an engineered lentivirus that could be retrogradely transported from muscle to motor neuron cell body (187). Injections of the *SMN1* expressing lentivirus into multiple muscles of *Smn-/-; SMN2; SMNΔ7* mice at a single time point decreased motor neuron death and increased survival by 3 to 5 days. Although integrating vectors offer stable transduction of cells, serious adverse events have been reported because of insertional mutagenesis in gene therapy treated patients with severe combined immunodeficiency (188-190). Recently, transduction of spinal cord lower motor neurons was achieved by systemic injection of a self complementary adeno-associated virus serotype 9 (scAAV9) expressing *SMN1* (191, 192). A single injection into the facial vein of one day old *Smn-/-; SMN2; SMNΔ7* mice was sufficient to significantly improve motor function and extend survival from 15 to 69 days. More preclinical work is required in rodents and non-human primates to determine dosage, toxicology, and the therapeutic window in SMA patients.

Other researchers have focused on non-SMN dependent therapies, such as neuroprotective or neurotrophic agents. Knockout of the ciliary neurotrophic factor resulted in decreased motor neuron sprouting and muscle strength in *Smn+/-* mice (193). Riluzole, a neuroprotective reagent, was shown to increase lifespan in a neuron specific *Smn* exon 7 knockout mouse (194). However, there was no improvement in motor function as assessed by rotarod tests. Furthermore, motor neuron axon loss was not reduced in treated animals. More research is needed to determine the efficacy of neuro-supportive reagents in the treatment of

SMA. It may be that effective treatment of SMA, especially in severe cases, will required a combination of therapeutic agents.

Summary

Proximal SMA is the second most common genetic disease and is the leading genetic cause of infant mortality. Despite intensive research for the past 15 years, the mechanism by which SMN depletion causes a motor neuron disease remains unidentified. What is apparent is that despite normal development motor neurons fail to be maintained in SMA. Animal models, both engineered and spontaneous, are critical to our understanding of SMA pathogenesis, testing and development of novel therapies, and identification of candidate genes for non-5q SMA. The remainder of this dissertation focuses on motor neuron pathogenesis in one particular model, feline SMA, and the function of its candidate disease gene, *LIX1*, in motor neurons.

REFERENCES

References

1. Nicholson SJ, Witherden AS, Hafezparast M, et al. Mice, the motor system, and human motor neuron pathology. Mamm Genome 2000;11:1041-1052.

2. Munsat TL, Davies KE. International SMA consortium meeting. Neuromuscul Disord 1992;2(5/6):423-428.

3. Wilkins RH, Brody IA. Infantile Spinal Muscular Atrophy. Arch Neurol 1971;25:24-26.

4. Pearn JH, Wilson J. Acute Werdnig-Hoffmann disease; acute infantile spinal muscular atrophy. Clin Genet 1973;48:425-430.

5. Thomas N, Dubowitz V. The natural history of type I (severe) spinal muscular atrophy. Neuromuscul Disord 1994;4(5/6):497-502.

6. Byers R, Banker B. Infantile muscular atrophy. Arch Neurol 1961;5:140-164.

7. Poirier R, Corbet RCB, Buckwold AE. Infantile spinal progressive muscular atrophy in twin. Can Med Assoc J 1951;65:342-343.

8. Dubowitz V. Infantile muscular atrophy a prospective study with particular reference to a slowly progressive variety. Brain 1964;5:707-722.

9. Messina S, Pane M, De Rose P, et al. Feeding problems and malnutrition in spinal muscular atrophy type I. Neuromuscul Disord 2008;18(5):389-393.

10. Kugelberg E, Welander L. Heredofamilial juvenile muscular atrophy simulating muscular dystrophy. AMA Arch Neurol Psych 1956;75(5):500-509.

11. Garvie J, Woolf A. Kugelberg-Welander syndrome (hereditary proximal spinal muscular atrophy). Br Med J 1966;1(5501):1458-1461.

12. Zerres K, Rudnik-Schöneborn S, Forrest E, et al. A collaborative study on the natural history of childhood and juvenile onset proximal spinal muscular atrophy (type II and III SMA): 569 patients. J Neurol Sci 1997;146(1):67-72.

13. Buchthal F, Olsen PZ. Electromyography and muscle biopsy in infantile spinal muscular atrophy. Brain 1970;93(1):15-30.

14. Crawford TO, Pardo CA. The neurobiology of childhood spinal muscular atrophy. [Internet]. Neurobiol Dis 1996;3(2):97-110.

15. Emery AEH. The nosology of the spinal muscular atrophies. J Med Genet 1971;481-495.

16. Moosa A, Dubowitz V. Motor nerve conduction velocity in spinal muscular atrophy of childhood. Br Med J 1976;51:974-977.

17. Hausmanowa-Petrusewicz I, Fidzianska A. Spinal muscular atrophy: foetal-like histopathological pattern in Werdig-Hoffman disease. Bull N Y Acad Med 1974;50(11):1157-1172.

18. Murayama S, Bouldin T, Suzuki K. Immunocytochemical and ultrastructural studies of Werdnig-Hoffmann disease. Acta Neuropathol 1991;81:408-417.

19. Walsh F, Moore S, Lake B. Cell adhesion molecule N-CAM is expressed by denervated myofibres in Werdnig-Hoffman and Kugelberg-Welander type spinal muscular atrophies. J Neurol Neurosurg Psychiatry 1987;50:439-442.

20. Ghatak NR. Spinal roots in Werdnig-Hoffmann disease. Acta Neuropathol 1978;41:1-7.

21. Araki S, Hayashi M, Tamagawa K, et al. Neuropathological analysis in spinal muscular atrophy type II. Acta Neuropathol 2003;106(5):441-448.

22. Kuru S, Sakai M, Konagaya M, et al. An autopsy case of spinal muscular atrophy type III (Kugelberg-Welander disease). Neuropathology 2009;29(1):63-67.

23. Lippa C, Smith T. Chromatolytic neurons in Werdnig-Hoffmann disease contain phosphorylated neurofilaments. Acta Neuropathol 1988;77:91-94.

24. Carpenter S, Watters G, Children M. Pathological involvement of primary sensory neurons in Werdnig-Hoffmann disease. Acta Neuropathol 1978;42:91-97.

25. Rudnik-Schöneborn S, Goebel HH, Schlote W, et al. Classical infantile spinal muscular atrophy with SMN deficiency causes sensory neuronopathy. Neurology 2003;60(6):983-987.

26. Winsor E, Murphy E, Thompson M, et al. Genetics of childhood spinal muscular atrophy. Br Med J 1971;8(2):143-148.

27. Pearn JH, Wilson J. Chronic generalized spinal muscular atrophy of infancy and childhood Arrested Werdnig-Hoffmann disease. Arch Dis Child 1973;48:768-774.

28. Pearn J. Incidence, prevalence and gene frequency studies of chronic childhood spinal muscular atrophy. J Med Genet 1978;15:409-413.

29. Pearn J. Genetics studies of acute spinal muscular atrophy (SMA type I): an analysis of sex ratios, segregation ratios and sex influence. J Med Genet 1978;15:414-417.

30. Rudnik-Schöneborn S, Röhrig D, Morgan G, et al. Autosomal recessive proximal spinal muscular atrophy in 101 sibs out of 48 families: clinical picture, influence of gender, and genetic implications. Am J Med Genet 1994;51(1):70-76.

31. Müller B, Melki J, Burlet P, et al. Proximal spinal muscular atrophy (SMA) types II and III in the same sibship are not caused by different alleles at the SMA locus on 5q. Am J Hum Genet 1992;50(5):892-895.

32. Capon F. Discordant clinical outcome in type III spinal muscular atrophy sibships showing the same deletion pattern. Neuromusc Disord 1996;6(4):261-264.

33. Cao A, Cianchetti C, Calisti L, et al. A family of juvenile proximal spinal muscular atrophy with dominant inheritance. J Med Genet 1976;13:131-135.

34. Pearn J. Classification of spinal muscular atrophies. Lancet 1980;315(8174):919-922.

35. Czeizel A, Hamula J. A Hungarian study on Werdnig-Hoffmann disease. J Med Genet 1989;26:761-763.

36. Emery AEH. Population frequencies of inherited neuromuscular diseases - a world survey. Neuromusc Disord1991;1(1):19-29.

37. Brzustowicz LM, Lehner T, Castilla LH, et al. Genetic mapping of chronic childhood-onset spinal muscular atrophy to chromosome 5q11.2-13.3. Nature 1990;344:540-541.

38. Gilliam TC, Brzustowicz LM, Castilla LH, et al. Genetic homogeneity between acute and chronic forms of spinal muscular atrophy. Nature 1990;345:823-825.

39. Melki J, Abdelhak S, Sheth P, et al. Gene for chronic proximal spinal muscular atrophy maps to chromosome 5q. Nature 1990;344:767-768.

40. Melki J, Sheth P, Abdelhak S, et al. Mapping of acute (type I) spinal muscular atrophy to chromosome 5q12-q14. Lancet 1990;336(8710):271-273.

41. Sheth P, Abdelhak S, Bachelot MF, et al. Linkage analysis in spinal muscular atrophy, by six closely flanking markers on chromosome 5. Am J Hum Genet 1991;48(4):764-768.

42. Brzustowicz LM, Kleyn PW, Boyce FM, et al. Fine-mapping of the spinal muscular atrophy locus to a region flanked by MAP1B and D5S6. Genomics 1992;13(4):991-998.

43. Daniels RJ, Thomas NH, MacKinnon RN, et al. Linkage analysis of spinal muscular atrophy. Genomics 1992;12(2):335-339.

44. Morrison KE, Daniels RJ, Suthers GK, et al. High-resolution genetic map around the spinal muscular atrophy (SMA) locus on chromosome 5. Am J Hum Genet 1992;50(3):520-7.

45. Melki J, Burlet P, Clermont O, et al. Refined linkage map of chromosome 5 in the region of the spinal muscular atrophy gene. Genomics 1993;15:521-524.

46. Soares VM, Brzustowicz LM, Kleyn PW, et al. Refinement of spinal muscular atrophy locus to the interval between D5S435 and MAP1B. Genomics 1993;15:365-371.

47. Wirth B, Voosen B, Rohrig D, et al. Fine mapping and narrowing of the genetic interval of the spinal muscular atrophy region by linkage studies. Genomics 1993;15:113-118.

48. Burghes AH, Ingraham SE, Kóte-Jarai Z, et al. Linkage mapping of the spinal muscular atrophy gene. Hum Genet 1994;93(3):305-312.

49. Francis MJ, Morrison KE, Campbell L, et al. A contig of non-chimaeric YACs containing the spinal muscular atrophy gene in 5q13. Hum Mol Genet 1993;2(8):1161-1167.

50. Thompson TG, Morrison KE, Kleyn P, et al. High resolution physical map of the region surrounding the spinal muscular atrophy gene. Hum Mol Genet 1993;2(8):1169-1176.

51. Melki J, Lefebvre S, Burglen L, et al. De novo and inherited deletions of the 5q13 region in spinal muscular atrophies. Science 1994;264(5164):1474-1477.

52. Theodosiou AM, Morrison KE, Nesbit AM, et al. Complex repetitive arrangements of gene sequence in the candidate region of the spinal muscular atrophy gene in 5q13. Am J Hum Genet 1994;55(6):1209-1217.

53. Daniels RJ, Campbell L, Rodrigues NR, et al. Genomic rearrangements in childhood spinal muscular atrophy: linkage disequilibrium with a null allele. J Med Genet 1995;32(2):93-96.

54. Lefebvre S, Burglen L, Reboullet S,et al. Identification and characterization of a spinal muscular atrophy-determining gene. Cell 1995;80:155-165.

55. Roy N, Mahadevan MS, McLean M, et al. The gene for neuronal apoptosis inhibitory protein is partially deleted in individuals with spinal muscular atrophy. Cell 1995;80(1):167-78.

56. Liston P, Roy N, Tamai K, et al. Suppression of apoptosis in mammalian cells by NAIP and a related family of IAP genes. Nature 1996;379:349-353.

57. Lunn MR, Wang CH. Spinal muscular atrophy. Lancet 2008;371:2120-2133.

58. Rodrigues NR, Owen N, Talbot K, et al. Deletions in the survival motor neuron gene on 5q13 in autosomal recessive spinal muscular atrophy. Hum Mol Genet 1995;4(4):631-634.

59. Parsons DW, McAndrew PE, Iannaccone ST, et al. Intragenic telSMN mutations: frequency, distribution, evidence of a founder effect, and modification of the spinal muscular atrophy phenotype by cenSMN copy number. Am J Hum Genet 1998;63(6):1712-1723.

60. Wang CH, Papendick BD, Bruinsma P, et al. Identification of a novel missense mutation of the SMN(T) gene in two siblings with spinal muscular atrophy. Neurogenetics 1998;1(4):273-6.

61. Wirth B, Herz M, Wetter A, et al. Quantitative analysis of Survival Motor Neuron copies: identification of subtle SMN1 mutations in patients with spinal muscular atrophy, genotype-phenotype correlation, and implications for genetic counseling. Am J Hum Genet 1999;64:1340-1356.

62. Hahnen E, Forkert R, Marke C, et al. Molecular analysis of candidate genes on chromosome 5q13 in autosomal recessive spinal muscular atrophy: evidence of homozygous deletions of the SMN gene in unaffected individuals. Hum Mol Genet 1995;4(10):1927-1933.

63. Burglen L, Lefebvre S, Clermont O, et al. Structure and organization of the human survival motor neurone (SMN) gene. Genomics 1996;32:479-482.

64. Battaglia G, Princivalle A, Forti F, et al. Expression of the SMN gene, the spinal muscular atrophy determining gene, in the mammalian central nervous system. Hum Mol Genet 1997;6(11):1961-1971.

65. Liu Q, Dreyfuss G. A novel nuclear structure containing the survival of motor neurons protein. EMBO J 1996;15(14):3555-3565.

66. Liu Q, Fischer U, Wang F, et al. The spinal muscular atrophy disease gene product, SMN, and its associated protein SIP1 are in a complex with spliceosomal snRNP proteins. Cell 1997;90:1013-1021.

67. Young PJ, Man N, Lorson CL, et al. The exon 2b region of the spinal muscular atrophy protein, SMN, is involved in self-association and SIP1 binding. Hum Mol Genet 2000;9(19):17-21.

68. Selenko P, Sprangers R, Stier G, et al. SMN Tudor domain structure and its interaction with the Sm proteins. Nat Struct Biol 2001;8(1):27-31.

69. Rossoll W, Bassell G. Spinal muscular atrophy and a model for survival of motor neuron protein function in axonal ribonucleoprotein complexes. Results Probl Cell Differ 2009;48:289-326.

70. Lorson CL, Strasswimmer J, Yao J-M, et al. SMN oligomerization defect correlates with spinal muscular atrophy severity. Nat Genet 1998;19:63-66.

71. Fischer U, Liu Q, Dreyfuss G. The SMN – SIP1 complex has an essential role in spliceosomal snRNP biogenesis. Cell 1997;90:1023-1029.

72. Pellizzoni L, Kataoka N, Charroux B, et al. A novel function for SMN, the spinal muscular atrophy disease gene product, in pre-mRNA splicing. Cell 1998;95(5):615-624.

73. Bühler D, Raker V, Lührmann R, et al. Essential role for the tudor domain of SMN in spliceosomal U snRNP assembly: implications for spinal muscular atrophy. Hum Mol Genet 1999;8(13):2351-2357.

74. Charroux B, Pellizzoni L, Perkinson RA, et al. Gemin3: a novel DEAD box protein that interacts with SMN, the spinal muscular atrophy gene product, and is a component of gems. J Cell Biol 1999;147(6):1181-1194.

75. Charroux B, Pellizzoni L, Perkinson RA, et al. Gemin4: a novel component of the SMN complex that is found in both gems and nucleoli. J Cell Biol 2000;148(6):1177-1186.

76. Friesen WJ, Dreyfuss G. Specific sequences of the Sm and Sm-like (Lsm) proteins mediate their interaction with the spinal muscular atrophy disease gene product (SMN). J Biol Chem 2000;275(34):26370-26375.

77. Baccon J, Pellizzoni L, Rappsilber J, et al. Identification and characterization of Gemin7, a novel component of the survival of motor neuron complex. J Biol Chem 2002;277(35):31957-31962.

78. Gubitz AK, Mourelatos Z, Abel L, et al. Gemin5, a novel WD repeat protein component of the SMN complex that binds Sm proteins. J Biol Chem 2002;277(7):5631-5636.

79. Pellizzoni L, Yong J, Dreyfuss G. Essential role for the SMN complex in the specificity of snRNP assembly. Science 2002;298(5599):1775-1779.

80. Pellizzoni L, Baccon J, Rappsilber J, et al. Purification of native survival of motor neurons complexes and identification of gemin6 as a novel component. J Biol Chem 2002;277(9):7540 -7545.

81. Pellizzoni L, Paushkin S, Mattaj IW, et al. The SMN complex is associated with snRNPs throughout their cytoplasmic assembly pathway. Mol Cell Biol 2002;22(18):6533-6541.

82. Zhang Z, Lotti F, Dittmar K, et al. SMN deficiency causes tissue-specific perturbations in the repertoire of snRNAs and widespread defects in splicing. Cell 2008;133(4):585-600.

83. Bäumer D, Lee S, Nicholson G, et al. Alternative splicing events are a late feature of pathology in a mouse model of spinal muscular atrophy. PLoS Genet 2009;5(12):e1000773.

84. McWhorter ML, Monani UR, Burghes AHM, et al. Knockdown of the survival motor neuron (Smn) protein in zebrafish causes defects in motor axon outgrowth and pathfinding. J Cell Biol 2003;162(5):919-931.

85. Carrel TL, McWhorter ML, Workman E, et al. Survival motor neuron function in motor axons is independent of functions required for small nuclear ribonucleoprotein biogenesis. J Neurosci 2006;26(43):11014-11022.

86. Burghes AHM, Beattie CE. Spinal muscular atrophy: Why do low levels of SMN make motor neurons sick? Nat Rev Neurosci 2009;10(8):597-609.

87. Mcwhorter ML, Boon K, Horan ES, et al. The SMN binding protein Gemin2 is not involved in motor axon outgrowth. Dev Neurobiol 2008;68(2);182-194.

88. Zhang HL, Pan F, Hong D, et al. Active transport of the survival motor neuron protein and the role of exon-7 in cytoplasmic localization. J Neurosci 2003;23(16):6627-6637.

89. Zhang H, Xing L, Rossoll W, et al. Multiprotein complexes of the survival of motor neuron protein SMN with gemins traffic to neuronal processes and growth cones of motor neurons. J Neurosci 2006;26(33):8622-8632.

90. Rossoll W, Jablonka S, Andreassi C, et al. Smn, the spinal muscular atrophy-determining gene product, modulates axon growth and localization of beta-actin mRNA in growth cones of motoneurons. J Cell Biol 2003;163(4):801-812.

91. Rossoll W, Kröning AK, Ohndorf UM,et al. Specific interaction of Smn, the spinal muscular atrophy determining gene product, with hnRNP-R and gry-rbp /hnRNP-Q: a role for Smn in RNA processing in motor axons? Mol Neurobiol 2002;11(1):93-106.

92. Glinka M, Herrmann T, Funk N, et al. The heterogeneous nuclear ribonucleoprotein-R is necessary for axonal beta-actin mRNA translocation in spinal motor neurons. Hum Mol Genet 2010;19(10):1951-1966.

93. Todd AG, Morse R, Shaw DJ, et al. SMN, Gemin2 and Gemin3 associate with beta-actin mRNA in the cytoplasm of neuronal cells in vitro. J Mol Biol 2010;401(5):681-9.

94. Giesemann T, Rathke-Hartlieb S, Rothkegel M, et al. A role for polyproline motifs in the spinal muscular atrophy protein SMN. J Biol Chem 1999;274(53):37908-37914.

95. Sharma A, Lambrechts A, Hao LT, et al. A role for complexes of survival of motor neurons (SMN) protein with gemins and profilin in neurite-like cytoplasmic extensions of cultured nerve cells. Exp Cell Res 2005;309(1):185-197.

96. Bowerman M, Anderson CL, Beauvais A, et al. SMN, profilin IIa and plastin 3: A link between the deregulation of actin dynamics and SMA pathogenesis. Mol Cell Neurosci 2009;42:66-74.

97. Oprea GE, Kröber S, Mcwhorter ML, et al. Plastin 3 is a protective modifier of autosomal recessive spinal muscular atrophy. Science 2008;320:524-527.

98. Bowerman M, Beauvais A, Anderson CL, et al. Rho-kinase inactivation prolongs survival of an intermediate SMA mouse model. Hum Mol Genet 2010;19(8):1468-1478.

99. Iwahashi H, Eguchi Y, Yasuhara N, et al. Synergistic anti-apoptotic activity between Bcl-2 and SMN implicated in spinal muscular atrophy. Nature 1997;390:413-417.

100. Sato K, Eguchi Y, Kodama TS, et al. Regions essential for the interaction between Bcl-2 and SMN, the spinal muscular atrophy disease gene product. Cell Death Differ 2000;7:374-383.

101. Young PJ, Day PM, Zhou J, et al. A direct interaction between the survival motor neuron protein and p53 and its relationship to spinal muscular atrophy. J Biol Chem 2002;277(4):2852-2859.

102. Pellizzoni L, Charroux B, Rappsilber J, et al. A functional interaction between the survival motor neuron complex and RNA polymerase II. Cell 2001;152(1):75-85.

103. Pellizzoni L, Baccon J, Charroux B, et al. The survival of motor neurons (SMN) protein interacts with the snoRNP proteins fibrillarin and GAR1. Curr Biol 2001:11:1079-1088.

104. Claus P, Doring F, Gringel S, et al. Differential intranuclear localization of fibroblast growth factor-2 isoforms and specific interaction with the survival of motoneuron protein. J Biol Chem 2003;278(1):479-485.

105. Lorson CL, Hahnen E, Androphy EJ, et al. A single nucleotide in the SMN gene regulates splicing and is responsible for spinal muscular atrophy. Genetics 1999;96:6307-6311.

106. Lorson CL, Androphy EJ. An exonic enhancer is required for inclusion of an essential exon in the SMA-determining gene SMN. Hum Mol Genet 2000;9(2):22-24.

107. Cartegni L, Krainer AR. Disruption of an SF2/ASF-dependent exonic splicing enhancer in SMN2 causes spinal muscular atrophy in the absence of SMN1. Nat Genet 2002;30(4):377-384.

108. Cartegni L, Hastings ML, Calarco JA, et al. Determinants of exon 7 splicing in the spinal muscular atrophy genes, SMN1 and SMN2. Am J Hum Genet 2006;78(1):63-77.

109. Hofmann Y, Lorson CL, Stamm S, et al. Htra2-b1 stimulates an exonic splicing enhancer and can restore full-length SMN expression to survival motor neuron 2 (SMN2). Proc Natl Acad Sci USA 2000;97(2):9618-9623.

110. Hofmann Y, Wirth B. hnRNP-G promotes exon 7 inclusion of survival motor neuron (SMN) via direct interaction with Htra2-b1. Hum Mol Genet 2002;11(17):2037-2049.

111. Vitte J, Fassier C, Tiziano FD, et al. Refined characterization of the expression and stability of the SMN gene products. Am J Path 2007;171(4):1269-80.

112. Burnett BG, Muñoz E, Tandon A, et al. Regulation of SMN protein stability. Mol Cell Biol 2009;29(5):1107-1115.

113. Zhang H, Xing L, Singer RH, et al. QNQKE targeting motif for the SMN-Gemin multiprotein complex in neurons. J Neurosci Res 2007;85:2657-2667.

114. Lefebvre S, Burlet P, Liu Q, et al. Correlation between severity and SMN protein level in spinal muscular atrophy. Nat Genet 1997;16(3):265-269.

115. Taylor JE, Thomas NH, Lewis CM, et al. Correlation of SMNt and SMNc gene copy number with age of onset and survival in spinal muscular atrophy. Eur J Hum Genet 1998;6(5):467-474.

116. Miller C, Degenhardt K, Sassoon DA, et al. Differential SMN2 expression associated with SMA severity. Nat Genet 1998;20:230-231.

117. Wirth B, Brichta L, Hahnen E. Spinal muscular Atrophy: from gene to therapy. Semin Pediatr Neurol 2006;1:121-131.

118. Ogino S, Gao S, Leonard DGB, et al. Inverse correlation between SMN1 and SMN2 copy numbers: evidence for gene conversion from SMN2 to SMN1. Eur J Hum Genet 2003;11(3):275-7.

119. van der Steege G, Grootscholten PM, Cobben JM, et al. Apparent gene conversions involving the SMN gene in the region of the spinal muscular atrophy locus on chromosome 5. Am J Hum Genet 1996;59(4):834-838.

120. Wirth B, Brichta L, Schrank B, et al. Mildly affected patients with spinal muscular atrophy are partially protected by an increased SMN2 copy number. Hum Genet 2006;119(4):422-8.

121. Vezain M, Saugier-Veber P, Goina E, et al. A rare SMN2 variant in a previously unrecognized composite splicing regulatory element induces exon 7 inclusion and reduces the clinical severity of spinal muscular atrophy. Hum Mutat 2010;31(1):E1110-1125.

122. Grohmann K, Varon R, Stolz P, et al. Infantile spinal muscular atrophy with respiratory distress type 1 (SMARD1). Ann Neurol 2003;1:719-724.

123. Grohmann K, Schuelke M, Diers A, et al. Mutations in the gene encoding immunoglobulin μ- binding protein 2 cause spinal muscular atrophy with respiratory distress type 1. Nat Genet 2001;29:75-77.

124. Finsterer J. Bulbar and spinal muscular atrophy (Kennedy's disease): a review. Eur J Neurol 2009;16(5):556-561.

125. Greenland KJ, Beilin J, Castro J, et al. Polymorphic CAG repeat length in the androgen receptor gene and association with neurodegeneration in a heterozygous female carrier of Kennedy's disease. J Neurol 2004;251(1):35-41.

126. La Spada AR, Wilson EM, Lubahn DB, et al. Androgen receptor gene mutations in X-linked spinal and bulbar muscular atrophy. Nature 1991;352:77-79.

127. LaSpada AR, Roling DB, Harding AE, et al. Meoitoc stability and genotype-phenotype correlation of the trinucleotide repeat in X-linked spinal and bulbar muscular atrophy. Nat Genet 1992;2:301-304.

128. Igarashi S, Tanno Y, Onodera O, et al. Strong correlation between the number of CAG repeats in androgen receptor genes and the clinical onset of features of spinal and bulbar muscular atrophy. Neurology 1992;42(12):2300-2302.

129. Schrank B, Götz R, Gunnersen JM, et al. Inactivation of the survival motor neuron gene, a candidate gene for human spinal muscular atrophy, leads to massive cell death in early mouse embryos. Proc Natl Acad Sci USA 1997;94(18):9920-9925.

130. Jablonka S, Schrank B, Kralewski M, et al. Reduced survival motor neuron (Smn) gene dose in mice leads to motor neuron degeneration: an animal model for spinal muscular atrophy type III. Hum Mol Genet 2000;9(3):341-346.

131. Monani UR, Sendtner M, Coovert DD, et al. The human centromeric survival motor neuron gene (SMN2) rescues embryonic lethality in Smn –/– mice and results in a mouse with spinal muscular atrophy. Hum Mol Genet 2000;9(3):333-340.

132. Hsieh-Li HM, Chang JG, Jong YJ, et al. A mouse model for spinal muscular atrophy. Nat Genet 2000;24(1):66-70.

133. McGovern VL, Gavrilina TO, Beattie CE, et al. Embryonic motor axon development in the severe SMA mouse. Hum Mol Genet 2008;17(18):2900-2909.

134. Avila AM, Burnett BG, Taye AA, et al. Trichostatin A increases SMN expression and survival in a mouse model of spinal muscular atrophy. J Clin Invest 2007;117(3):659-671.

135. Rudnik-Schöneborn S, Vogelgesang S, Armbrust S, et al. Digital necroses and vascular thrombosis in severe spinal muscular atrophy. Muscle Nerve 2010;42(1):144-1447.

136. Shababi M, Habibi J, Yang HT, et al. Cardiac defects contribute to the pathology of spinal muscular atrophy models. Hum Mol Genet 2010;19(2):4059-4071.

137. Menke LA, Poll-The BT, Clur S, et al. Congenital heart defects in spinal muscular atrophy type I: A clinical report of two siblings and a review of the literature. Am J Med Genet 2008;146A:740-744.

138. Rudnik-Schöneborn S, Heller R, Berg C, et al. Congenital heart disease is a feature of severe infantile spinal muscular atrophy. J Med Genet 2008;45:63-638.

139. Le TT, Pham LT, Butchbach MER, et al. SMNDelta7, the major product of the centromeric survival motor neuron (SMN2) gene, extends survival in mice with spinal muscular atrophy and associates with full-length SMN. Hum Mol Genet 2005;14(6):845-857.

140. Butchbach MER, Edwards JD, Burghes AHM. Abnormal motor phenotype in the SMNDelta7 mouse model of spinal muscular atrophy. Neurobiol Dis 2007;27(2):207-219.

141. Murray LM, Comley LH, Thomson D, et al. Selective vulnerability of motor neurons and dissociation of pre- and post-synaptic pathology at the neuromuscular junction in mouse models of spinal muscular atrophy. Hum Mol Genet 2008;17(7):949-962.

142. Monani UR, Pastore MT, Gavrilina TO, et al. A transgene carrying an A2G missense mutation in the SMN gene modulates phenotypic severity in mice with severe (type I) spinal muscular atrophy. Cell 2003;160(1):41-52.

143. Gavrilina TO, McGovern VL, Workman E, et al. Neuronal SMN expression corrects spinal muscular atrophy in severe SMA mice while muscle-specific SMN expression has no phenotypic effect. Hum Mol Genet 2008;17(8):1063-1075.

144. Frugier T, Tiziano FD, Cifuentes-diaz C, et al. Nuclear targeting defect of SMN lacking the C-terminus in a mouse model of spinal muscular atrophy. Hum Mol Genet 2000;9(5):849-858.

145. Cifuentes-Diaz C, Nicole S, Velasco ME, et al. Neurofilament accumulation at the motor endplate and lack of axonal sprouting in a spinal muscular atrophy mouse model. Hum Mol Genet 2002;11(12):1439-1447.

146. Ferri A, Melki J KA. Progressive and selective degeneration of motoneurons in a mouse model of SMA. Neuroreport 2004;15(2):275-280.

147. Cifuentes-Diaz C, Frugier T, Tiziano FD, et al. Deletion of murine SMN exon 7 directed to skeletal muscle leads to severe muscular dystrophy. J Cell Biol 2001;152(5):1107-1114.

148. Gladman JT, Bebee TW, Edwards C, et al. A humanized Smn gene containing the SMN2 nucleotide alteration in exon 7 mimics SMN2 splicing and the SMA disease phenotype. Hum Mol Genet 2010;19(21):4239-4252.

149. Duchen LW, Strich SJ. An hereditary motor neurone disease with progressive degeneration of muscle in the mouse: the mutant 'wobbler'. J Neurol Neurosurg Psych 1968:31:535-542.

150. Schmitt-John T, Drepper C, Mu A, et al. Mutation of Vps54 causes motor neuron disease and defective spermiogenesis in the wobbler mouse. Nat Genet 2005;37(11):1213-1215.

151. Schmalbruch H, Jensen HJ, Bjaerg M, et al. A new mouse mutant with progressive motor neuronopathy. J Neuropathol Exp Neurol 1991;50(3):192-204.

152. Bömmel H, Xie G, Rossoll W, et al. (Tbce) gene in the mouse mutant progressive motor neuronopathy, a model of human motoneuron disease. J Cell Biol 2002;159(4):563-570.

153. Grohmann K, Rossoll W, Kobsar I, et al. Characterization of Ighmbp2 in motor neurons and implications for the pathomechanism in a mouse model of human spinal muscular atrophy with respiratory distress type 1 (SMARD1). Hum Mol Genet 2004;13(18):2031-2042.

154. Troyer D, Cash WC, Vestweber J, et al. Review of spinal muscular atrophy (SMA) in Brown Swiss cattle. J Vet Diagn Invest 1993;5:303-306.

155. Troyer D. Upper motor neurone and descending tract pathology in bovine spinal muscular atrophy. J Comp Pathol 1992;107(3):305-317.

156. Krebs S, Medugorac I, Röther S, et al. A missense mutation in the 3-ketodihydrosphingosine reductase FVT1 as candidate causal mutation for bovine spinal muscular atrophy. Proc Natl Acad Sci USA 2007;104(16):6746-6751.

157. Cork LC, Price DL, Griffin JW, et al. Hereditary canine spinal muscular atrophy: canine motor neuron disease. Can J Vet Res 1990;54(1):77-82.

158. Green SL, Tolwani RJ, Varnma S, et al. Analysis of the canine Cu/Zn superoxide dismutase (SOD1) gene. J Hered 2002 93(2):119-124.

159. Blazej RG, Mellersh CS, Cork LC, et al. Hereditary canine spinal muscular atrophy is phenotypically similar but molecularly distinct from human spinal muscular atrophy. J Hered 1998;89:531-537.

160. Wirth B, Schmidt T, Hahnen E, et al. De novo rearrangements found in 2% of index patients with spinal muscular atrophy: mutational mechanisms, parental origin, mutation rate, and implications for genetic counseling. Am J Hum Genet 1997;61(5):1102-1111.

161. Prior TW, Swoboda KJ, Scott HD, et al. Homozygous SMN1 deletions in unaffected family members and modification of the phenotype by SMN2. Am J Med Genet 2004;130A(3):307-310.

162. Cusin V, Clermont O, Gerard B, et al. Prevalence of SMN1 deletion and duplication in carrier and normal populations: implication for genetic counseling. J Med Genet 2003;40(4):e39.

163. Wang CH, Lunn MR. Spinal muscular atrophy: advances in research and consensus on care of patients. Curr Treat Options Neurol 2008;10(6):420-428.

164. Oskoui M, Levy G, Garland CJ, et al. The changing natural history of spinal muscular atrophy type 1. Neurology 2007;69(20):1931-1936.

165. Brichta L, Hofmann Y, Hahnen E, et al. Valproic acid increases the SMN2 protein level: a well-known drug as a potential therapy for spinal muscular atrophy. Hum Mol Genet 2003;12(19):2481-2489.

166. Sumner CJ, Huynh TN, Markowitz JA, et al. Valproic acid increases SMN levels in spinal muscular atrophy patient cells. Ann Neurol 2003;54(5):647-654.

167. Brichta L, Holker I, Haug K, et al. In vivo activation of SMN in spinal muscular atrophy carriers and patients treated with valproate. Ann Neurol 2006;59(6):970-975.

168. Swoboda KJ, Scott CB, Reyna SP, et al. Phase II open label study of valproic acid in spinal muscular atrophy. PloS ONE 2009;4(5):e5268.

169. Swoboda KJ, Scott CB, Crawford TO, et al. SMA CARNI-VAL trial part I: double-blind, randomized, placebo-controlled trial of L-carnitine and valproic acid in spinal muscular atrophy. PLoS ONE 2010;5(8):e12140.

170. Chang JG, Hsieh-Li HM, Jong YJ, et al. Treatment of spinal muscular atrophy by sodium butyrate. Proc Natl Acad Sci USA 2001;98(17):9808-9813.

171. Brahe C, Vitali T, Tiziano FD, et al. Phenylbutyrate increases SMN gene expression in spinal muscular atrophy patients. Eur J Hum Genet 2005;13(2):256-259.

172. Jakubik M, Riessland M, Ackermann B, et al. SAHA ameliorates the SMA phenotype in two mouse models for spinal muscular atrophy. Hum Mol Genet 2010;19(8):1492-1506.

173. Hua Y, Vickers TA, Baker BF, et al. Enhancement of SMN2 exon 7 inclusion by antisense oligonucleotides targeting the exon. PLoS Biol 2007;5(4):e73.

174. Hua Y, Vickers TA, Okunola HL, et al. Antisense masking of an hnRNP A1/A2 intronic splicing silencer corrects SMN2 splicing in transgenic mice. J Hum Genet 2008;82:834-848.

175. Geib T, Hertel KJ. Restoration of full-length SMN promoted by adenoviral vectors expressing RNA antisense oligonucleotides embedded in U7 snRNAs. PLoS ONE 2009;4(12):e8204.

176. Williams JH, Schray RC, Patterson CA, et al. Oligonucleotide-mediated survival of motor neuron protein expression in CNS improves phenotype in a mouse model of spinal muscular atrophy. J Neurosci 2009;29(24):7633-7638.

177. Skordis LA, Dunckley MG, Yue B, et al. Bifunctional antisense oligonucleotides provide a trans-acting splicing enhancer that stimulates SMN2 gene expression in patient fibroblasts. Proc Natl Acad Sci USA 2003;100(7):4114-4119.

178. Dickson A, Osman E, Lorson CL. A negatively acting bifunctional RNA increases survival of motor neuron both in vitro and in vivo. Hum Gene Ther 2008;19:1307-1315.

179. Baughan TD, Dickson A, Osman EY, et al. Delivery of bifunctional RNAs that target an intronic repressor and increase SMN levels in an animal model of spinal muscular atrophy. Hum Mol Genet 2009;18(9):1600-1611.

180. Grzeschik SM, Ganta M, Prior TW, Heavlin WD, Wang CH. Hydroxyurea enhances SMN2 gene expression in spinal muscular atrophy cells. Ann Neurol 2005;58(2):194-202.

181. Liang WC, Yuo CY, Chang JG, et al. The effect of hydroxyurea in spinal muscular atrophy cells and patients. J Neurol Sci 2008;268(1-2):87-94.

182. Wolstencroft EC, Mattis V, Bajer AA, et al. A non-sequence-specific requirement for SMN protein activity: the role of aminoglycosides in inducing elevated SMN protein levels. Hum Mol Genet 2005;14(9):1199-1210.

183. Mattis VB, Bowerman M, Kothary R, et al. A SMNDelta7 read-through product confers functionality to the SMNDelta7 protein. Neurosci Lett 2008;442(1):54-58.

184. Heier CR, DiDonato CJ. Translational readthrough by the aminoglycoside geneticin (G418) modulates SMN stability in vitro and improves motor function in SMA mice in vivo. Hum Mol Genet 2009;18(7):1310-1322.

185. Mattis VB, Fosso MY, Chang CW, et al. Subcutaneous administration of TC007 reduces disease severity in an animal model of SMA. BMC Neurosci 2009;10:142.

186. Mattis VB, Ebert AD, Fosso MY, et al. Delivery of a read-through inducing compound, TC007, lessens the severity of a spinal muscular atrophy animal model. Hum Mol Genet 2009;18(20):3906-3913.

187. Azzouz M, Le T, Ralph GS, et al. Lentivector-mediated SMN replacement in a mouse model of spinal muscular atrophy. J Clin Invest 2004;114(12):1726-1731.

188. Hacein-Bey-Abina S, Von Kalle C, Schmidt M, et al. LMO2-associated clonal T cell proliferation in two patients after gene therapy for SCID-X1. Science 2003;302(5644):415-419.

189. Howe SJ, Mansour MR, Schwarzwaelder K, et al. Insertional mutagenesis combined with acquired somatic mutations causes leukemogenesis following gene therapy of SCID-X1 patients. J Clin Invest 2008;118(9):3143-3150.

190. Hacein-Bey-Abina S, Garrigue A, Wang GP, et al. Insertional oncogenesis in 4 patients after retrovirus-mediated gene therapy of SCID-X1. J Clin Invest 2008;118(9):3132-3142.

191. Valori CF, Ning K, Wyles M, et al. Systemic delivery of scAAV9 expressing SMN prolongs survival in a model of spinal muscular atrophy. Sci Transl Med 2010;2(35):35ra42.

192. Foust KD, Wang X, McGovern VL, et al. Rescue of the spinal muscular atrophy phenotype in a mouse model by early postnatal delivery of SMN. Nat Biotechnol 2010;28(3):271-274.

193. Simon CM, Jablonka S, Ruiz R, et al. Ciliary neurotrophic factor-induced sprouting preserves motor function in a mouse model of mild spinal muscular atrophy. Hum Mol Genet 2010;19(6):973-986.

194. Haddad H, Cifuentes-Diaz C, Miroglio A, et al. Riluzole attenuates spinal muscular atrophy disease progression in a mouse model. Muscle Nerve 2003;28(4):432-437.

CHAPTER 2: Failure of axon radial growth in feline SMA

Abstract

Feline SMA is a fully penetrant, autosomal recessive lower motor neuron disease in domestic cats that clinically resembles human SMA Type III. Affected cats demonstrate clinical signs at 12 to 13 weeks of age. A whole genome linkage scan identified a ~140 kilobase pair deletion that abrogates expression of *LIX1,* a novel SMA candidate gene of unknown function. To characterize the progression of feline SMA, we assessed pathological changes in muscle and spinal cord from 3 days of age to beyond clinical onset. Quadriceps femoris muscle fibers from affected cats appeared smaller at 10 weeks; by 12 weeks atrophic fibers were more prevalent than in age-matched controls. Significant loss of L5 ventral root axons in affected cats coincided with onset of clinical signs, and by 21 weeks of age, affected cats had 40% fewer L5 motor axons. There was no significant difference in L5 soma number, even at 21 weeks. Morphometric analysis of L5 ventral roots and horns revealed that prior to axon loss affected cats failed to develop large caliber motor neurons, suggesting a role for LIX1 in radial growth of axons.

Introduction

The human spinal muscular atrophies (SMA) are a group of lower motor neuron disorders that vary in age of onset, clinical severity and survival time. Individuals with the severest form (SMA I; Werdnig-Hoffmannn disease) never gain the ability to sit upright or walk and do not survive beyond a few years of age. Type II SMA patients develop clinical symptoms after six months of age and are unable to walk. SMA III (Kugelberg-Welander disease) is the mildest juvenile onset form of the disease; individuals are able to walk, although this ability may be lost as the disease progresses. The adult-onset form of the disease (SMA IV) has the mildest clinical severity and does not result in shortened life expectancy (1). SMA is the leading genetic cause of infant mortality, and mutations in the ubiquitously expressed *survival of motor neuron 1* (*SMN1*) account for 98% of cases (2, 3). Copy number variation in a nearly identical gene, *survival of motor neuron 2* (*SMN2*), modifies clinical severity; eight copies are sufficient to complement homozygous loss of *SMN1* (4). Only 10% of SMN2 transcripts are full-length due to a single nucleotide difference in exon 7 that disrupts an exonic splice enhancer (5-7). Currently, there is limited understanding of the mechanisms by which mutations of ubiquitously expressed genes result in SMA and other motor neuron-specific diseases, such as amyotrophic lateral sclerosis and spinal bulbar muscular atrophy. Treatment for SMA has focused on increasing levels of full length SMN produced from the SMN2 locus (8). Naturally occurring and engineered animal models offer insight into motor neuron development and maintenance that is critical for the discovery and testing of effective treatments.

Feline SMA is a fully penetrant, autosomal recessive disease resembling SMA III in severity and time of onset (9). In affected cats, lower motor neuron degeneration leads to muscle atrophy and gait abnormalities. Affected cats demonstrate clinical signs at 12 to 13 weeks of age with disease progression reaching a plateau around 8 months. Life expectancy is ~8 years. A whole genome linkage scan and fine mapping identified a 140 kilobase pair deletion that disrupts expression of *limb expression 1* (*LIX1*) and *leucyl/cystinyl aminopeptidase (LNPEP*) (10). We hypothesize that *LIX1* is the feline SMA disease gene because it is highly expressed in the spinal cord and a *LNPEP* knockout did not produce an overt neuromuscular phenotype (11, 12). LIX1 is poorly annotated but is predicted to possess a double-stranded RNA binding domain at its amino terminus. This is particularly intriguing because SMN1 is critical for small nuclear ribonucleoprotein (snRNP) biogenesis (13-15) and co-localizes with mRNA granules in motor neurons (16). Thus far only the end-stage of feline SMA pathology has been reported. In this study we sought to characterize the onset and progression of disease through histological and morphometric techniques.

Materials and Methods

Animals

All cats were produced and housed in breeding colonies at Michigan State University. Animals at MSU were raised and euthanized according to IUCAC approved protocols and adhered to National Institutes of Health guidelines. Cats were genotyped by multiplex PCR as previously described (10).

Histology

Quadriceps femoris muscles from two affected cats and two age-matched controls (homozygous normal and heterozygous) at 6, 8, 10, 12 and 21 weeks were fixed by immersion in 10% (w/v) neutral buffered formalin, paraffin embedded, sectioned and stained with hematoxylin-eosin (H&E). Unfixed tibialis anterior (TA), extensor digitorum longus (EDL) and

soleus muscles from 10 and 12 week old cats were embedded in Tissue-Tek® OCT medium (Sakura Finetek, Torrance, CA) and frozen in liquid nitrogen cooled 95% ethanol. Muscles were stored at -80^{o}C until transversely sectioned at 12 μm with a cryostat and thaw mounted on gelatin-coated glass slides. Muscle sections were fiber-typed by ATPase enzymatic reactions at pH 4.6 and 9.4. Five random, non-overlapping images with a 40x objective of a single H&E section and 2 images at 10x magnification of a fiber-typed section per cat were captured on an Eclipse 90i microscope with a DS-Fi1 digital camera (Nikon, Tokyo, Japan) for fiber shape examination. The diameters of 50 fibers in H&E stained quadriceps femoris muscle sections from 10 week old cats were measured at 40x magnification with NIS Elements software (Nikon, Tokyo, Japan).

One fifth of the frozen sections were screened for neuromuscular junctions (NMJs) with a modified cholinesterase stain (17). Prior to staining, sections were warmed to room temperature and fixed in 4% (w/v) paraformaldehyde in 0.1 M sodium phosphate buffer pH 7.4. Staining was terminated after 15 minutes with distilled water; sections were dehydrated with graded ethanol washes, cleared with xylene and cover-slipped with Permount (Thermo Fisher Scientific, Waltham, MA). Sections were examined for the presence of motor endplates. Sections adjacent to those exhibiting cholinesterase staining were labeled for acetylcholine receptors by sequential incubation in 1:500 dilution of biotin conjugated anti-bungarotoxin (Invitrogen, Carlsbad, CA), avidin horseradish peroxidase conjugate (Kirkegaard and Perry Laboratories, Gaithersburg, MD) and Nova Red peroxidase substrate (Vector Laboratories, Burlingame, CA).

Tissue-Tek® OCT embedded TA and EDL muscles were also longitudinally sectioned at 20 μm with a cryostat and thaw mounted on gelatin-coated glass slides. To label the pre and post-synaptic regions of the NMJs, sections were first stained for acetylcholine receptors as above, except that the peroxidase substrate was Vector® Red (Vector Laboratories,

Burlingame, CA). Sections were then labeled with a 1:1000 dilution of mouse anti-phosphorylated neurofilaments antibody cocktail (α-SMI312; Abcam, Cambridge, MA) and a 1:500 dilution of Alexa Fluor® 488 labeled goat anti-mouse IgG (Invitrogen, Carlsbad, CA). Sections were cover-slipped in ProLong Gold antifade reagent (Invitrogen, Carlsbad, CA) and stored at 4°C in the dark for laser scanning confocal microscopy.

Spinal cords were fixed by immersion in 10% neutral buffered formalin and the L5 ventral roots and L5 segment were dissected. L5 spinal cord segments were paraffin embedded and thirty-two 10 μm thick serial sections were stained with cresyl violet for cell body counts and morphometric analysis. L5 ventral roots were embedded in Poly/Bed 812- Araldite, thick sectioned and stained with toluidine blue for axon counts and morphometry.

Motor neuron and myelin sheath morphometry

All axons within a single, toluidine blue stained cross-section of L5 ventral roots were counted with Neurolucida (MBF Bioscience, Williston, VT) and a Nikon FX-A microscope (Tokyo, Japan) at 20x magnification. Non-overlapping images of ventral root cross sections were captured at 40x. Diameters of two hundred and fifty axons, excluding the myelin sheath, were measured from these images with Image-Pro Plus 5.1 (Media Cybernetics, Bethesda, MD). Axon diameters were grouped in 2 μm increments, and the number of axons within each bin was determined. For the 12 and 21 week time-points, the axon morphometrics were normalized to correct for over-sampling due to axon loss in affected cats. The number of axons within a size bin was multiplied by the average number of L5 axons in affected cats and then divided by the average number of L5 axons in control cats.

Average myelin sheath thicknesses were also determined from the toulidine blue stained ventral root images. Using Image-Pro Plus 5.1, two concentric circles were fitted to one hundred axons. The larger circle contained the axon and myelin sheath; and the smaller circle

contained only the axon. Subtraction of the smaller radius from the larger radius was taken as the myelin sheath thickness.

Cresyl violet positive cell bodies with a distinct nucleus and nucleolus at 10x magnification were counted with Neurolucida in alternate, 10 μm thick cross-sections of L5 spinal cord to prevent double counting of cells. Only a single ventral horn was counted in each section. Overlapping images of a single cross section at 10x were collected for cell body morphometrics. Major and minor diameters from 50 cells with distinct nucleoli were measured by fitting two circles to the soma, one that was contained within the soma and one that surrounded the soma (18), with Image Pro 5.1. Major and minor diameters were averaged to obtain the average soma diameter. The average diameters were grouped in 10 μm increments and the number of cell bodies within each bin was determined.

Confocal laser scanning microscopy

Stained longitudinal muscle sections were examined for fluorescence on an Olympus Fluoview 1000 laser-scanning microscope (Center Valley, PA) equipped with a 40x oil immersion objective NA=1.30. Autofluorescence of Vector® Red labeled acetylcholine receptors (red) was excited at 542 nm and emission was detected through a LP 560 nm filter. Fluorescence of Alexa Fluor 488 labeled neurofilaments (green) was excited at 488 nm and emission detected through a BP 505-525 nm filter. Structural integrity of NMJs was determined in red-green merged extended focus images that were optimized for brightness and contrast with Fluoview v5 software. Junctions in which red and green signals failed to overlay were scored as denervated.

Data analysis and figure generation

Averages, standard deviations (S.D.), two-tailed Student's t-test (α=0.05) and all graphs were generated with Microsoft Excel (Microsoft Corporation Redmond, WA). Figures were

created in Microsoft PowerPoint and then converted to .tif files in Adobe Photoshop CS4 (San Jose, CA).

Results

We examined muscle fiber morphology in quadriceps femoris muscle of two normal (N) and two affected (A) cats aged 6, 8, 10, 12 and 21 weeks (Figure 2.1). We observed no noticeable difference in fiber shape at 6 and 8 weeks of age (Figure 2.1A-D). At 10 weeks (Figure 2.1E and F), affected cats had smaller muscle fiber diameters than age-matched controls (N=17.2 ± 3.8 μm and 22.9 ± 4.3 μm; A=11.6 ± 1.9 μm and 14.5 ± 2.6 μm). Small, angular fibers were more prevalent in affected cats at 12 weeks of age and occasional centralized nuclei were observed. Groups of atrophic fibers and hypertrophied muscle fibers were observed in affected cats at 21 weeks (Figure 2.1J). Fiber typing of TA and EDL muscles (Figure 2.2A, B, D, E) at 12 weeks old (N=2) revealed both slow twitch (Type 1) and fast twitch (Type 2) atrophic fibers. However, the majority of atrophic fibers in the TA and EDL were fast twitch (affected TA = 79%, 78%; affected EDL = 83%, 81%). In contrast, we observed few atrophic fibers in the soleus (Figure 2.2C and F), a slow twitch muscle, in affected cats. These observations indicated that neurons innervating fast twitch muscle fibers are primarily affected in feline SMA.

Neuromuscular junctions (NMJs) in the TA and EDL muscles of affected cats were structurally intact at 10 weeks of age (Figure 2.3A, B, E, and F), and there was no apparent difference in end-plate size at 12 weeks (data not shown). However, we observed end-plate denervation at 12 weeks (Figure 2.3G and H). In the TA muscle, 6 of 21 and 9 of 33 NMJs were denervated in two affected cats. Six of 18 and 9 of 36 NMJs were denervated in EDL muscles. In the 12 week control animal, only 1 of 15 and none of 18 NMJs were denervated in TA and EDL muscle sections, respectively (Figure 2.3C and D). No abnormal accumulations of

neurofilament were identified in affected cats at either time-point. Therefore, structural disruption of neuromuscular junctions coincided with the presence of atrophic fibers.

To understand the progression of neurodegeneration in feline SMA, we assessed the total number of L5 ventral root axons in affected cats and age-matched controls (Figure 2.4A). At 10 weeks of age, there was no significant difference between the two groups (N=4312 ± 747, A=4481 ± 194; n=3, p=0.6). Loss of L5 motor axons coincided with the onset of clinical signs 2 weeks later (N=4544 ± 396, A=3647 ± 369; n=3, p=0.03), and by 21 weeks of age, affected cats had 40% fewer L5 motor axons than controls (N=4575 ± 648, A=2734 ± 472; n=5, $p=9x10^{-4}$).

Figure 2.1. Photomicrographs of H&E stained cross sections of quadriceps muscle. B, D, F, H and J are representative images from affected cats. A, C, E, G and I are from age-matched controls. Cats were aged 6 wks (A, B), 8 wks (C, D), 10 wks (E, F), 12 wks (G, H) or 21 wks (I, J) when euthanized. Bars = 20 μm.

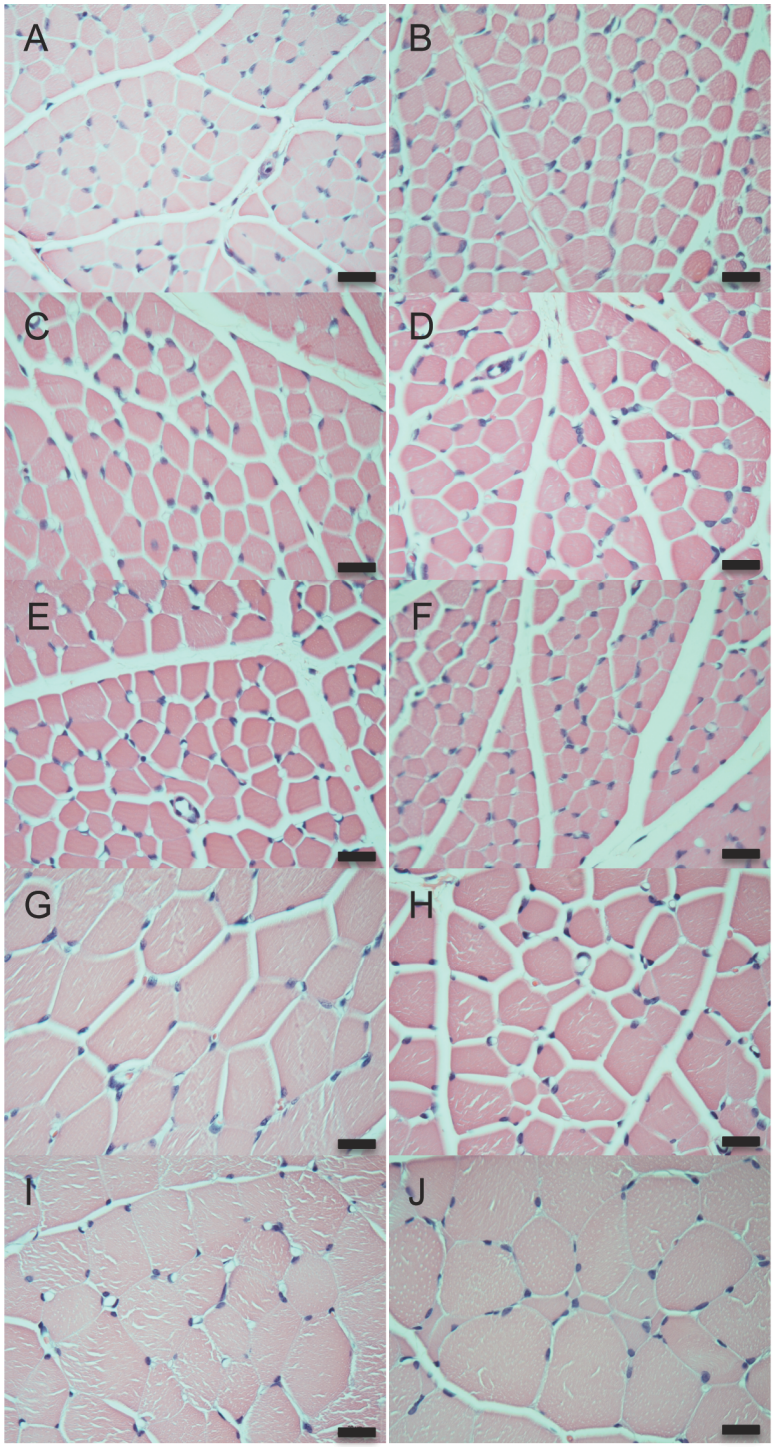

Figure 2.2. Photomicrographs of fiber-typed hindlimb muscles. TA (A, D), EDL (B, E) and soleus (C, F) from 12 week old SMA affected (D-F) and control (A-C) cats were fiber typed by myofibrillar ATPase reaction at pH 4.6. Both slow and fast twitch atrophic fibers were observed in affected cats, although the majority of atrophic fibers were fast twitch. Bars = 20 μm.

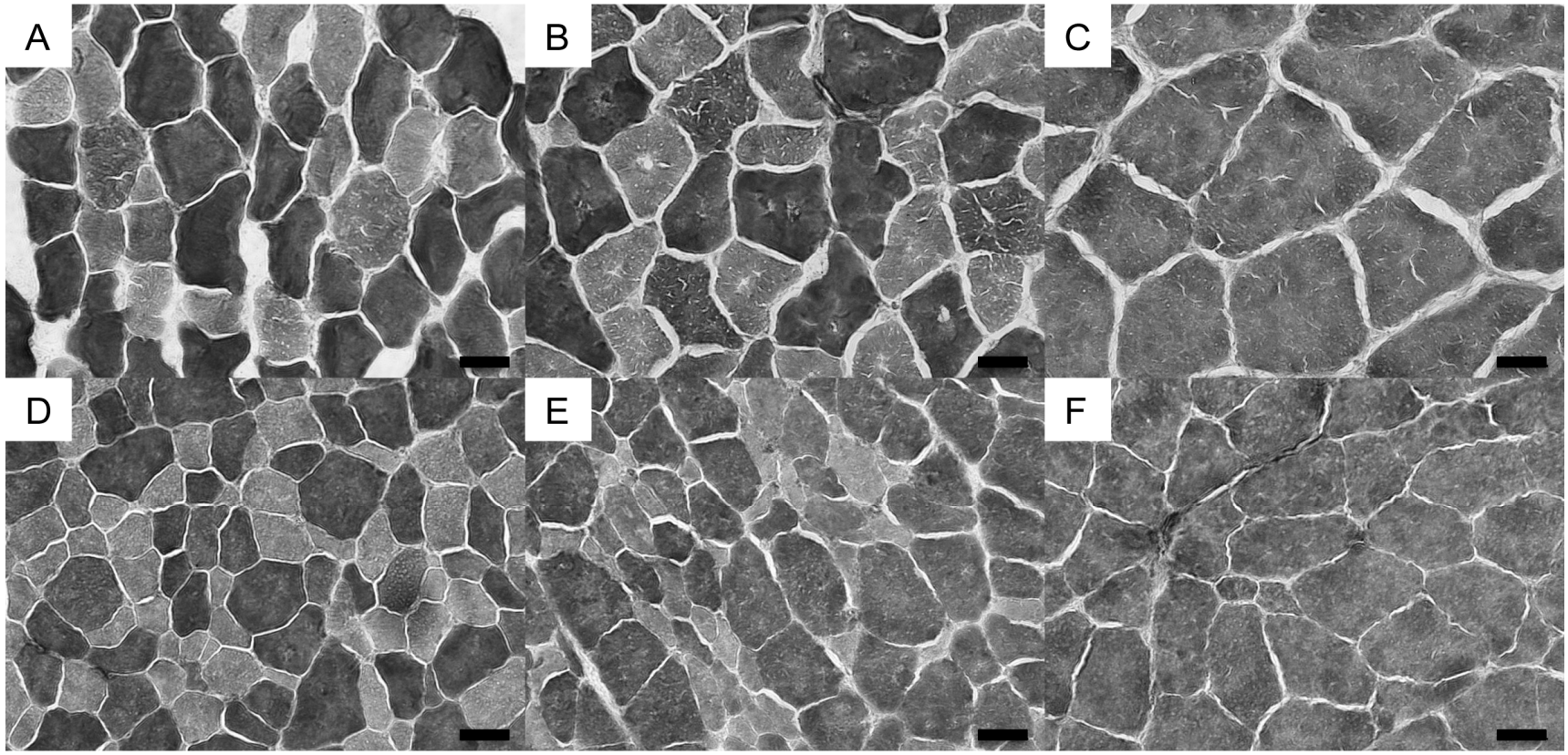

Figure 2.3. Confocal laser scanning microscopy extended focus images of TA and EDL neuromuscular junctions. Acetylcholine receptors are labeled in red and neurofilaments are labeled in green. E-H are representative images from SMA affected TA (E and G) and EDL (F and H) sections at 10 (E and F) and 12 weeks (G and H). A-D are representative images from age and tissue matched controls. A) 35 optical sections representing a thickness of 10.5 μm. B) 71 optical sections representing a thickness of 14.2 μm. C) 68 optical sections representing a thickness of 20 μm. D) 76 optical sections representing a thickness of 15.2 μm. E) 60 optical sections representing a thickness of 18 μm. F) 61 optical sections representing a thickness of 18.3 μm. G) 65 optical sections representing a thickness of 19.5 μm. H) 91 optical sections representing a thickness of 18.2 μm. Bar = 50 μm.

Figure 2.3 continued.

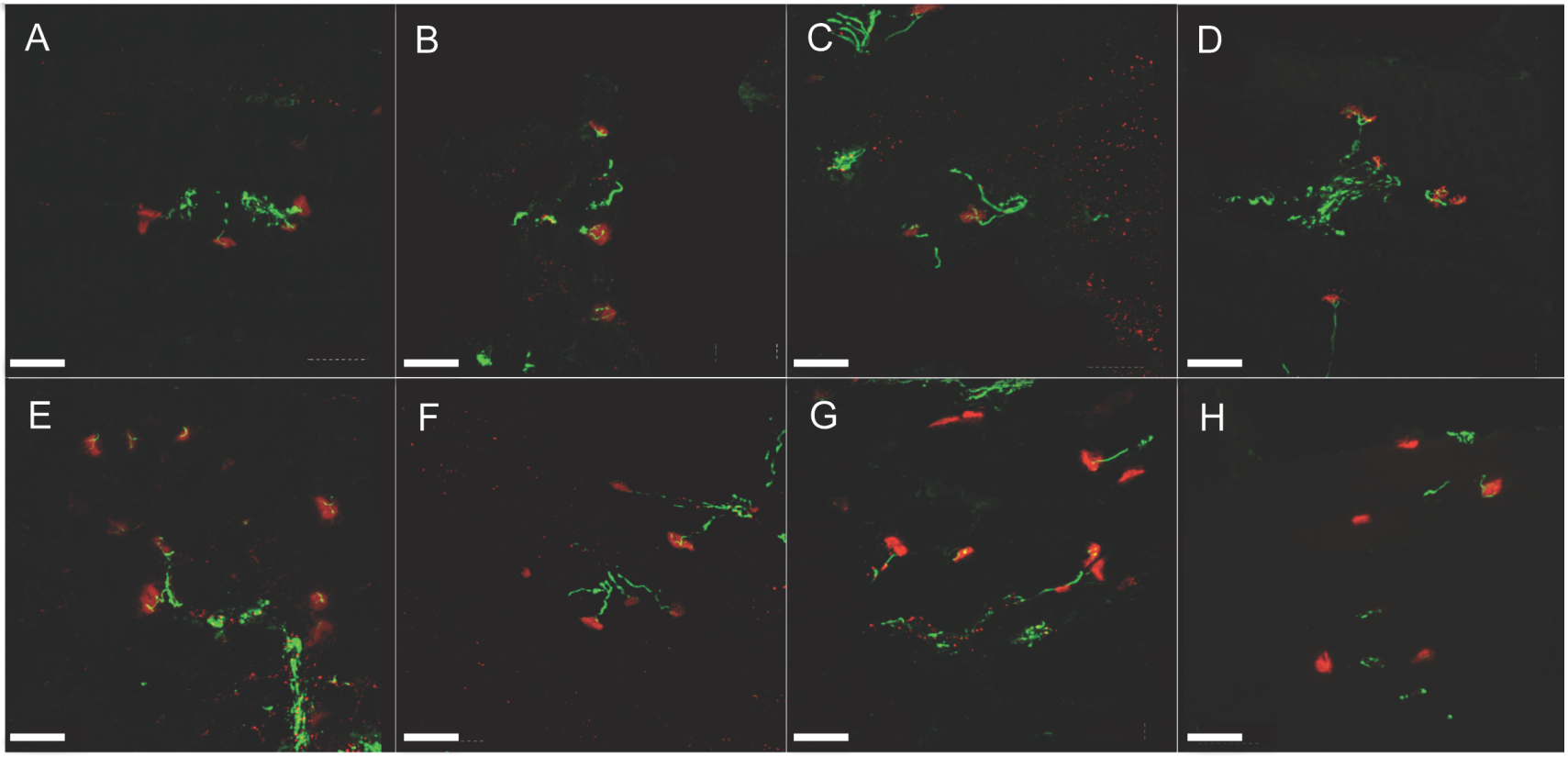

The axon deficit was not mirrored in L5 motor neuron somas even at 21 weeks (Figure 2.4B). However, the presence of chromatolysis and acentric nuclei in anterior horn cells beginning at 8-9 weeks (Figure 2.8A and B) provided evidence of somal degeneration. Thus, this observation of axonal loss prior to cell body loss indicated a mechanism of retrograde degeneration.

During axon counts we observed a lack of large caliber motor axons in affected cats beginning at 8 weeks of age (Figure 2.5A-H). This finding is consistent with previous morphometric analysis of a C5 ventral root in an affected adult cat (9). To investigate this further, we measured axon diameter in 250 L5 ventral root axons in affected and age-matched cats. At 3 days (data not shown) and 4.5 weeks (Figure 2.6A), the distribution of axon diameter in affected cats was comparable to normal controls. Distributions in normal and affected cats broadened as axon calibers increased with age. Beginning at 8 weeks of age, normal cats developed the characteristic bimodal distribution of ventral root motor axon diameters, but axons in affected cats maintained a unimodal distribution (Figure 2.6B). Eight week old affected cats had significantly fewer axons with diameters measuring 6 μm and greater. This disparity was even more pronounced at 12 and 21 weeks of age; axons with calibers equal to or greater than 8 μm are significantly reduced in affected cats (Figure 2.6C and D). Small caliber axons were present in greater numbers in affected cats at 8, 10 and 12 weeks, but this over-representation disappeared at 21 weeks of age, presumably due to progressive axon loss.

We observed no overt differences in myelin sheath thickness in affected cats at any age examined. To properly exclude myelin defects in feline SMA, we measured both myelin thickness and axon caliber in 100 axons at 8-9, 10, 12 and 21 weeks (Figure 2.7). Even though a significant decrease in average axon radius was detected at all ages, there was no difference in average myelin thickness. Thus, affected cats failed to reach normal caliber despite comparable ensheathment.

Figure 2.4. L5 motor neuron axon and soma counts. A) Total number of myelinated axons in L5 ventral root in normal (shaded) and affected (unshaded) cats. B) Number of motor neuron somas in 160 μm thickness of cresyl violet stained L5 spinal cord. Average ± S.D shown. Asterisks denote statistical significance by Student's t-test ($p<0.03$, n=3 except at 21 weeks, where n=5).

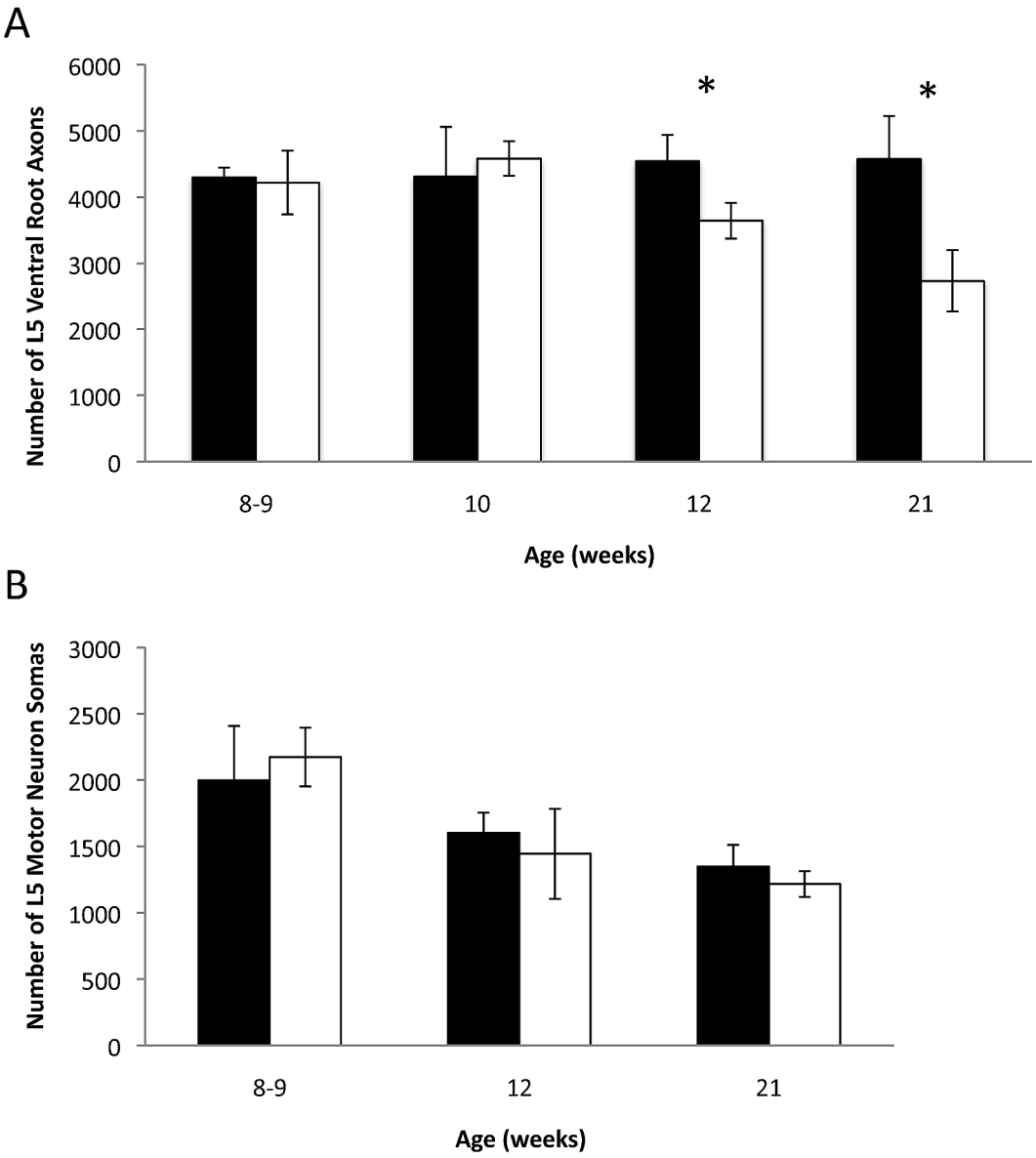

Figure 2.5. L5 toluidine blue stained ventral roots. Panels A-H are representative images of normal (A, C, E, and G) and affected cat (B, D, F, and H) ventral roots at 4.5 weeks (A and B), 8-9 weeks (C and D), 12 weeks (E and F) and 21 weeks (G and H). Bar = 20 μm.

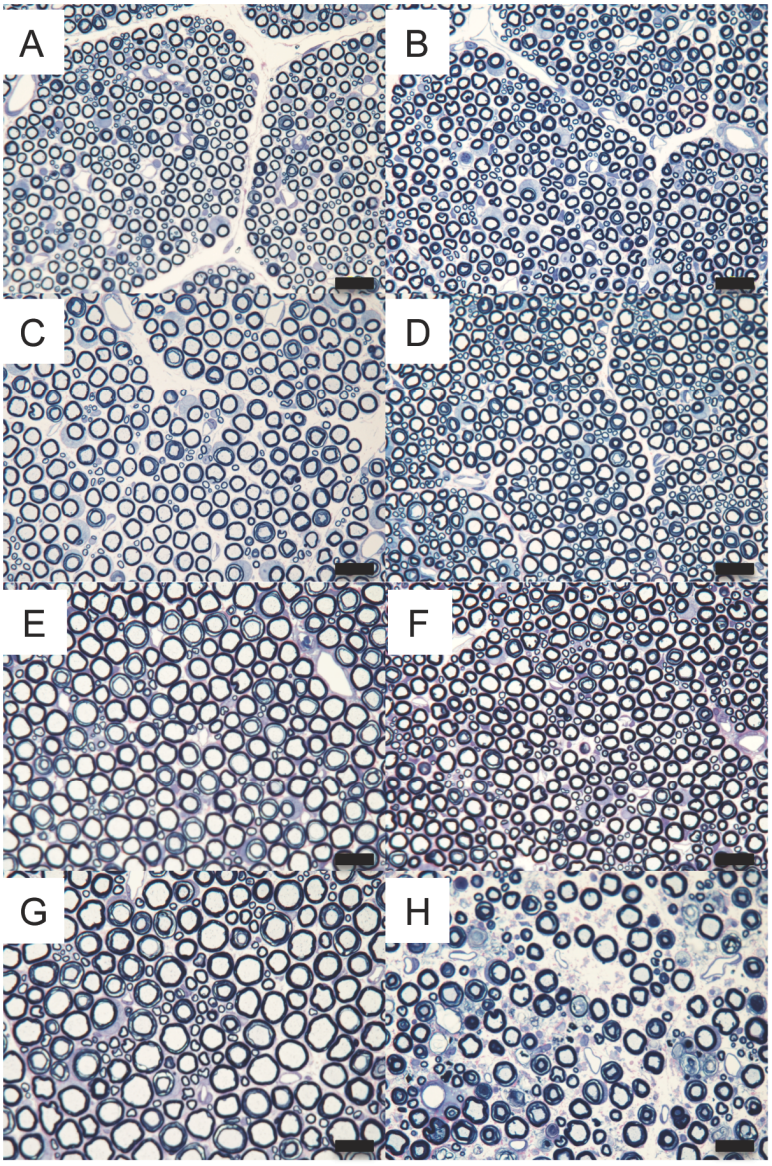

Figure 2.6. L5 ventral roots axon morphometrics at 4.5 weeks (A), 8-9 weeks (B), 12 weeks (C) and 21 wks (D) of normal (shaded) and affected cats (unshaded). In A, n=2. At all other time points, n was greater than or equal to 3, and thus averages ± S.D. were graphed. The data in C and D were adjusted to account for over-sampling in affected cats (See Material and Methods). Asterisks denote statistical significance by Student's t-test ($p \leq 0.05$).

Figure 2.6 continued.

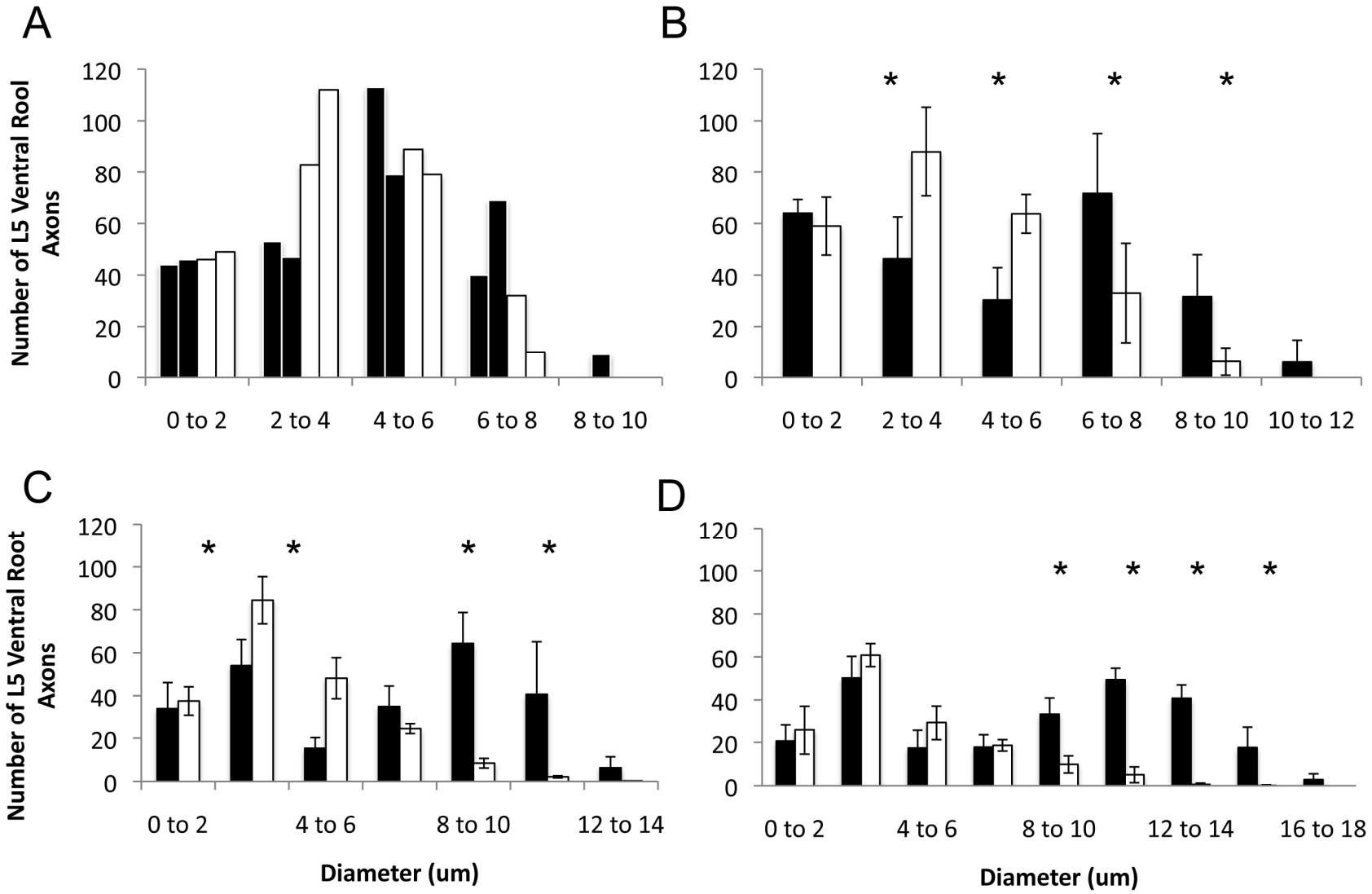

Figure 2.7. Average axon radius and myelin thickness. A) Average L5 ventral root axon radius as measured in 100 axons. B) Average myelin sheath thickness measured in the same 100 axons (n=3 except at 21 weeks where n=5). Asterisks indicate statistical significance by Student's t-test ($p \leq 0.02$).

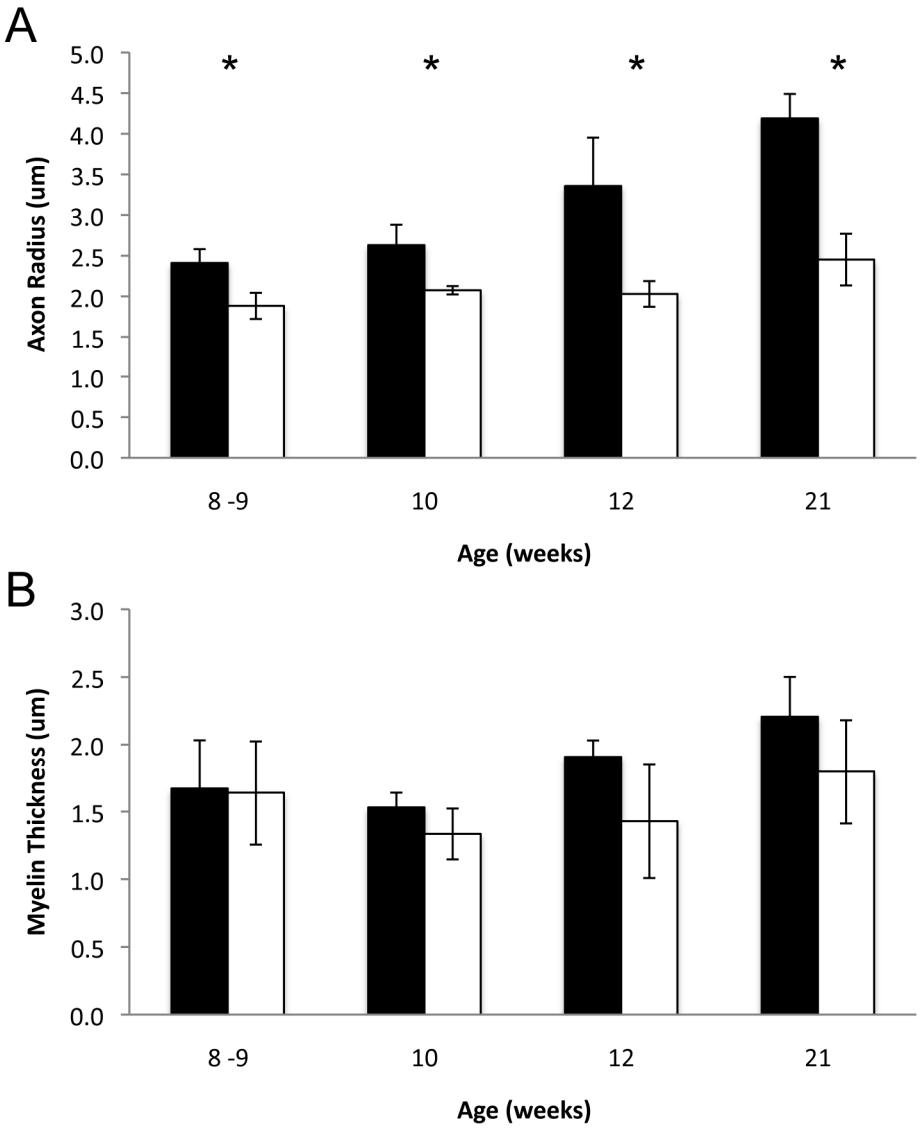

Morphometric analysis of L5 ventral horn somas also revealed a dearth of large cell bodies, although this phenomenon occurred at a later age than the deficit in large axon diameters in the ventral roots. At 8-9 weeks, affected cats had similar distributions of cell body diameters as age matched controls (Figure 2.8G). No single size increment demonstrated a significant difference at 12 weeks (Figure 2.8H), but when soma were grouped into two pools, cells with diameters from 0 to 40 μm or cells with diameters greater than 40 μm, affected cats had significantly fewer somas with an average diameter greater than 40 μm (N=8 ± 1.2, A=3 ± 1.7; n=4, p=0.002). At 21 weeks of age, affected cats still had significantly fewer cells with diameters of greater than 40 μm (Figure 2.8I). The lack of large caliber motor axons preceded any changes to the cell bodies by ~4 weeks, and was consistent with the primary site of feline SMA pathogenesis being distal to the soma.

Discussion

We undertook a systematic histological examination of muscles, motor neuron axons and cell bodies to identify the earliest pathological changes in feline SMA and to follow their progression. Small, atrophic muscle fibers became apparent at 12 weeks of age, although fibers appeared smaller at 10 weeks. The appearance of muscle atrophy coincided with structural denervation of motor end-plates and statistically significant loss of L5 ventral root axons. There was no significant loss of L5 motor neuron somas by 21 weeks, indicating retrograde neurodegeneration in feline SMA. This finding is consistent with engineered mouse models of SMA (19-21).

Myofibrillar ATPase fiber typing of TA, EDL and soleus muscles demonstrated that a majority of atrophic fibers were Type 2 (fast twitch). Fast twitch muscle fibers belong to larger motor units and are innervated by larger diameter motor neurons than slow twitch fibers (22,

Figure 2.8.Cresyl violet stained L5 spinal cord and soma morphometrics. Photomicrographs of L5 anterior horns from normal cats aged 8 wks (A) 12 wks (C) and 21 wks (E) and from age-matched affected cats B, D, and F, respectively. Bars=200 μm. Cell body morphometrics at 8-9 wks (G), 12 wks (H) and 21 wks (I). Averages ± S.D. for normal (shaded) and affected cats (unshaded) are shown. Asterisks indicate statistical significance by Student's t-test at $p \leq 0.03$.

Figure 2.8 continued

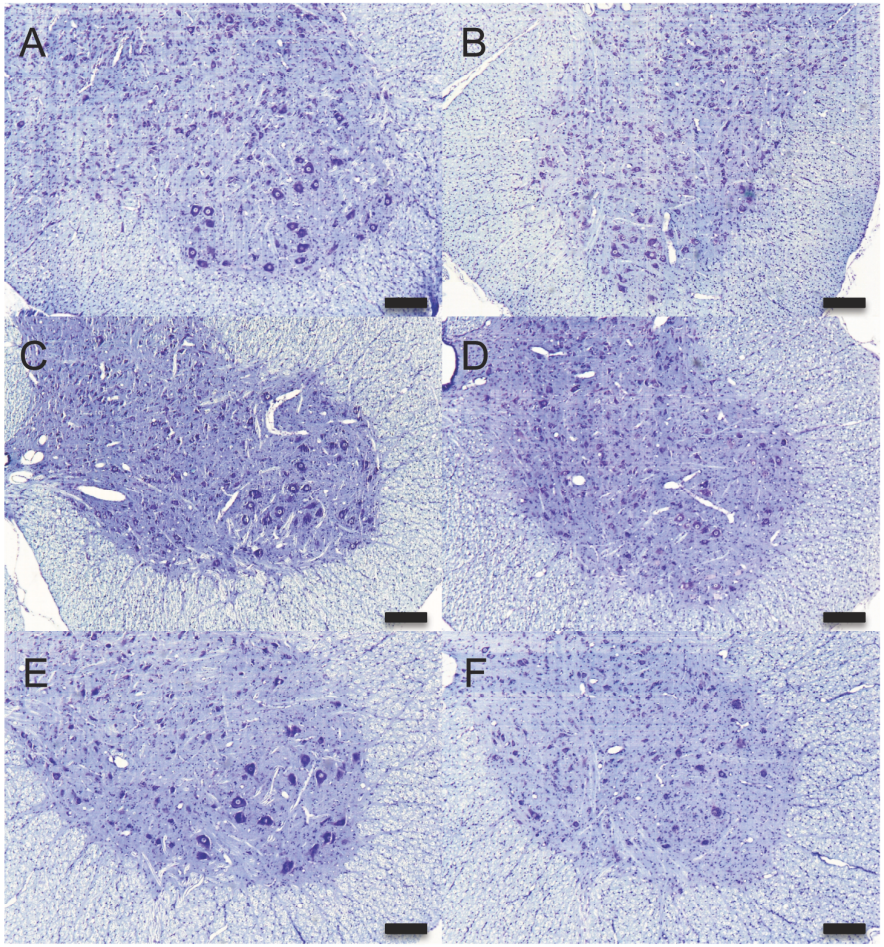

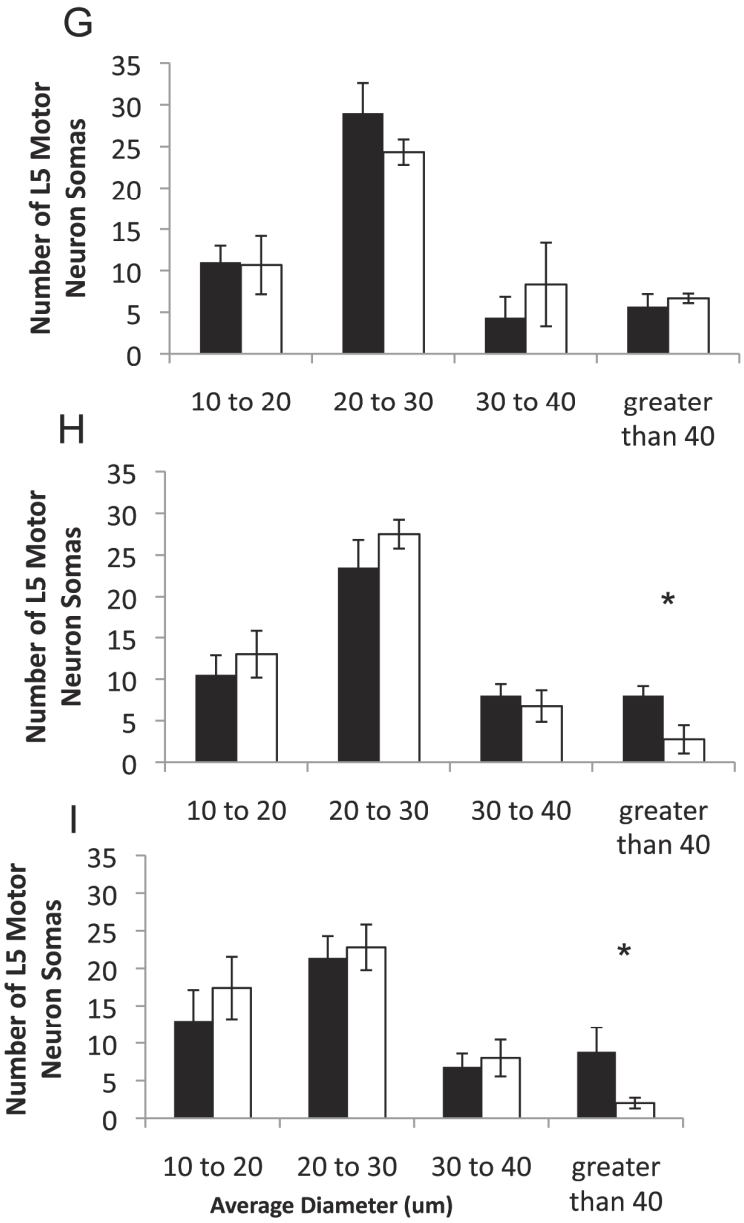

23). Concordantly, morphometric analysis of L5 ventral root axons demonstrated that motor neurons in affected cats failed to develop a normal bimodal size distribution at 8-9 weeks. The dearth of large caliber axons was echoed in L5 ventral horn somas at 12 weeks of age and thereafter is similar to what is observed in autopsy specimens from human SMA patients (24).

Our colleagues at the University of Nantes, France have conducted extensive neurological and electromyography (EMG) exams in SMA affected and normal cats aged 4 to 36 weeks. Affected cats developed EMG abnormalities in hindlimb muscles at 12 weeks. Significant decreases in compound motor action potential (CMAP) amplitudes were detected at 8-11 weeks, indicating a functional denervation of NMJs. Despite reduced axon calibers at earlier ages, changes in nerve conduction velocity (NCV) of the sciatic and radial nerves were not observed until 16 weeks of age. This is likely explained by the contribution of sensory axons, which are unaffected in feline SMA, to the overall NCV. Thus the functional changes observed by our French collaborators coincide with the pathology we identified in muscles and the loss of L5 ventral root axons.

Taken together this work describes the onset and early disease course of feline SMA. Neuromuscular development proceeds normally in affected cats until ~8 weeks of age. At this point, motor axons in affected cats fail to undergo radial growth. Degeneration of these axons begins between 10 and 12 weeks of age, with significant axon loss by 12 weeks. EMG abnormalities, muscle atrophy and clinical signs are also present by 12 weeks of age. Neurodegeneration continues to progress, although cell body numbers are maintained (but smaller in size) even at 21 weeks.

Thus, our study supports a defect of axon radial growth as the earliest observed pathological change in feline SMA. Two critical factors in axon diameter regulation are neurofilaments (NFs) and myelin. NFs are intermediate filaments composed of three polypeptides, NF-L (light), NF-M (medium), NF-H (heavy). They are the most abundant cytoskeleton component in neurons. During development, increases in NF expression occur

after synapse formation and concurrent with myelination and axon radial growth (25). Increases in NF expression and transport are also seen after axon crush or transection (26, 27). NF-L is critical for neurofilament assembly and axon radial growth (28). The carboxyl termini of NF-M and NF-H form the side arms of NFs and are heavily phosphorylated in axons. These negatively charged phosphate groups are hypothesized to increase NF spacing and, therefore, axon caliber. Due to the larger number of KSP repeats in NF-H, it was originally thought that the heavy subunit was more important for axon radial growth. However, knockout of NF-H or deletion of its tail domain failed to disrupt radial growth and resulted only in a mild decrease in motor axon number (29, 30). In contrast, deletion of the NF-M tail domain severely inhibited axon caliber expansion (31, 32). The NF-M tail domain contains few KSP repeats; whose position and number are not conserved and recent evidence suggests that these residues are not required for axon radial growth (33).

Another key determinant in axon caliber is myelination. Unmyelinated axons have smaller calibers than myelinated fibers. Furthermore, within myelinated axons, the unmyelinated nodes of Ranvier are smaller in diameter than surrounding axonal segments and have reduced neurofilament spacing and phosphorylation (34). Schwann cells are currently thought to signal to axons via an unidentified receptor to increase cellular kinase activity and neurofilament phosphorylation (35, 36). We have excluded demyelination as an explanation of reduced axon caliber in feline SMA. However, more work is required to determine expression and phosphorylation levels of neurofilaments and whether LIX1 has a direct role in this or the signaling between Schwann cells and motor neurons. The research described herein increases our knowledge of disease progression in a naturally occurring animal model of SMA. This understanding will greatly aid in the assessment of therapeutic benefits of LIX1 gene therapy or new pharmacological agents in feline SMA.

REFERENCES

References

1. Russman BS. Spinal muscular atrophy: clinical classification and disease heterogeneity. J Child Neurol 2007;22(8):946-951.

2. Lefebvre S, Bürglen L, Reboullet S, et al. Identification and characterization of a spinal muscular atrophy-determining gene. Cell 1995;80:155-165.

3. Wirth B, Herz M, Wetter A, et al. Quantitative analysis of survival motor neuron copies: identification of subtle SMN1 mutations in patients with spinal muscular atrophy, genotype-phenotype correlation, and implications for genetic counseling. Am J Hum Genet 1999;64(5):1340-1356.

4. Wirth B, Brichta L, Hahnen E. Spinal muscular atrophy: from gene to therapy. Semin Pediatr Neurol 2006;13(2):121-131.

5. Lorson CL, Androphy EJ. An exonic enhancer is required for inclusion of an essential exon in the SMA-determining gene SMN. Hum Mol Genet 2000;9(2):259-265.

6. Lorson CL, Hahnen E, Androphy EJ, et al. A single nucleotide in the SMN gene regulates splicing and is responsible for spinal muscular atrophy. Proc Natl Acad Sci USA1999;96(11):6307-6311.

7. Monani UR, Lorson CL, Parsons DW, et al. A single nucleotide difference that alters splicing patterns distinguishes the SMA gene SMN1 from the copy gene SMN2. Hum Mol Genet 1999;8(7):1177-1183.

8. Burnett BG, Crawford TO, Sumner CJ. Emerging treatment options for spinal muscular atrophy. Curr Treat Options Neurol 2009;11(2):90-101.

9. He Q, Lowrie C, Shelton GD, et al. Inherited motor neuron disease in domestic cats: a model of spinal muscular atrophy. Pediatr Res 2005;57(3):324-330.

10. Fyfe JC, Menotti-Raymond M, David VA, et al. An ~ 140-kb deletion associated with feline spinal muscular atrophy implies an essential LIX1 function for motor neuron survival. Genome Res 2006;1084-1090.

11. Moeller C, Yaylaoglu MB, Alvarez-Bolado G, et al. Murine Lix1, a novel marker for subtantia nigra, cortical layer 5, and hindbrain structures. Brain Res Gene Expr Patt 2002;1:199-203.

12. Keller SR, Davis AC, Clairmont KB. Mice deficient in the insulin-regulated membrane aminopeptidase show substantial decreases in glucose transporter GLUT4 levels but maintain normal glucose homeostasis. J Biol Chem 2002;277(20):17677-17686.

13. Pellizzoni L, Kataoka N, Charroux B, et al. A novel function for SMN, the spinal muscular atrophy disease gene product, in pre-mRNA splicing. Cell 1998;95(5):615-624.

14. Pellizzoni L, Yong J, Dreyfuss G. Essential role for the SMN complex in the specificity of snRNP assembly. Science 2002;298(5599):1775-1779.

15. Massenet S, Pellizzoni L, Paushkin S, et al. The SMN complex is associated with snRNPs throughout their cytoplasmic assembly pathway. Mol Cell Biol 2002;22(18):6533-6541.

16. Zhang H, Xing L, Singer RH, et al. QNQKE targeting motif for the SMN-Gemin multiprotein complex in neurons. J Neurosci Res 2007;2657-2667.

17. Pestronk A, Drachman DB. A new stain for quantitative measurement of sprouting at neuromuscular junctions. Muscle Nerve 1978;1(1):70-74.

18. Tatton WG, Theriault E. Postnatal growth of medial gastrocnemius motoneurons in the kitten. Brain Res 1988;471(2):191-206.

19. Cifuentes-Diaz C, Nicole S, Velasco ME, et al. Neurofilament accumulation at the motor endplate and lack of axonal sprouting in a spinal muscular atrophy mouse model. Hum Mol Genet 2002;11(12):1439-1447.

20. Ferri A, Melki J, Kato AC. Progressive and selective degeneration of motoneurons in a mouse model of SMA. Neuroreport 2004;15(2):275-280.

21. Michaud M, Arnoux T, Bielli S, et al. Neuromuscular defects and breathing disorders in a new mouse model of spinal muscular atrophy. Neurobiol Dis 2010;38(1):125-135.

22. Sato M, Mizuno N, Konishi A. Postnatal differentiation of cell body volumes of spinal motoneurons innervating slow-twitch and fast-twitch muscles. J Comp Neurol 1977;175(1):27-36.

23. Purves D, Augustine GJ, Fitzpatrick D et al. *Neuroscience*. Sunderland, MA: Sinauer Associates 2001.

24. Crawford TO, Pardo CA. The neurobiology of childhood spinal muscular atrophy. Neurobiol Dis 1996;3(2):97-110.

25. Lee MK, Cleveland DW. Neuronal intermediate filaments. Annu Rev Neurosci 1996;19:187-217.

26. Hoffman PN, Cleveland DW, Griffin JW, et al. Neurofilament gene expression: a major determinant of axonal caliber. Proc Natl Acad Sci USA 1987;84:3472-3476.

27. Hoffman PN, Thompson GW, Griffin JW, et al. Changes in neurofilament transport coincide temporally with alterations in the caliber of axons in regenerating motor fibers. J Cell Biol 1985;101(4):1332-1340.

28. Sakaguchi T, Okada M, Kitamura T, et al. Reduced diameter and conduction velocity of myelinated fibers in the sciatic nerve of a neurofilament-deficient mutant quail. Neurosci Lett 1993;153(1):65-68.

29. Rao MV, Garcia ML, Miyazaki Y, et al. Gene replacement in mice reveals that the heavily phosphorylated tail of neurofilament heavy subunit does not affect ax;onal caliber or the transit of cargoes in slow axonal transport. J Cell Biol 2002;158(4)681-693.

30. Rao MV, Houseweart MK, Williamson TL, et al. Neurofilament-dependent radial growth of motor axons and axonal organization of neurofilaments does not require the neurofilament heavy subunit (NF-H) or its phosphorylation. J Cell Biol 1998;143(1):171-181.

31. Rao MV, Campbell J, Yuan A, et al. The neurofilament middle molecular mass subunit carboxyl-terminal tail domains is essential for the radial growth and cytoskeletal architecture of axons but not for regulating neurofilament transport rate. J Cell Biol 2003;163(5):1021-031.

32. Garcia ML, Lobsiger CS, Shah SB, et al. NF-M is an essential target for the myelin-directed "outside-in" signaling cascade that mediates radial axonal growth. J Cell Biol 2003;163(5):1011-1020.

33. Garcia ML, Rao MV, Fujimoto J, et al. Phosphorylation of highly conserved neurofilament medium KSP repeats is not required for myelin-dependent radial axonal growth. J Neurosci 2009;29(5):1277-1284.

34. Hsieh T, Kidd GJ, Crawford TO, et al. Regional modulation of neurofilament organization by myelination in normal axons. J Neurosci 1994;14(11):6392-6401.

35. Yin X, Crawford TO, Griffin JW, et al. Myelin-associated glycoprotein is a myelin signal that modulates the caliber of myelinated axons. J Neurosci 1998;18(6):1953-1962.

36. Dashiell SM, Tanner SL, Pant HC, et al. Myelin-associated glycoprotein modulates expression and phosphorylation of neuronal cytoskeletal elements and their associated kinases. J Neurochem 2002;81(6):1263-1272.

CHAPTER 3: *Lix1* knockout does not produce a SMA phenotype

Abstract

Feline SMA is an autosomal recessive, juvenile onset lower motor neuron disease caused by ~140 kilobase pair deletion, which disrupts expression of two genes, *limb expression 1* (*LIX1*) and *leucyl/cystinyl aminopeptidase* (*LNPEP*). A *Lnpep* knockout mouse has been previously generated and did not demonstrate any overt neuromuscular phenotype. Little is known currently about *LIX1*, except that it is highly expressed in spinal cord motor neurons. To confirm that loss of *Lix1* alone is responsible for the feline SMA phenotype, a *Lix1* knockout (KO) mouse line derived from an intron 1 gene trap clone was ordered from Lexicon Genetics. Mating of F1 heterozygotes produced offspring in the expected Mendelian ratio. Disruption of *Lix1* expression did not result in any neuromuscular phenotype even at two years of age as determined by hanging latency, rotarod, footprint ink tests and histological methods. RT-PCR analysis of spinal cord RNA identified a *Lix1* alternative transcript beginning in intron 4 and containing exons 5 and 6. This transcript appears to be mouse-specific and its expression is not disrupted in *Lix1* KO mice. The expression of this shorter transcript may compensate for the loss of *Lix1* in the KO mice and thus protect against motor neuron degeneration.

Introduction

Feline spinal muscular atrophy (SMA) is a juvenile onset lower motor neuron disease that is clinically analogous to Type 3 human SMA (1). Affected cats develop hindlimb muscle weakness and gait abnormalities at 12-13 weeks with atrophy becoming apparent at 5 months. Linkage and molecular analysis identified an ~140 kilobase deletion on feline chromosome A1q (2). This deletion spans intron 3 of *limb expression 1* (LIX1) to intron 1 of *leucyl/cystinyl aminopeptidase* (*LNPEP*) and abrogates expression of both genes. *LNPEP* is widely expressed, with its strongest expression occurring in the placenta, heart, kidney and small intestine. Knockout (KO) of *Lnpep* decreased trafficking of a glucose transporter, GLUT4, to the plasma membrane in response to insulin stimulation. In mice examined at one year of age, no overt neuromuscular phenotype was reported (3).

In contrast, relatively little is known about *LIX1*. *LIX1* is highly conserved; the deduced feline amino acid sequence is >92% identical to that of dog, cow, human, and mouse. *In situ* hybridization experiments in chicken identified *LIX1* expression in the developing limb bud and facial primordia (4). Similar experiments in mice found strong expression in spinal cord lower motor neurons, dorsal root ganglia and some interneurons (5). Thus far, there have been no cases of human SMA to date that can be linked to *LIX1* (2, 6, 7). However the *LIX1* expression profile data and failure of *Lnpep* KO mice to produce any neuromuscular phenotype support the hypothesis that *LIX1* is responsible for feline SMA. Therefore, we sought to characterize neuromuscular structure and function in *Lix1* KO mice.

Materials and Methods

Mice

We ordered a KO mouse line derived from a *Lix1* intron 1 gene trap embryonic stem cell clone (OST262711) from Lexicon Genetics (The Woodlands, TX). Two male and two female

heterozygotes (C57BL6/129 Sv Ev Brd) were received and bred to produce F2 *Lix1*$^{-/-}$ mice and homozygous normal controls that were used for subsequent behavioral testing and histology. Mice were housed and handled at Michigan State University according to IUACAC approved protocols and National Institutes of Health guidelines.

Genotyping

Genomic DNA (gDNA) was isolated from mouse tail biopsies (8). These were digested overnight at 55°C in 10mM Tris, pH 7.5, 400mM NaCl, 100mM EDTA, 0.6% SDS and 0.5 mg/ml Proteinase K. DNA was ethanol precipitated, and pellets were air dried. DNA was resuspended in 100 μl of 10mM Tris, pH 8.0, 1mM EDTA and stored at -20°C until used in multiplex polymerase chain reaction (PCR). One μl of gDNA was PCR amplified in 25 μl reactions containing a final concentration of 250 nM forward and reverse primers (Integrated DNA Technologies, Coralville, IA), 1 mM dNTPs (Invitrogen, Carlsbad, CA) and 0.05 U/μl Choice-Taq™ DNA polymerase and 10 mM Tris-HCl, pH 9.0, 10 mM KCl, 1.5 mM $MgSO_4$, 8 mM $(NH_4)_2SO_4$, 1.5 mM $MgCl_2$, and 0.05% NP-40 (Denville Scientific, South Plainfield, NJ). One set of primers (5'-GCCCTCGGTTGGCTTTTGAT-3' and 5'-GCCCACCTCATCCCAAACTTC-3') flanked the trapping cassette insertion site and a second reverse primer, 5'-ATAAACCTCTTGCAGTTGCATC-3', was located in the 5' long terminal repeat (LTR) of the trapping cassette (Figure 3.1A). Thermocycling conditions were as follows: 2 minutes 95°C initial denaturation, 35 cycles at 94°C for 30 seconds (s), 58°C for 30 s, and 72°C for 30 s and a final extension at 72°C for 10 minutes. Amplification from the wild-type locus yielded a 359 bp product, whereas, amplification from the mutated locus produced a 219 bp product. Products were analyzed by agarose gel electrophoresis.

Hanging latency

Mice were allowed to grip a wire cage lid 40 cm above a cage with bedding. The cage lid was inverted for 120 s and the time at which the mouse fell was recorded (9). Mice were tested weekly beginning at 3 weeks of age until 9 months and then were tested monthly until 2 years. After 8 months, the test was extended to 240 s.

Accelerating rotarod

Mice were tested for endurance and motor coordination by an accelerating rotarod (Columbus Instruments, Columbus OH; axle diameter 3.6 cm). The test began at 4 rpm and speed was increased 0.1 rpm/s for 360 s, and the time that the mouse remained on the rod was recorded (10). Each animal was given three trials with a 10 minute rest between each trial. After one week on training, mice were tested three times per week and the best trial time from each day was recorded and averaged to obtain a value for the week. At 9 months of age, the mice were tested one week per month until 2 years of age.

Footprint ink test

The front and rear paws of mice were painted with red and blue non-toxic acrylic paint, respectively. Mice were placed at one end of a tube lined with paper and guided to walk to the other end (9). Three measurements of forelimb stride length, hindlimb stride length, front base width and hind base width were taken and averaged together to yield a single value for each parameter. Mice were tested once weekly from 19 weeks until 9 months and once monthly thereafter.

Histology

After euthanasia by CO_2 asphyxiation, whole hind limbs were immersion fixed in 10% neutral buffered formalin. Anterior tibialis (TA) muscles were dissected, paraffin embedded, transversely sectioned at 5 μm and stained with hematoxylin and eosin (H&E). Five random, non-overlapping fields of view at 40x magnification were examined for muscle fiber morphology.

Dorsal laminectomies of vertebral columns were performed in 10% neutral buffered formalin. After 1 week of immersion fixation, L4 ventral roots and L4 spinal cord segments were harvested. L4 ventral roots were embedded in Poly/Bed 812-Araldite, sectioned at 1 μm and stained with toluidine blue for axon counts and morphometrics. L4 spinal cord was paraffin embedded, sectioned at 5 μm and stained with cresyl violet.

L4 ventral root counts and morphometry

All axons within a single L4 ventral root cross section were counted with Neurolucida (MBF Bioscience, Williston, BT) and a Nikon FX-A microscope (Tokyo, Japan) at 20x magnification. A single image of the cross section was captured at 40x magnification and 250 axon diameters, excluding the myelin sheath, were measured with Image-Pro Plus 5.1 (Media Cybernetics, Bethesda, MD). Axon diameters were grouped in 2 μm increments and the number of axons within a bin was determined.

cDNA amplification by PCR

Whole spinal cord was expelled from the vertebral column of 6 week old mice with a 20 ml syringe filled with 0.1 M phosphate buffered saline (PBS), pH 7.4, and a dulled 18 gauge needle. Spinal cords were flash frozen in liquid nitrogen and then stored at -80°C until RNA extraction with RNeasy® Lipid Tissue Midi Kit (Qiagen, Venlo, Netherlands) according to manufacturer's instructions. RNA was analyzed by gel electrophoresis and spectrophotometry. One μg of total RNA was reverse transcribed in a 20 μl reaction at 50°C for 50 minutes with SuperScript III® and oligo dT_{20} (Invitrogen, Carlsbad, CA) according to manufacturer's recommendations or with no added reverse transcriptase (no RT). Two μl of cDNA amplification reactions or no RT reactions were PCR amplified in 50 μl reactions containing a final concentration of 250 nM forward and reverse primers (Integrated DNA Technologies, Coralville, IA), 1 mM dNTPs (Invitrogen, Carlsbad, CA) and 0.05 U/μl Choice-Taq™ DNA polymerase and

10 mM Tris-HCl, pH 9.0, 10 mM KCl, 1.5 mM $MgSO_4$, 8 mM $(NH_4)_2SO_4$, 1.5 mM $MgCl_2$, and 0.05% NP-40 (Denville Scientific, South Plainfield, NJ). Primers used for RT-PCR are listed below. Cycling conditions for *Lix1* amplification were initial denaturation at 95°C for 2 minutes, 35 cycles of 30 s denaturation at 94°C, 30 s primer annealing at 62°C, 1 min extension at 72°C and final extension at 72°C for 10 min. Reaction conditions for γ *actin* (*Actg1)* were identical except that the annealing temperature was 58°C and the extension time was 30 s. Products were analyzed by agarose gel electrophoresis.

Lix1 exon 1 F: 5'-CCAGCCTGTCAGCCAGCCTT-3'

Lix1 exon 2 F: 5'-CTGGGCCTCCCTTTGTGAGCTA-3'

Lix1 exon 5 F: 5'-CCAACTACTGCACTGGAATGA-3'

Lix1alt exon 1 F: 5'-TCCTGCTGCGCTGAGGAACC-3'

Lix1 3' UTR R: 5'- ACCTGCCACCTGGCCTTGCT-3'

Actg1 exon 1 F: 5'-AATCGCCGCACTCGTCATTG-3'

Actg1 exon 2 R: 5'-TGTGGTGCCAGATCTTCTCC-3'

Quantitative RT-PCR (RT-qPCR)

Whole spinal cords were expelled from 2, 4 and 8 week old mice as described above, flash frozen and stored at -80°C until RNA extraction. These mice were from a 6 generation backcross to C57BL6 mice (Jackson Labs, Bar Harbor, ME) to reduce variation in expression due to genetic background differences. Total RNA was extracted with PureLink™ RNA Mini Kit (Invitrogen, Carlsbad, CA) according to manufacturer's specifications. RNA was analyzed by gel electrophoresis and spectrophotometry. Five hundred ng of RNA per sample was reverse transcribed with SuperScriptIII® and oligo dT_{20} primer. The resulting cDNA and no RT controls were diluted 1:2.5 for subsequent PCR amplification. Two μl of cDNA or no RT controls were

amplified with 200 nM of primers and Fast SYBR® Green Master Mix (Applied Biosytems, Carlsbad, CA) in 20 μl reactions on a Step-One Plus Real-Time PCR system (Applied Biosystems). Samples were incubated at 95°C for 20 s prior to 40 cycles of 95°C for 3 s and 60°C for 30 s. Melt curves were generated for each sample. Data were analyzed with Step-One Plus® software by the relative standard curve method with β actin (*Actb1*) and *Cyclophilin* (*Cyp*) serving as reference genes. Primer sequences are listed below. Each gene was replicated in three technical replicates of three biological replicates.

Lix1: 5'-GCCTCCCTTTGTGAGCTATG-3' and 5'-GCCTGGCCTCAGCTCTACT-3'

Lix1alt: 5'-CGCAATAGGCTTCAGCTTTCC-3' and 5'-CTTCCTGTCGAGAGCACTTTG-3'

Actb1: 5'-ACGGCCAGGTCATCACTATT-3' and 5'-CGGATGTCAACGTCACACTT-3'

Cyp: 5'-ACTGTCGCTTTTCGCCG-3' and 5'-GCTGTCTTTGGAACTTTGTCTG-3'

Data analysis and figure generation

Averages, standard deviations, X^2 tests and Student's t-tests (α = 0.05) were performed with Excel software (Microsoft Corporation, Redmond, WA). All graphs were generated in Excel. Figures were created in PowerPoint and converted to tiff files in Photoshop CS4 (Adobe, San Jose, CA).

Results

Matings of *Lix1*$^{+/-}$ mice received from Lexicon Genetics produced 85 F2 offspring. Genotyping of these mice by multiplex PCR (Figure 3.1B) revealed that 25 mice were homozygous normal, 37 were heterozygous and 23 were homozygous for the *Lix1* gene trap allele. This ratio does not differ significantly from the expected 1:2:1 Mendelian genotypic ratio (X^2=1.9, p=0.1) and thus insertional mutagenesis of *Lix1* is not embryonic lethal. To confirm that gene trapping resulted in disruption of *Lix1* expression, I performed RT-PCR on total RNA

extracted from six week old whole spinal cord. No amplification of Lix1 cDNA was detected in homozygous KO mice (Figure 3.1C).

Mice were examined for signs of neuromuscular dysfunction by weighing, hanging latency, accelerating rotarod and footprint ink test weekly until 9 months of age, and monthly thereafter until two years of age. At all ages, there was no difference between *Lix1*$^{-/-}$ and *Lix1*$^{+/+}$ control animals (Figures 3.2 and 3.3). Furthermore, *Lix1* KO did not result in decreased survival (Figure 3.4). The failure of *Lix1*$^{-/-}$ mice to show any overt difference in motor function led me to examine the mice for more subtle motor phenotypes. Therefore, I assessed L4 ventral root axon number and size distribution at three ages, six months, one year and two years. No axon loss was observed in *Lix1*$^{-/-}$ mice (Figure 3.5). There were significantly more axons with diameters of 4 to 6 μm in knockout mice at two years of age (Figure 3.6I), however there was no difference in the range of axon diameters observed. Examination of TA muscle and L4 spinal cord did not reveal any overt pathology (Figure 3.7, n = 3). Thus in mice, disruption of *Lix1* was not sufficient to reproduce the feline SMA phenotype as determined by motor functions tests and spinal cord and muscle histology.

In an effort to explain the lack of phenotype in our *Lix1* gene trap mouse, I undertook further RT-PCR examination of the *Lix1* locus. No amplification was detected in *Lix1*$^{-/-}$ mice when primers were located in exon 2 and the 3' UTR (Figure 3.8A). However, a product was detected when the forward primer was moved downstream to exon 5 (Figure 3.8B). Query of the *Lix1* locus on the University of California Santa Cruz genome browser, identified a mouse specific, alternative *Lix1* transcript beginning in intron 4 and containing exons 5 and 6 of *Lix1*. Primers were designed to PCR amplify this alternative transcript and a product was detected in

Figure 3.1. Insertional mutagenesis of *Lix1* is non-embryonic lethal null allele. A) Schematic of wild-type and *Lix1* intron 1 gene trapped loci. Black arrows represent approximate position of genotyping primers. LTR = long terminal repeats. SA and SD = splicing acceptor and donor site, respectively. pA = polyadenylation signal. NEO = neomyocin resistance gene. PGK = *phosphoglycerate kinase* promoter. BTK = *Bruton tyrosine kinase* exon. B) Representative image of multiplex PCR genotyping results of F2 progeny. Lane 1: Molecular weight marker. Lane 2: H_2O negative control. Lane 3: F1 $Lix1^{+/-}$ positive control. Lanes 4-6: $Lix1^{+/+}$. Lanes 7-9: $Lix1^{-/-}$. Lanes 10 and 11: $Lix1^{+/-}$. C) RT-PCR of *Lix1* and *Actg1*. Lane 1: $Lix1^{+/+}$. Lane 2: $Lix1^{+/+}$ no RT. Lane 3: $Lix1^{+/-}$. Lane 4: $Lix1^{+/-}$ no RT. Lane 5: $Lix1^{-/-}$. Lane 6: $Lix1^{-/-}$ no RT. Lane 7: H_2O negative control.

Figure 3.1 continued.

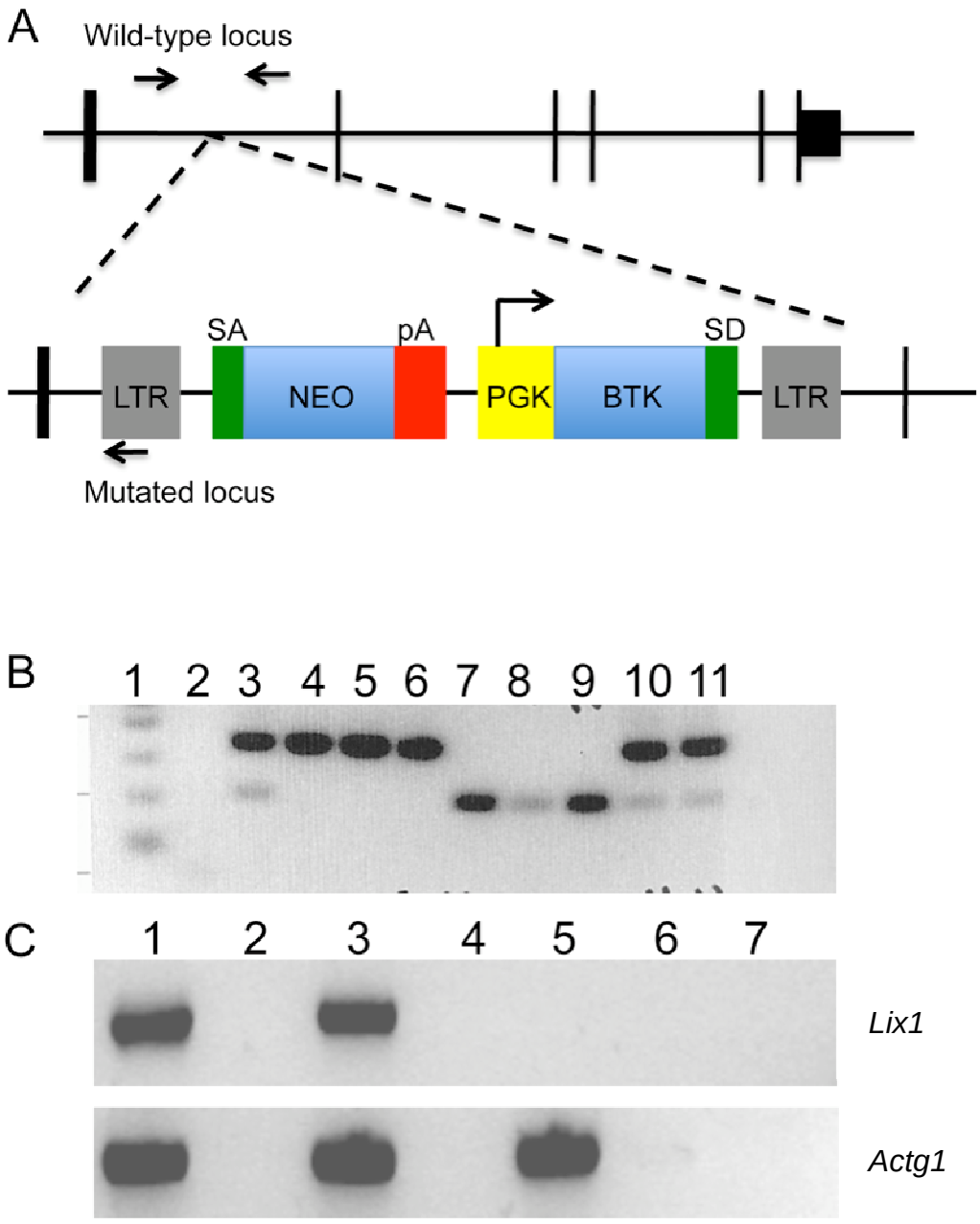

Figure 3.2. Weights and motor function tests at 6 months, 1 year and 2 years. A) Average weights of mice (6 months n = 18; 1 year n = 12; 2 years n = 5). B) Hanging latency test results (6 months n = 14; 1 year n = 12; 2 years n = 5). C) Accelerating rotarod test results (6 months n = 4; n = 12; 2 year n = 5). Averages ± S.D. are shown. For all $p > 0.05$ Shaded bars represent *Lix1*$^{+/+}$ mice. Unshaded bars represent *Lix1*$^{-/-}$.

Figure 3.2 continued.

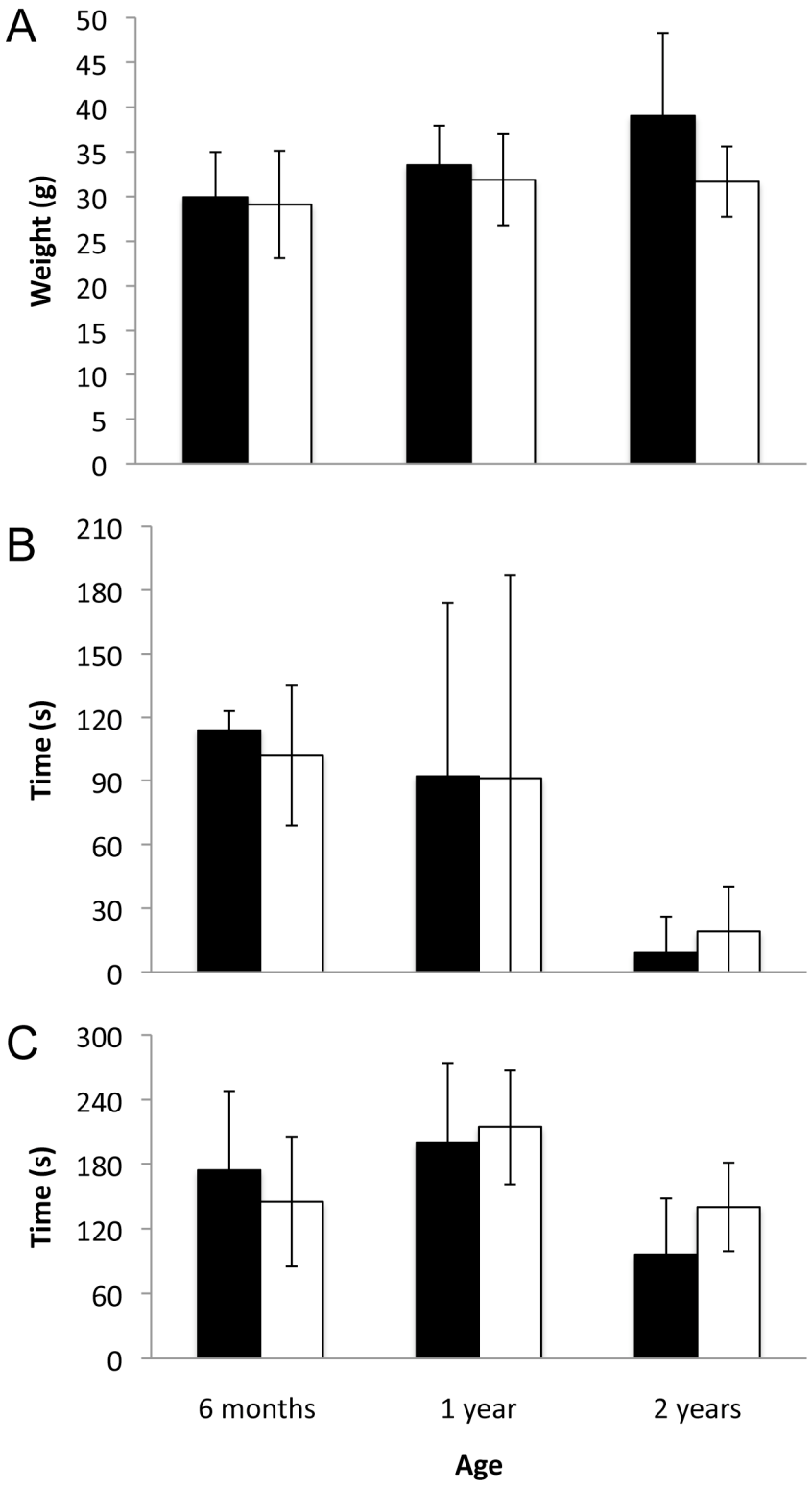

Figure 3.3. Footprint ink tests. A) 6 months n = 5. B) 1 year n = 9. C) 2 years n = 5. Averages ± S.D are shown. For all $p > 0.05$. Shaded bars represent *Lix1*$^{+/+}$ mice. Unshaded bars represent *Lix1*$^{-/-}$.

Figure 3.3 continued.

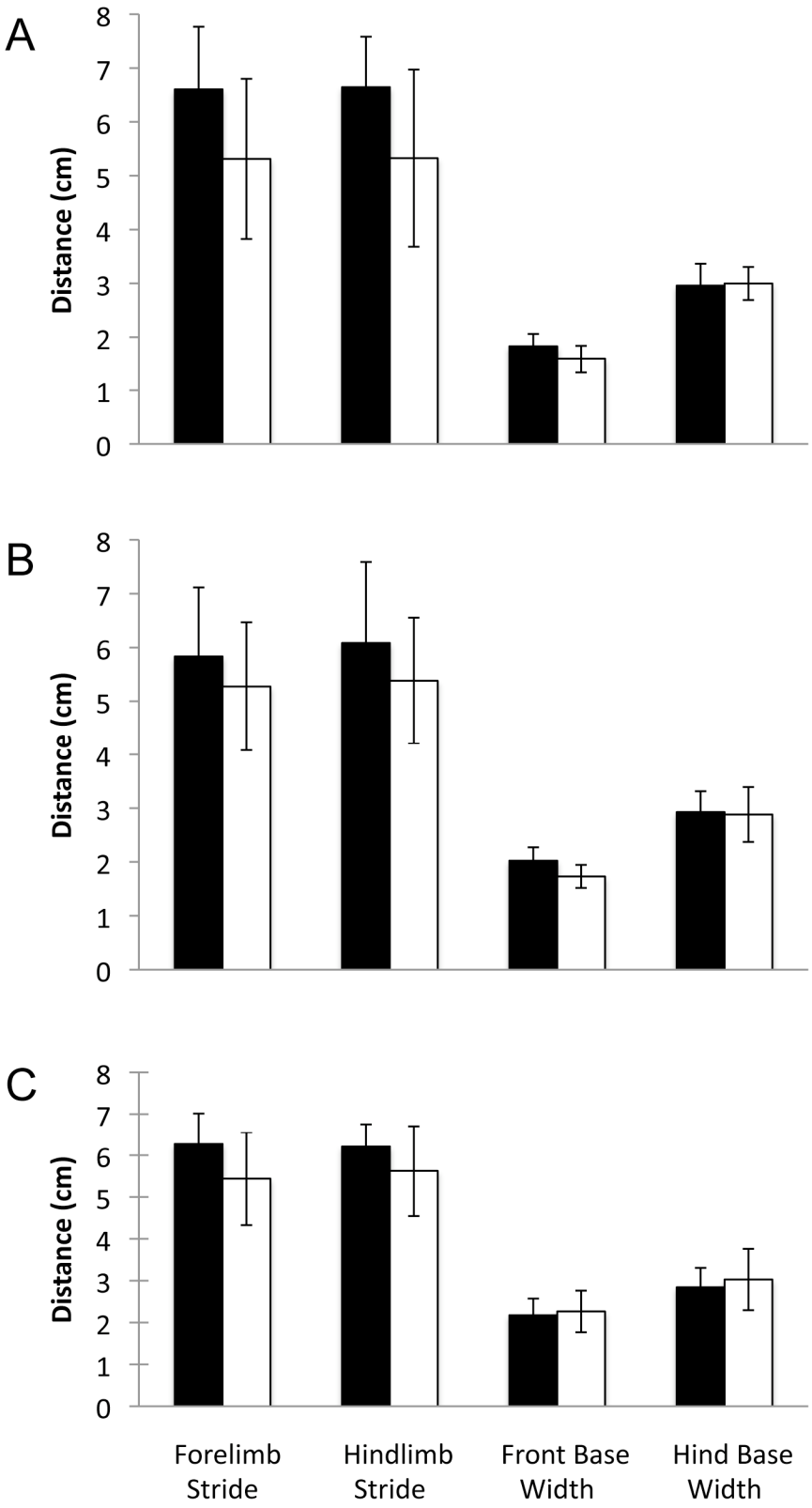

Figure 3.4. Survival of *Lix1*$^{-/-}$ mice. KO of *Lix1* did not result in decreased lifespan (n = 7). Mice were sacrificed at 2 years of age for histology. *Lix1*$^{+/+}$ = solid line, *Lix1*$^{-/-}$ = dashed line.

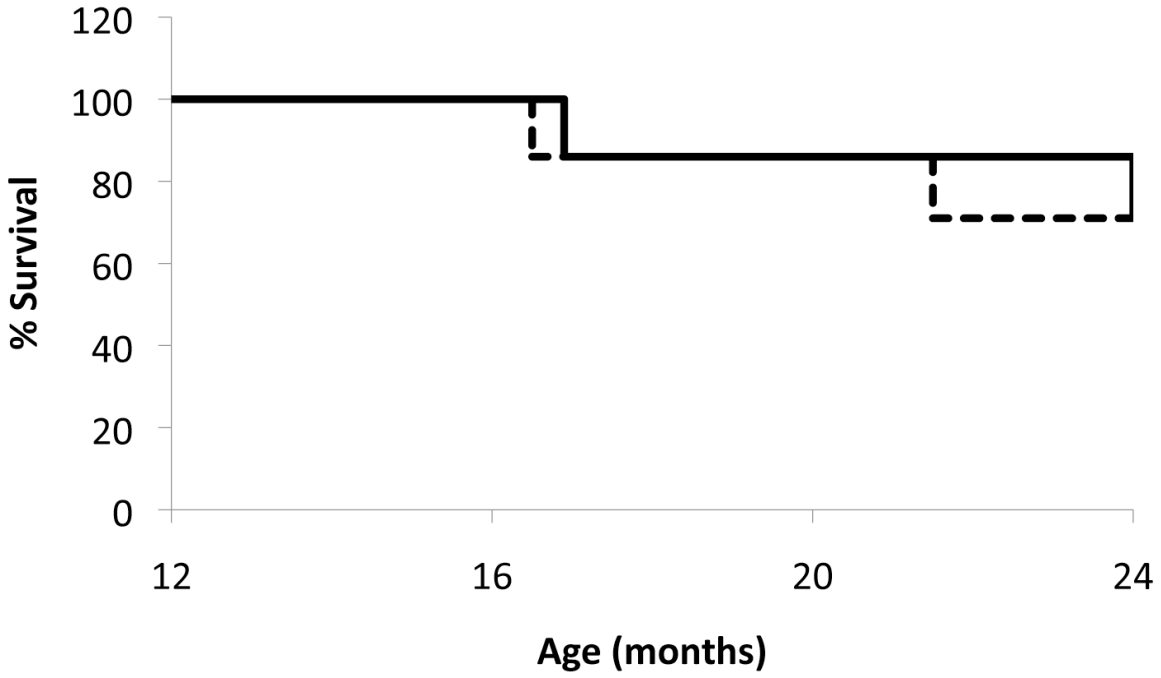

Figure 3.5. Total number of L4 ventral root axons at 6 months (n = 4), 1 year (n = 5) and 2 years (n = 5) of age. Averages ± S.D. are shown. For all $p > 0.05$. Shaded bars represent *Lix1*$^{+/+}$ mice. Unshaded bars represent *Lix1*$^{-/-}$ mice.

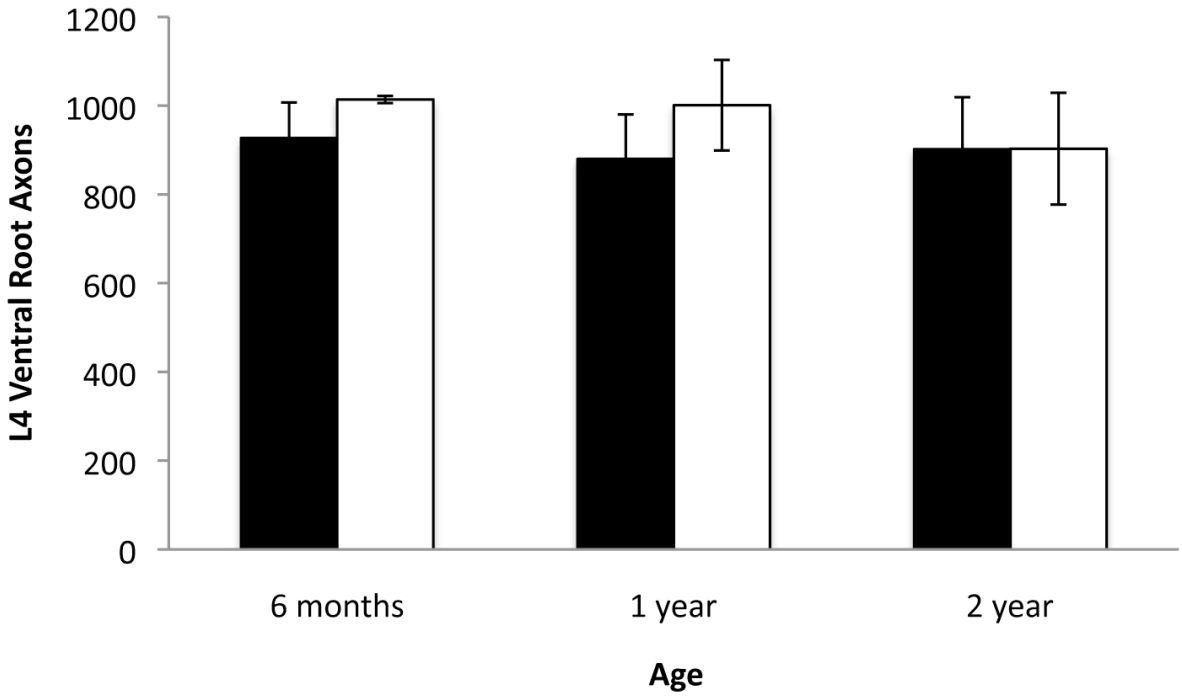

Figure 3.6. Photomicrographs of toluidene blue stained L4 ventral roots and morphometrics. Representative images of *Lix1*$^{-/-}$ mice at 6 months (B), 1 year (D) and 2 years (F) and age-matched controls (A, C, and E). Bar = 20 μm. Ventral root morphometrics at 6 months (G, n = 4), 1 year (H, n = 5) and 2 years (I, n = 5). Averages ± S.D. are shown. For all $p > 0.05$. except 4-6 μm at 2 years where asterisk denotes statisitical significance at $p \leq 0.05$ by Student's t-test. Shaded bars represent *Lix1*$^{+/+}$ mice. Unshaded bars represent *Lix1*$^{-/-}$ mice.

Figure 3.6 continued.

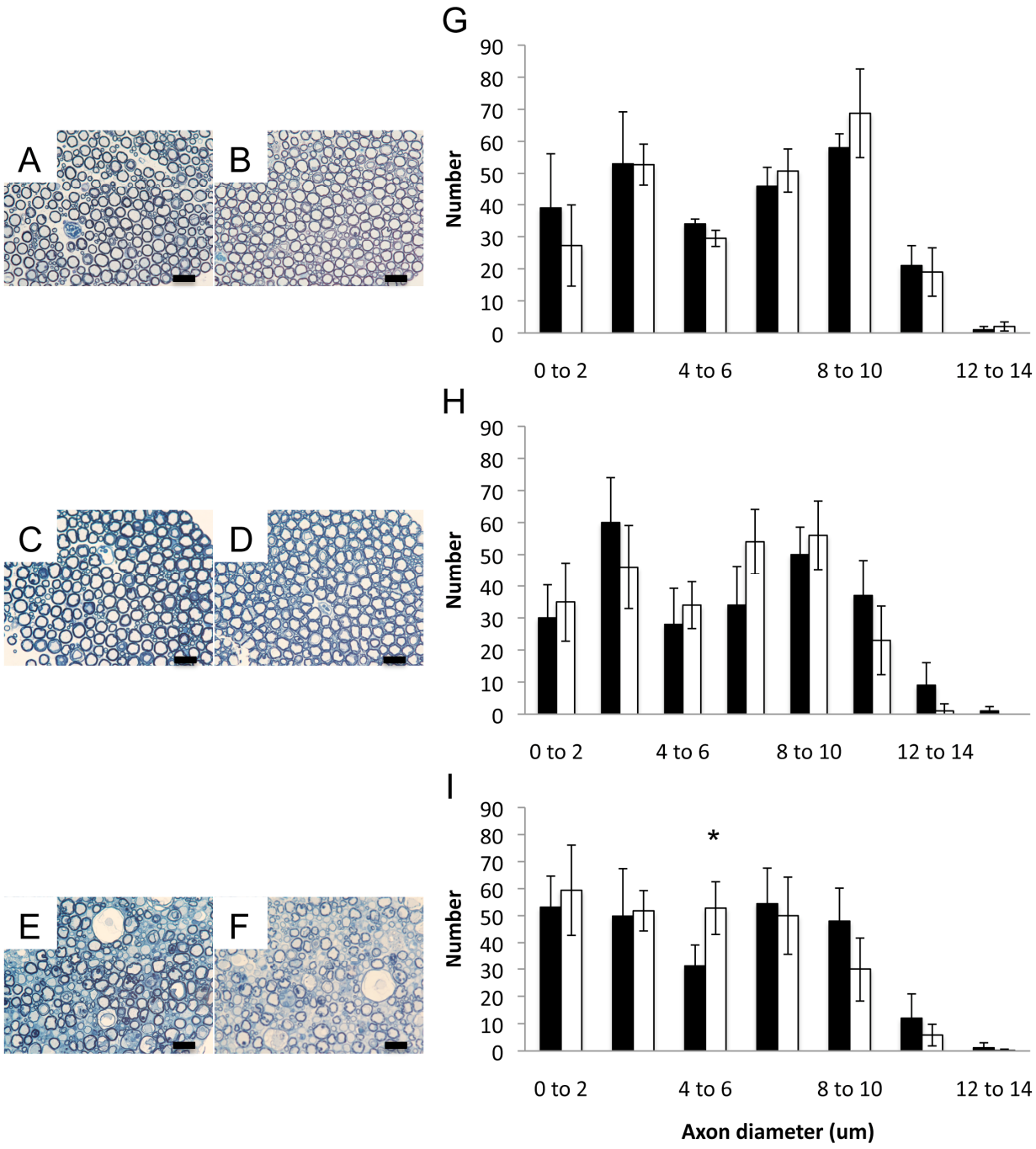

Figure 3.7. Photomicrographs of L4 spinal cords and TA muscles at 2 years. Representative images of cresyl violet stained ventral horns from *Lix1*$^{+/+}$ (A) and *Lix1*$^{-/-}$ mice (B). Representative images of H & E stained TA muscles from *Lix1*$^{+/+}$ (C) and *Lix1*$^{-/-}$ mice (D). Bars = 100 μm in A and B. Bars = 20 μm in C and D.

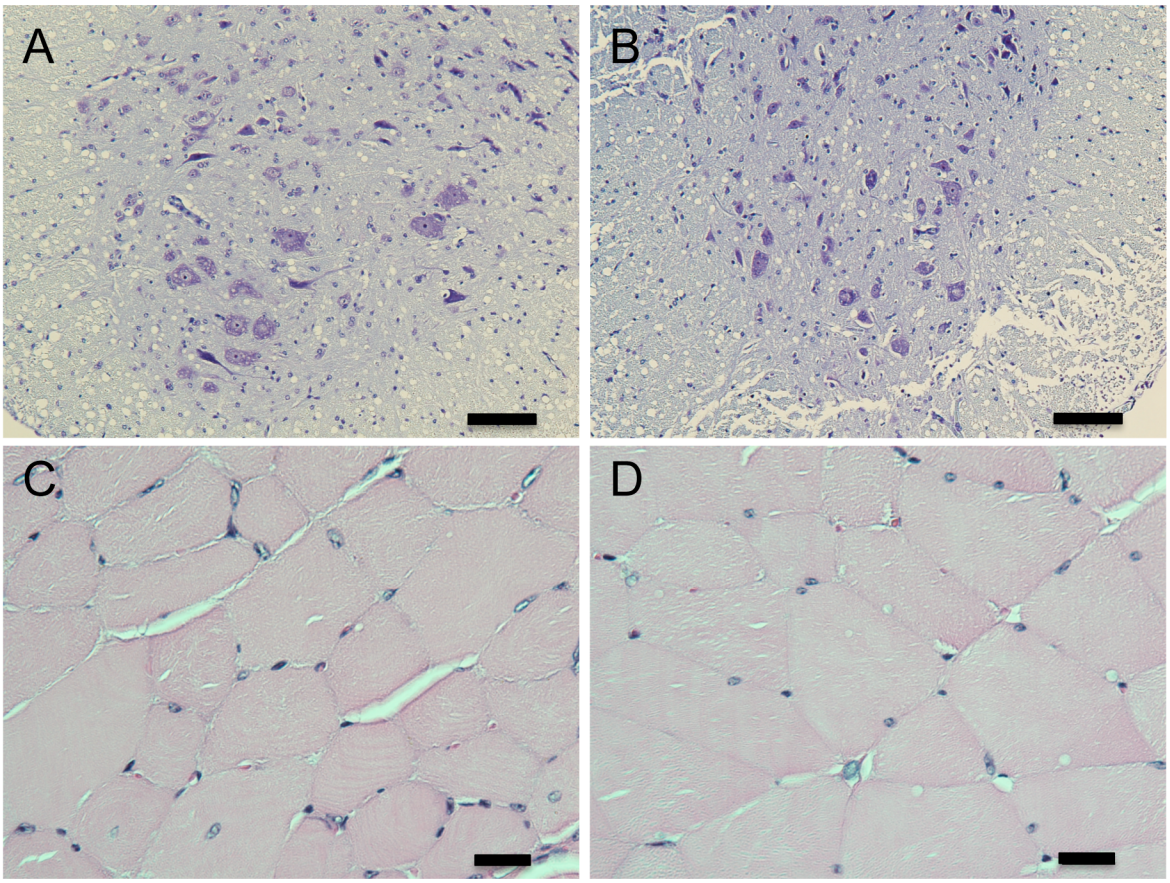

Figure 3.8. RT-PCR analysis of *Lix1* locus. A) Forward primer is located in exon 2 of *Lix1*. B) Forward primer is located in exon 5 of *Lix1*. C) Forward primer is located in exon 1 of the *Lix1* alternative transcript. For A-C the reverse primer is located in the *Lix1* 3' UTR. D) *Actg1* control. For all: Lane 1: Molecular weight marker. Lane 2: $Lix1^{+/+}$. Lane 3: $Lix1^{+/+}$ no RT. Lane 4: $Lix1^{+/-}$. Lane 5: $Lix1^{+/-}$ no RT. Lane 6: $Lix1^{-/-}$. Lane 7: $Lix1^{-/-}$ no RT. Lane 8: H_2O negative control.

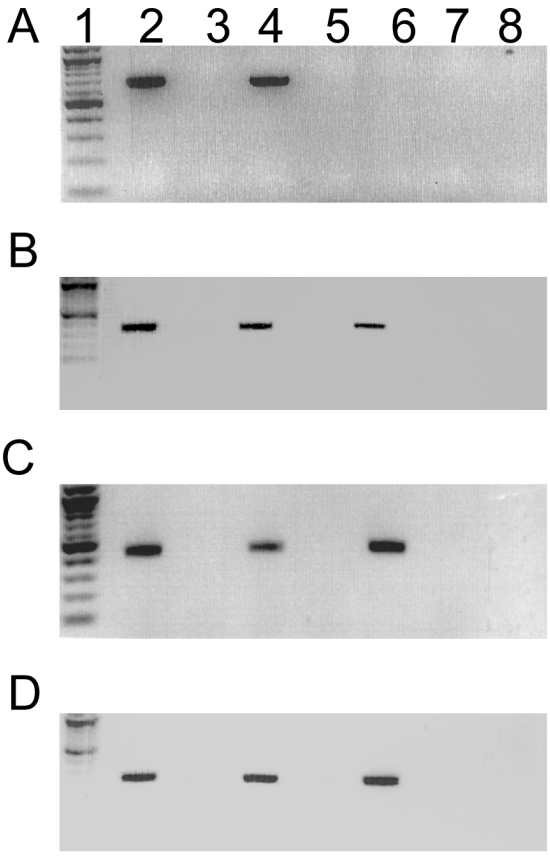

Lix1$^{-/-}$ mice (Figure 3.8C). Therefore the intron 1 gene trap does not abrogate expression of this alternative transcript, which will be referred to as *Lix1alt* from this point forward.

To determine whether *Lix1alt* expression is up regulated in *Lix1*$^{-/-}$ or whether it is the predominant transcript in mice, I performed RT-qPCR on whole spinal cord from 2, 4, and 8 week old mice (Table 3.1, Figure 3.10). There was no increase in *Lix1alt* expression in *Lix1*$^{-/-}$ mice nor was it expressed at a higher level than the longer *Lix1* transcript in normal controls. However, our lack of a Lix1 antibody has prevented evaluation of Lix1 and Lix1alt protein expression in normal and *Lix1* knockout mice.

Discussion

The feline SMA mutation disrupts expression of two genes, *LIX1* and *LNPEP*. Based on expression profiles and results from a previous *Lnpep* KO mouse, we hypothesized that loss of *LIX1* was responsible for lower motor neuron disease in SMA affected cats. To test this hypothesis, I assessed *Lix1* gene trap mice for neuromuscular dysfunction by several motor function tests

and histological methods. *Lix1* KO mice did not demonstrate any deficit in strength, endurance or coordination as determined by hanging latency, rotarod and footprint ink tests. Furthermore, *Lix1* KO did not result in axon loss or decreased axon caliber as was observed in SMA affected cats.

RT-PCR analysis did identify a mouse specific *Lix1* alternative transcript, *Lix1alt*, whose expression persisted in *Lix1*$^{-/-}$ mice. This transcript begins in intron 4 of *Lix1* and contains *Lix1* exons 5 and 6. This transcript contains a 468 base pair open reading frame that is predicted to encode an 18 kDa protein with the final 120 residues being identical to Lix1. *Lix1alt* expression is not increased in *Lix1* KO mice, nor is the alternative transcript a major transcript in normal

Figure 3.9. Testing of RT-qPCR primers for *Lix1* (A), *Lix1alt* (B), *Actb1* (C), and *Cyp* (D). Lane 1: *Lix1*$^{+/+}$. Lane 2: *Lix1*$^{+/+}$ no RT control. Lane 3: H_2O negative control. Cycling conditions were identical to RT-qPCR except that annealing (60℃ 30 s) and extension (72℃ 30 s) were separate steps. Total number of cycles is 35.

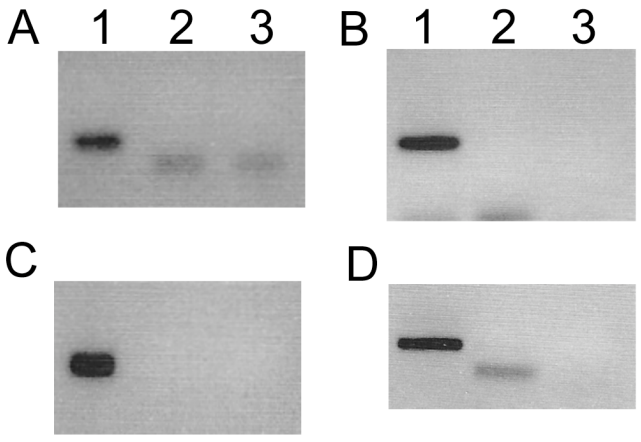

Table 3.1. Cycle thresholds (C_T) from RT-qPCR. Averages ± S.D. from three technical replicates of three biological replicates at 2, 4 and 8 weeks of age.

		Average C_T ± S.D.			
Genotype	Age	*Lix1*	*Lix1alt*	*Actb1*	*Cyp*
Lix1$^{+/+}$	2 weeks	26.0 ± 0.24	34.3 ± 0.6	15.7 ± 0.98	18.8 ± 0.7
Lix1$^{-/-}$			34.3 ± 0.53	16.2 ± 0.99	18.9 ± 0.94
Lix1$^{+/+}$	4 weeks	23.3 ± 0.52	32.4 ± 0.42	19.9 ± 0.14	18.3 ± 0.12
Lix1$^{-/-}$			33.4 ± 0.85	21.0 ± 0.99	18.6 ± 0.4
Lix1$^{+/+}$	8 weeks	24.2 ± 0.45	31.9 ± 0.82	20.4 ± 0.99	19.9 ± 1.5
Lix1$^{-/-}$			30.4 ± 0.48	17.3 ± 0.29	18.8 ± 0.29

Figure 3.10. Relative expression of Lix1 and Lix1alt in 2 (A), 4 (B), and 8 (C) week old animals. *Lix1* and *Lix1alt* expression is normalized to *Cyp* and *Actb*. Averages ± S.D. are shown. For all p > 0.05. Shaded bars represent *Lix1*$^{+/+}$. Unshaded bars represent *Lix1*$^{-/-}$ mice.

Figure 3.10 continued.

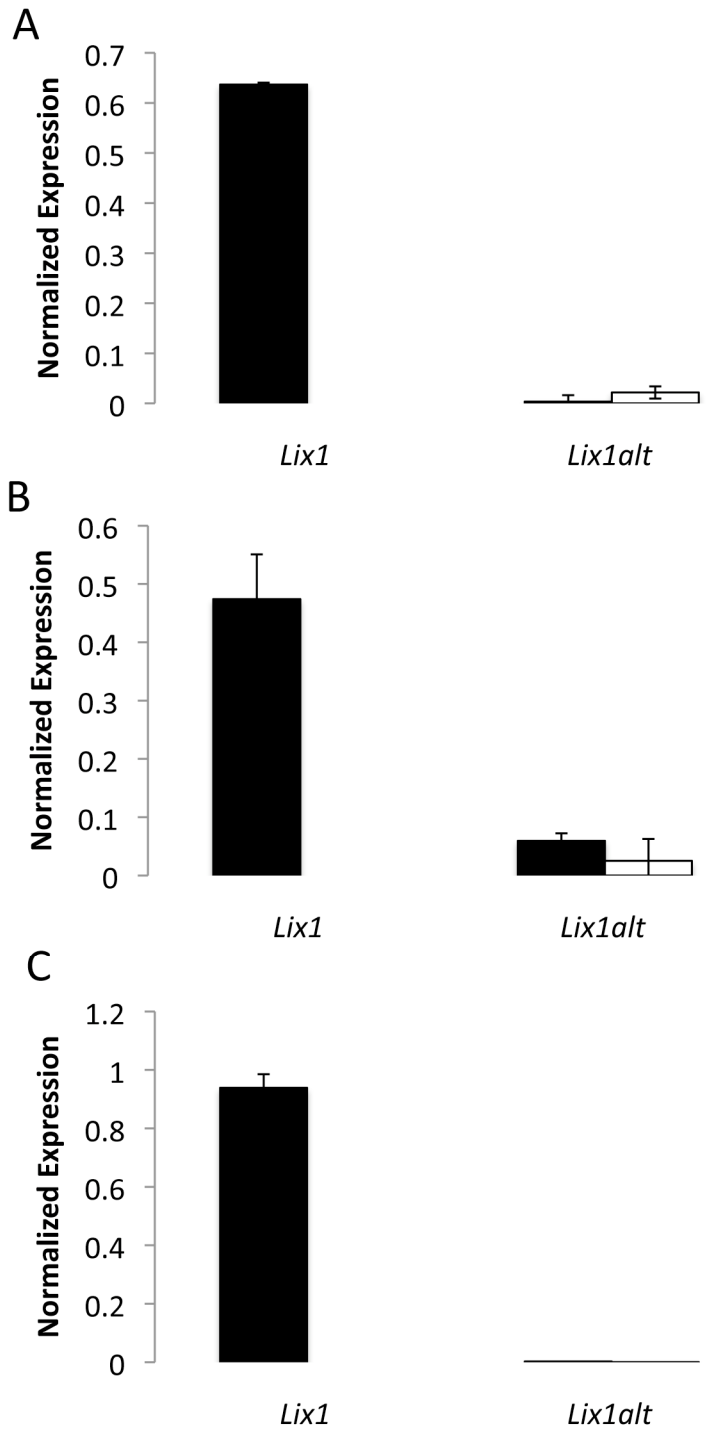

mice. However, protein translated from the *Lix1alt* transcript may be functionally redundant to Lix1 and thus protect against SMA in *Lix1* KO mice.

Functional redundancy has been previously documented in several mouse models that fail to mimic human disease. Lesch-Nyhan syndrome is (LHS) a severe X-linked recessive disease characterized by self-injurious behavior and is caused by a deficiency of hypoxanthine-guanine phosphoribosyltransferase (HPRT) enzyme. However, HPRT deficient mice failed to demonstrate self-mutilation or motor defects seen in human patients (11, 12). Recapitulation of the human phenotype was seen after administration of an adenine phosphoribosyltransferase (APRT) inhibitor that disrupted an alternative purine salvage pathway that is more active in mice (13). Another example of functional redundancy is seen in a naturally occurring mouse model of Duchenne muscular dystrophy (DMD). In humans and golden retrievers, null mutations in the *dystrophin* gene result in severe muscle wasting and premature death. The *mdx* mouse has a nonsense mutation in *dystrophin*; however, these mice show little muscle weakness and have a normal lifespan (14). A more severe phenotype is prevented by functional redundance of a *dystrophin* homolog, *utrophin* (15, 16). Thus to exclude *Lix1* as the feline SMA disease gene, another knockout mouse in which both *Lix1* and *Lix1alt* are disrupted is required.

There is also evidence of varying phenotypic robustness in similar mutations of mouse and human orthologous genes. A comparison of 120 essential genes in humans and the knockout of the mouse ortholog identified that ~20% of the genes were non-essential in mice (17). In humans, a valine for alanine substitution at residue 4 of Cu, Zn superoxide dismutase (SOD1) causes amyotrophic lateral sclerosis, a fatal, late onset motor neuron disease (18). However, transgenic mice over-expressing this mutant SOD1 failed to develop any signs of motor neuron disease (19). It is possible that another knockout mouse, in which expression from the *Lix1* locus is completely disrupted, will still fail to show a neuromuscular phenotype.

Two other hypotheses exist to explain the discrepancy between *Lix1* KO mice and SMA affected cats. First, feline SMA could be due to deletion of a regulatory element. An example of

enhancer mutation resulting in disease is found in pre-axial polydactyly. Disruption of a long-range *sonic hedgehog* enhancer by point mutations or targeted deletion causes limb defects in humans and mice (20, 21). Identification of enhancer elements in the feline SMA deletion would require comparative genomics to identify putative regulatory elements followed by reporter gene assays to assess those sequences for regulatory function. Finally, targeted deletion of those sequences in mice with the Cre-Lox system would be necessary. Alternatively, loss of *Lix1* and *Lnpep* could be required to recapitulate feline SMA in mice. Unfortunately, the close proximity between *Lix1* and *Lnpep* makes it impossible to create *Lix1* and *Lnpep* double knockouts through breeding. Instead, a chromosome engineering strategy based on the Cre-Lox system would be required (22). In summary, I was unable to exclude or prove *Lix1* as a candidate feline SMA disease gene in this study. Further research is required to prove or disprove a role for *Lix1* in motor neuron disease. We are currently working with colleagues at the University to Nantes to deliver *LIX1* by adeno-associated virus based gene therapy in affected cats. The amelioration or delay of clinical signs in treated SMA cats will provide evidence that *LIX1* is indeed the feline SMA disease gene.

REFERENCES

References

1. He Q, Lowrie C, Shelton GD, Castellani RJ, et al. Inherited motor neuron disease in domestic cats: a model of spinal muscular atrophy. Pediatr Res 2005;57(3):324-330.

2. Fyfe JC, Menotti-Raymond M, David VA, et al. An ~ 140-kb deletion associated with feline spinal muscular atrophy implies an essential LIX1 function for motor neuron survival. Gen Res. 2006:1084-1090.

3. Keller SR, Davis AC, Clairmont KB. Mice deficient in the insulin-regulated membrane aminopeptidase show substantial decreases in glucose transporter GLUT4 levels but maintain normal glucose homeostasis. J Biol Chem 2002;277(20):17677-17686.

4. Swindell E, Moeller C, Thaller C, et al. Cloning and expression analysis of chicken Lix1, a founding member of a novel gene family. Mech Dev 2001;109:405-408.

5. Moeller C, Yaylaoglu MB, Alverez-Bolado G, et al. Murine Lix1, a novel marker for substantia nigra, cortical layer 5, and hindbrain structures. Gene Expr Patt 2002:199-203.

6. Parkinson N, Baumer D, Rose-Morris A, et al. Candidate screening of the bovine and feline spinal muscular atrophy genes reveals no evidence for involvement in human motor neuron disorders. Neuromuscul Disord 2008;18:394-397.

7. Sasongko TH, Gunadi, Yusoff S, et al. Screening of the LIX1 gene in Japanese and Malaysian patients with SMA and/or SMA-like disorder. Brain Dev. 2010;32(5):385-389.

8. Miller S, Dykes D, Polesky H. A simple salting out procedure for extracting DNA from human nucleated cells. Nucl Acids Res 1988;16(3):1215.

9. Monks DA, Johansen JA, Mo K, et al. Overexpression of wild-type androgen receptor in muscle recapitulates polyglutamine disease. Proc Natl Acad Sci USA. 2007;104(46):18259-18264.

10. Crawley JN. Behavioral phenotyping of transgenic and knockout mice: experimental design and evaluation of general health, sensory functions, motor abilities, and specific behavioral tests. Brain Res 1999;83:518-26.

11. Kuehn M, Bradley A, Robertson E, et al. A potential animal model for Lesch-Nyhan syndrome through induction of HPRT mutations into mice. Nature 987;32(6):295-298.

12. Hooper M, Hardy K, Handyside A, et al. HPRT-deficient mice (Lesch-Nyhan) mouse embryos derived from germline colonization by cultured cells. Nature 1987;32(6)295-298.

13. Wu C, Melton DW. Production of a model for Lesch-Nyhan syndrome in hypoxanthine phosphoribosyltransferase-deficient mice. Nat Genet 1993;3:235-240.

14. Sicinski P, Geng Y, Ryder-Cook AS, et al. The molecular basis of muscular dystrophy in the mdx mouse: a point mutation. Science 1989;244(4912):1578-1580.

15. Grady RM, Teng H, Nichol MC, et al. Skeletal and cardiac myopathies in mice lacking utrophin and dystrophin: a model for Duchenne Muscular Dystrophy. Cell 1997;90(4):729-738.

16. Deconinck AE, Rafael JA, Skinner JA, et al. Utrophin-dystrophin-deficient mice as a model for Duchenne Muscular Dystrophy. Cell 1997;90(4):717-727.

17. Liao B, Zhang J. Null mutations in human and mouse orthologs frequenlty result in different phenotypes. Proc Natl Acad Sci USA 2008;105(19):6987-6992.

18. Deng HX, Hentati A, Tainer JA, et al. Amyotrophic lateral sclerosis and structural defects in Cu,Zn superoxide dismutase. Science 1993;261(5124):1047-1051.

19. Gurney M, Pu H, Chiu A, et al. Motor neuron degeneration in mice that express a human Cu, Z superoxide dismutase mutation. Science 1994;264(5166):1772-1775.

20. Sagai T, Hosoya M, Mizushina Y, et al. Elimination of a long-range cis-regulatory module causes complete loss of limb-specific Shh expression and truncation of the mouse limb. Development 2005;132(4):797-803.

21. Lettice L, Heaney S, Purdie L, et al. A long-range Shh enhancer regulates expression in the developing limb and fin and is associated with preaxial polydactyly. Hum Mol Genet 2003;12(14):1725-1735.

22. Mills AA, Bradley A. From mouse to man: generating megabase chromosome rearrangements. Trends Genet 2001;17(6):331-339.

CHAPTER 4: DCHS1 is a LIX1 interacting partner

Abstract

LIX1, the candidate feline SMA disease gene, has no known function. A yeast two-hybrid screen of a human fetal brain cDNA library was conducted to identify putative LIX1 interacting partners and thus assign a function for LIX1. This screen of 2×10^7 clones identified twelve unique preys, three of which were identified multiple times. Confirmation of the protein interactions was accomplished by *in vitro* co-immunoprecipitation and band shift assays. The cytoplasmic domain of Dachsous1 (DCHS1) was identified 20 times in the yeast two-hybrid screen and was the only prey that had a confirmed interaction with LIX1 *in vitro*. GFP-tagged Lix1 and Lix1alt, a murine specific transcript from an alternative promoter, both co-localized strongly with DsRed-tagged Dchs1 in tranfected Cos7 and NSC34 cells. However no interaction between Lix1 and Dchs1 was detected in co-immunoprecipitation experiments of Cos7 and NSC34 cell lysate. The large GFP and DsRed tags may interfere with the interaction between Dchs1 and Lix1, as another group has recently reported the successful co-immunoprecipitation of these proteins from cultured cells. Nothing is yet known about the function of DACHSOUS1 in vertebrates; therefore, the role of the LIX1 and DACHSOUS interaction remains unclear.

Introduction

The putative feline SMA disease gene, *LIX1*, is poorly annotated. Prior to our laboratory's report in 2006, there were only two other published reports on *LIX1*. These were two *in situ* hybridization studies, one in chicken and one in mouse, which demonstrated *LIX1* expression in the developing limb bud, facial primordia and central nervous system, particularly in spinal cord lower motor neurons and dorsal root ganglia (1, 2). Semi-quantitative RT-PCR by our lab confirmed that *LIX1* is expressed in the central nervous system and most strongly in the spinal cord (3). The deduced amino acid sequence (282 residues) of feline LIX1 is highly conserved among dog (99% identical), human (97%), cow (97%), mouse (92%), chicken (85%), and *Drosophila melanogaster* (51%). Residues 22-99 of LIX1 are predicted by computerized secondary structure analysis to fold into a double-stranded RNA-binding domain (see Chapter 5); however no other conserved protein domains were identified. With the relatively little information available about LIX1 it was difficult to propose pathogenic mechanisms by which loss of LIX1 resulted in feline SMA. Therefore, I undertook a yeast two-hybrid screen to identify putative LIX1 interacting partners and thus impute a function for LIX1. Interactions between LIX1 and proteins identified by yeast two-hybrid were confirmed by *in vitro* co-immunoprecipitation and band shift assays. The interaction between LIX1 and DACHSOUS1 was further investigated by confocal microscopy and co-immunoprecipitation from cultured cells.

Material and Methods

Yeast Two-Hybrid Analysis

The human LIX1 open reading frame was PCR amplified from a full-length cDNA IMAGE clone (ID #: 5264055) in a 50 μl reaction containing a final concentration of 250 μM dNTPs (Invitrogen, Carlsbad, CA), 0.05 U/μl AmpliTaq Gold® DNA polymerase and 10 mM Tris-HCl, pH 8.3, 50 mM KCl, 1.5 mM $MgCl_2$, and 0.001% gelatin (Applied Biosystems, Carlsbad, CA)

with 250 nM of primers 5'-TTTTCATATGGACATAACCTTGGAATCT-3' and 5'-TTTTCCCGGGCTAGTGATAGGCCACACAGGGC'-3' (MSU Macromolecular Structure Core, East Lansing, MI) to introduce NdeI and XmaI restriction sites. Thermocycling conditions were as follows: 2 minutes 95°C initial denaturation, 35 cycles at 94°C for 30 seconds (s), 62°C for 30 s, and 72°C for 1 minute and a final extension at 72°C for 10 minutes. The PCR product and pGBKT7 vector (Clontech Laboratories, Mountainview, CA) were double digested with NdeI and XmaI (New England Biolabs, Ipswich, MA) restriction enzymes according to manufacturer's recommendations. The digested vector and insert were ligated with T4 DNA ligase (Promega, Madison, WI) according to manufacturer's specifications and transformed into chemically competent *Escherichia coli* (*E. coli*) DH5α by heat shock. The pGBKT7-hLIX1 vector was purified from overnight liquid cultures with the Qiaprep Spin Miniprep kit (Qiagen, Hilden, Germany), and the insert was sequenced at the University of Michigan DNA Sequencing Core (Ann Arbor, MI) with the T7 sequencing primer and 3' DNA-BD sequencing primer (Qiagen).

Saccharomyces cerevisiae (*S. cerevisiae*) strain AH109 was transformed with pGBKT7-hLIX1 by the lithium acetate mediated method as described in the Matchmaker™ Gal4 Two-Hybrid System 3 Yeast Protocols Handbook (Clontech Laboratories). AH109 yeast expressing GAL4-LIX1 were mated with *S. cerevisiae* strain Y187 that was pre-transformed with a human fetal brain cDNA library (Clontech Laboratories). Diploid yeast were selected and tested for activation of yeast-two hybrid reporter genes on minimal medium containing 5-bromo-4-chloro-3-indolyl α-D-galactopyranoside (Glycosynth, Warrington, England) and lacking leucine, tryptophan, adenine and histidine. Bait and prey vectors were extracted from yeast-two hybrid positive clones by lyticase/SDS lysis and Qiaprep Spin Miniprep kit purification (Qiagen). Prey vector (pGADT7) inserts were PCR amplified as described above except with primers 5'-CGATGATGAACATACCCCACCA-3' and 5'-TGGTGCACGATGCACAGTTG-3'. Thermocycling conditions were as follows: 2 minutes 95°C initial denaturation, 35 cycles at 94°C for 30 s, 62°C

for 30 s, and 72°C for 3 minutes and a final extension at 72°C for 10 minutes. PCR products were sequenced with the T7 sequencing primer at the University of Michigan DNA Sequencing Core and the sequences were compared to the human genomic plus transcript DNA database with the BLAST computer algorithm on the National Center for Biotechnology Information (NCBI) website.

In vitro co-immunoprecipitation

Myc-tagged hLIX1 and HA-tagged prey proteins were *in vitro* transcribed and translated according to manufacturer's specifications with the T_NT® Quick Coupled T7 Transcription/Translation System (Promega) and Redivue L-[^{35}S] methionine (GE Healthcare, Waukesha, WI) from yeast two hybrid system vectors. Ten μl of c-Myc-hLIX1 was incubated at room temperature for one hour with ten μl of HA-tagged prey proteins. Complexes were immunoprecipitated with 5 μl of either mouse anti-c-Myc monoclonal antibody (Clontech) or mouse anti-HA monoclonal antibody (Sigma Aldrich, Saint Louis, MO) and 10 μl Protein A agarose beads (Sigma). Immunoprecipitates were washed three times with 500 μl of 20 mM Tris HCl pH 8.0, 137 mM NaCl, 1% nonidet P-40, 2 mM EDTA, 1 mM N-ethylmaleimide and 1 mM phenylmethylsulfonyl fluoride. Proteins were eluted in 15 μl of 1x SDS sample buffer (50 mM Tris HCl pH 6.8, 2% SDS, 0.1% bromophenol blue, 10% glycerol, 100 mM dithiothreitol) at 80°C for 5 minutes. Eluted proteins were separated on 10% SDS-polyacrylamide gels. Gels were fixed for 30 minutes in 50% methanol, 10% acetic acid and vacuum dried to 3M Whatman paper. Gels were exposed to phosphor screens overnight and visualized by autoradiography.

In vitro band shift assays

Three μl of *in vitro* transcribed and translated c-Myc-LIX1 and three μl of HA tagged prey protein were incubated at room temperature for five to sixty minutes. Samples were loaded onto 13% polyacrylamide,10 mM MOPS-KOH pH 6.8 gels or 13% polyacrylamide, 37.5 mM Tris-

glycine pH 8.8 gels and run at 4°C, 175 V for 2 hrs in 10mM MOPS-KOH pH 6.8 or 25 mM Tris, 192 mM glycine pH 8.3, respectively. Gels were fixed and dried as described above and then exposed to phosphor screens overnight and visualized by autoradiography.

Cloning of mammalian expression vectors

Mouse spinal cord total RNA was extracted and reverse transcribed as described in Chapter 3. The open reading frames of *Lix1* and *Lix1alt* with and without a stop codon were PCR amplified to introduce flanking attB1 and attB2 λ recombination sites in 50 μl reactions containing a final concentration of 250 nM forward and reverse primers (see below) (Integrated DNA Technologies, Coralville, IA), 1 mM dNTPs (Invitrogen) and 0.02 U/μl Phusion® DNA polymerase and 1x Phusion® HF buffer (New England Biolabs). Thermocycling conditions for *Lix1* were as follows: 30 s 98°C initial denaturation, 35 cycles at 98°C for 10 s, 58°C for 30 s, and 72°C for 45 s and a final extension at 72°C for 10 minutes. Thermocycling conditions for *Lix1alt* were identical except that the annealing temperature was 56°C and the extension time was 30 s. PCR products were purified with the Wizard® SV Gel and PCR Clean-Up System (Promega) and cloned into pDONR™221 vector (Invitrogen) by λ recombination with the BP Clonase™ enzyme according to manufacturer's recommendations (Invitrogen). Chemically competent *E. coli* DH5α were transformed by heat shock wth 5 μl of the BP Clonase™ reaction and transformants were selected for on LB/kanamycin plates. Plasmid DNA was purified from kanamycin resistant clones with PureYield™ Plasmid Miniprep System (Promega) and sequenced at the University of Michigan DNA Sequencing Core (Ann Arbor, MI) with M13 forward and reverse sequencing primers. After sequence verification, *Lix1* and *Lix1alt* inserts were cloned into pcDNA-DEST47 and pcDNA-DEST53 vectors with LR Clonase™ enzyme according to manufacturer's instructions (Invitrogen). Chemically competent *E. coli* DH5α were

transformed by heat shock wth 5 µl of the LR Clonase™ reaction and transformants were selected for on LB/ampicillin plates. Plasmids were purified from ampicillin resistant clones with the PureYield™ Plasmid Midiprep System (Promega) for transfections.

Lix1 without stop codon F and R:

5'-GGGGACAAGTTTGTACAAAAAAGCAGGCTTCACCATGGACAGAACCTTGGAATC-3' and

5'-GGGGACCACTTTGTACAAGAAAGCTGGGTCATGATAGCCACACAGAGC-3'

Lix1 with stop codon F and R:

5'-GGGGACAAGTTTGTACAAAAAAGCAGGCTTCATGGACAGAACCTTGGAATC-3' and 5'-

GGGGACCACTTTGTACAAGAAAGCTGGGTCCTAATGATAGCCACACAGA-3'

Lix1alt without stop codon F and R:

5'-GGGGGACAAGTTTGTACAAAAAAGCAGGCTTCACCATGCCCTTGGATTTTCTGT-3' and

5'-GGGGACCACTTTGTACAAGAAAGCTGGGTCATGATAGCCACACAGAGC-3'

Lix1alt with stop codon F and R:

5'-GGGGACAAGTTTGTACAAAAAAGCAGGCTTCATGCCCTTGGATTTTCTGT-3' and 5'-

GGGGACCACTTTGTACAAGAAAGCTGGGTCCTAATGATAGCCACACAGA-3'

Nucleotides 1 through 723 of *Dchs1* cDNA were PCR amplified in a 50 µl reaction containing a final concentration of 250 µM dNTPs (Invitrogen, Carlsbad, CA), 0.02 U/µl Phusion® DNA polymerase and 1x Phusion® HR buffer with 250 nM of primers 5'-TTTTAAGCTTACCATGCAGAAGGAGCTGAGTGTC-3' and 5'-TTTTGAATTCGTCCAGAAGTGTCACATCTAGC-3' (Integrated DNA Technologies), to introduce HindIII and EcoRI restriction sites. Thermocycling conditions were as follows: 30 s 98°C initial denaturation, 35 cycles at 98°C for 10 s, 62°C for 30 s, and 72°C for 45 s and a final extension at 72°C for 10 minutes. Nucleotides 8754 to 9873 of Dchs1 cDNA were PCR amplified as above with primers 5'-TTTTGAATTCGCACCTGACCTCAACTTGCTA-3' and 5'-

TTTTGGTACCGTGATGCGCAGCTCTGTGTCATC-3' (Integrated DNA Technologies), to introduce EcoRI and KpnI restriction sites. Thermocycling conditions were as above except for a 60°C annealing temperature. PCR products were analyzed by agarose gel electrophoresis. The N-terminal PCR product was double digested with HindIII and EcoRI restriction enzymes according to manufacturer's recommendations, and the C-terminal PCR product was double digested with EcoRI and KpnI accord to manufacturer's recommendations (New England Biolabs). The vector, pDsRed-Monomer-N1 (Clontech), was double digested with HindIII and KpnI and all three digestion products were ligated with T4 DNA ligase according to manufacturer's directions (Promega) and transformed into chemically competent *E. coli* DH5α by heat shock. The pDsRed-Monomer-N1-Dchs1ΔECD plasmid was purified from kanamycin resistant clones with the PureYield™ Plasmid Miniprep System (Promega) and sequenced with at the University of Michigan DNA Sequencing Core with the following primers: 5'-CTTGGAGCCGTACTGGAACT-3' and 5'-GGAGGTCTATATAAGCAGAG-3'.

Dchs1ΔECD lacking the last 300 nucleotides (Dchs1ΔECDΔC) was PCR amplified from pDsRed-Monomer-N1-Dchs1ΔECD as above with primers 5'-TTTTAAGCTTACCATGCAGAAGGAGCTGAGTGTC-3' and 5'-TTTTGGTACCCTTATCGTCGTCATCCTTGTAATCAATACGGGGAGCTGGAGGAC-3' to introduce flanking HindIII and KpnI restriction sites and FLAG tag. Thermocycling conditions were as above except for a 57°C annealing temperature. The PCR product was cloned into pDsRed-Monomer N1 via the HindIII and KpnI restrictions sites, transformed, purified and sequenced as described above. Both pDsRed-Monomer-N1-Dchs1ΔECD and pDsRed-Monomer-N1-Dchs1ΔECDΔC were purified from transformed *E. coli* DH5α with the PureYield™ Plasmid Midiprep System (Promega) for transfections.

Rabbit anti-Dchs1 custom antibody

Custom anti-mouse Dchs1 peptide sera and affinity-purified antibodies were generated by immunizing rabbits with synthetic peptide CTESGLEPPDDTELR (Dchs1 residues 3277-3291) at ProSci (Poway, CA). For western blots and immunocytochemistry experiments to test the Dchs1 antibody, the affinity-purified antibody was incubated overnight a 4°C with five fold immunizing peptide in PBS, pH 7.4 or PBS alone. The antibody was centrifuged for 1 minute at 4°C 14,000 x *g* to pellet any aggregate, and the supernatant was used as the primary antibody for western blots and immunocytochemistry.

Cell culture and transfection

Cos7 cells (provided by Dr. Karen Friderici) were cultured in Dulbecco's Modified Eagle Medium (D-MEM) with 1,000 mg/L glucose, 110 mg/L sodium pyruvate, 2 mM L-glutamine and 10% fetal bovine serum (FBS) (Invitrogen) at 37°C, 5% CO_2. Cos7 cells were passaged 1:4 when they were ~95% confluent. Cos7 cells grown in 60 mm dishes or sterile glass coverslips were transfected with *Lix1*, *Lix1alt* and *Dchs1* expression vectors with Lipofectamine™ 2000 according to manufacturer's recommendations (Invitrogen). Twenty-four to 48 hours after transfection, cells were harvested for western blots or those grown on coverslips were fixed in 4% paraformaldehyde in 100 mM phosphate buffered saline (PBS), pH 7.4. Coverslips were washed three times in PBS, pH 7.4 and then dehydrated in graded ethanol washes before being mounted on glass slides in SlowFade® Gold antifade reagent with DAPI (Invitrogen).

NSC34 cells (provided by Dr. William Atchison) were maintained in D-MEM with 4.5 g/L d-glucose, 100 mg/L sodium pyruvate, 2 mM L-glutamine, 5-10% FBS (Invitrogen) and 1x antibiotic-antimycotic (15240-096, Invitrogen) at 37°C, 5% CO_2. Cells were passaged 1:4 when 95% confluency was reached. To differentiate NSC34 cells and induce neuritogenesis, cells were cultured in Ham's F12 medium with 1% FBS. NSC34 cells grown in 60 mm dishes or on

sterile glass coverslips were transfected with Fugene® HD at a ratio of 8 μl transfection reagent to 2 μg expression vector according to manufacturer's instructions (Roche Applied Science, Basel, Switzerland). Eight hours after transfection, mediim was replaced with Ham's F12/1% FBS or fresh high glucose D-MEM/10% FBS. Cells in dishes were harvested for reverse transcriptase-polymerase chain reaction and western blots or cells on coverslips were fixed in 4% paraformaldehyde in PBS, pH 7.4 for immunocytochemistry.

Reverse transcriptase polymerase chain reaction (RT-PCR)

Total RNA from cultured NSC34 cells was extracted with PureLink™ RNA Mini kit according to manufacturer's instructions (Invitrogen). RNA was analyzed by gel electrophoresis and spectrophotometry. One μg of total RNA was reverse transcribed at 50°C for 50 minutes with SuperScript III® and oligo dT_{20} (Invitrogen) according to manufacturer's recommendations or with no added reverse transcriptase (no RT). Two μl of cDNA amplification reactions or no RT reactions were PCR amplified in 50 μl reactions containing a final concentration of 250 nM forward and reverse primers (Integrated DNA Technologies), 1 mM dNTPs (Invitrogen) and 0.05 U/μl Choice-Taq™ DNA polymerase and 10 mM Tris-HCl, pH 9.0, 10 mM KCl, 1.5 mM $MgSO_4$, 8 mM $(NH_4)_2SO_4$, 1.5 mM $MgCl_2$, and 0.05% NP-40 (Denville Scientific, South Plainfield, NJ). Cycling conditions for *Lix1* and *Dchs1* amplification were initial denaturation at 95°C for 2 minutes (min), 35 cycles of 30 s denaturation at 94°C, 30 s primer annealing at 60°C, 1 min extension at 72°C and final extension at 72°C for 10 min. Reaction conditions for *Lix1alt* were identical except that the annealing temperature was 62°C and the extension time was 30 s. Products were analyzed by agarose gel electrophoresis. Primers used for cDNA amplification by PCR are listed below.

Lix1 F: 5'-CCAGCCTGTCAGCCAGCCTTT-3'

Lix1 and *Lix1alt* R: 5'-ACCTGCCACCTGGCCTTGCT-3'

Lix1alt F: 5'-TCCTGCTGCGCTGAGGAACC-3'

Dchs1 F: 5'-CAGCGCCATTCTCTCCGTCTCT-3'

Dchs1 R: 5'-CCTCAAGGCACCCGAGTTCTCA-3'

Immunocytochemistry

NSC34 cells were cultured and transfected on sterile glass coverslips as described above. After 24 hours in Ham's F12 medium with 1% fetal bovine serum, cells were rinsed with phospate buffered saline, pH 7.4, and fixed for 30 minutes in 4% paraformaldehyde in phosphate buffered saline (PBS), pH 7.4. Cells were then permeabliized with ice-cold acetone for 5 minutes. After 3 washes with PBS, cells were blocked with 10% normal goat serum in PBS with 0.1% Tween 20 (PBST). Cells were then incubated overnight at 4^{o}C in rabbit anti-Dchs1 polyclonal antibody (1:100 dilution; ProSci, Poway, CA) and/or mouse anti-neurofilament heavy subunit (NF-H) monoclonal antibody (1:500 dilution of SMI-32; AbCam, Cambridge, MA). Cells were washed 3 times with PBS prior to a 2 hour incubation at room temperature in goat anti-rabbit IgG Alexa Flour® 488 (1:500) and/or goat anti-mouse IgG Alexa Fluor® 350 (Invitrogen, Carlsbad, CA). After washing with PBS, coverslips were mounted onto glass slides with Prolong Gold antiFade (Invitrogen) and sealed with clear nail polish.

Confocal laser scaning microscopy

Immunolabeled cells or transfected cells were imaged for fluorescence on an Olympus Fluoview 1000 laser-scanning microscope (Center Valley, PA) equipped with a 40x (NA=1.3) and 60x (NA=1.42) oil immersion objectives. Fluorescence of Alexa Fluor® 350 labeled NF-H (blue) or DAPI stained nuclei was excited at 405 nm and emission was detected through a 430-470 nm band pass filter. Fluorescence of GFP tagged Lix1 and Lix1alt or Alexa Fluor® 488 labeled Dchs1 (green) was excited at 488 nm and emission detected through a 505-525 nm band pass filter. Fluorescence of DsRed tagged Dchs1 (red) was excited at 543 and emission

was detected through a LP 560 nm filter. Co-localization of Lix1 or Lix1alt with Dchs1 was determined in red-green merged images that were optimized for brightness and contrast with Fluoview v5 software.

In vivo co-immunoprecipitation

Cos7 or NSC34 cells were transfected with Lix1 and Dchs1 expression vectors as described above. Twenty-four hours after transfection, cells were harvested in 1 ml PBS, pH 7.4 and centrifuged at 3,000 x *g* for 3 minutes at 4°C. Cells were lysed on ice for ten minutes in 25 mM Tris-HCl pH7.4, 150 mM NaCl, 0.5% nonidet P-40, 0.02% NaN_3 and EDTA-free complete protease inhibitor cocktail (Roche Applied Science, Basel, Switzerland) with frequent vortexing. Lysate was cleared at 14,000 x *g* for 10 minutes at 4°C, and protein was quantified by Bradford assay (Bio-Rad Laboratories, Hercules, CA). Seven hundred and fifty µg of total protein was incubated overnight at 4°C with 20 µl of rabbit anti-GFP sepharose beads (AbCam, Cambridge, MA). Beads were washed three times with Tris-buffered saline (25 mM Tris, 150 mM NaCl pH 7.2 with EDTA-free complete protease inhibitor cocktail), and protein was eluted in 1x non-reducing SDS sample buffer (50 mM Tris HCl pH 6.8, 2% SDS, 0.1% bromophenol blue, 10% glycerol) at 100°C for 5 minutes. Proteins were separated by electrophoresis on 10% SDS-acrylamide gels and analyzed by western blotting.

Western blots

After SDS-PAGE, proteins were transferred to PVDF membrane (Millipore, Billerica, MA) at 4°C 20 V overnight or 100 V for 1 hour. Membranes were blocked for 1 hour at room temperature in 5% non-fat milk in 20 mM Tris-HCl pH 7.4, 150 mM NaCl and 0.1% Tween 20 (TBST). Primary antibodies were appropriately diluted with 5% non-fat milk in TBST and membranes were incubated in the dilution overnight at 4°C. After four TBST washes, membranes were incubated for 2 hours at room temperature in diluted secondary antibodies.

Signals were visualized with enhanced chemiluminescence (ECL) plus detection kit (PerkinElmer, Waltham, MA) after four more TBST washes. When necessary, blots were stripped in 200 mM glycine, 0.1% SDS, 1% Tween 20 pH 2.2 followed by two PBS, pH 7.4 washes and a TBST wash. Membranes were re-hydrated in methanol and washed once with TBST prior to blocking and incubation in another primary antibody. Antibodies used for western blots are listed below.

Primary Antibody	Working Dilution	Manufacturer
rabbit anti-GFP polyclonal	1:2000	Invitrogen (Carlsbad, CA)
goat anti-GFP polyclonal	1:2500	AbCam (Cambridge, MA)
rabbit anti-Dchs1 polyclonal	1:1000	ProSci Incorporated (Poway, CA)
mouse anti-FLAG monoclonal M2	1:500	Sigma-Aldrich (Saint Louis, MO)
Living Colors® DsRed rabbit polyclonal	1:1000	Clontech (Mountainview, CA)
mouse monoclonal to alpha tubulin	1:1000	AbCam (Cambridge, MA)

Secondary Antibody	Working Dilution	Manufacturer
rabbit anti-mouse IgG (whole molecule) peroxidase	1:80,000	Sigma-Aldrich
goat anti-rabbit IgG (whole molecule) peroxidase	1:80,000	Sigma-Aldrich
donkey anti-goat IgG horseradish peroxidase	1:5000	Santa Cruz Biotechnology (Santa Cruz, CA)

Results

For the yeast two-hybrid screen, a GAL4-DBD-LIX1 fusion protein bait was used to screen a human fetal brain cDNA library. A screen of >2 x 10^7 clones resulted in 54 reporter-positive interactions. Sequencing the cDNA insert of the prey plasmid and a BLAST search of the human genomic and transcript database determined identity of each interacting prey protein. Table 4.1 summarizes the identified LIX1 interacting partners, some of which were identified

Table 4.1. Putative LIX1 interacting proteins identified by yeast-two hybrid analysis.

Candidate Interacting Protein	Gene Symbol	Function	# of clones
Bromodomain adjacent to zinc finger domain 2B	*BAZ2B*	Unknown	1
Chromosome 6 open reading frame 134	*C6orf134*	Unknown	1
Chromosome 11 open reading frame 17	*C11orf17*	Unknown	1
Dachsous1	*DCHS1*	planar cell polarity, proximal-distal patterning	20
Deleted in azoospermia associated protein 2	*DAZAP2*	Unknown	1
Electron transport flavoprotein α subunit	*ETFA*	electron transfer from dehydrogenases to mitochondrial respiratory chain	2
Leucine zipper, putative tumor suppressor 2	*LZTS2*	putative - cell cycle control	1
Mitochondrial ribosomal protein subunit 6	*MRPS6*	translation of mitochondrial encoded polypeptides	1
n-myc downstream regulated gene 4	*NDRG4*	putative - neurite outgrowth	2
Splicing factor 3A 60 kDa subunit	*SF3A3*	subunit of snRNP2	1
Zinc finger protein 33A	*ZNF33A*	Unknown	1
Zinc finger protein 74	*ZNF74*	Unknown	1

multiple times. The preys listed below represent 34 of the positive interaction clones; the remaining 17 clones could not be amplified or did not represent any known transcript. Of these putative interacting proteins, four have fairly well described functions. Dachsous1 (DCHS1) is a cell-surface adhesion and signaling protein that has been extensively studied in *Drosophila melanogaster* and found to play a role in the proximal-distal patterning of the wings and legs (4). The electron transfer flavoprotein α subunit is one of two protein subunits involved in the transfer of electrons from several dehydrogenases to the mitochondrial respiratory chain (5). The mitochondrial ribosomal protein subunit 6 is a nuclear encoded protein that is involved in translation of the thirteen polypeptides encoded in the mitochondrial genome, including subunits of the respiratory chain (6). Finally, splicing factor 3A 60 kDa subunit is one of three subunits of splicing factor 3A, itself a subunit of the U2 snRNP which recognizes the 3' splice site in pre-mRNA (7). The functions of C11orf17, DAZAP2 and NDRG4 have yet to be determined. However, RNA interference experiments demonstrated that reduced NDRG4protein resulted in decreased neurite outgrowth in rat pheochromocytoma (PC12) cells differentiated with nerve growth factor (8). Although the yeast two-hybrid system is useful for identifying novel protein interactions, disadvantages of the yeast two-hybrid system are 1) that there is a significant false positive rate, 2) protein-protein interactions identified in the yeast nucleus may not occur in mammalian cells where the proteins may be compartmentalized differently and 3) the temporal and spatial expression of the two proteins may differ. Therefore, it is necessary to confirm putative protein interactions through biochemical methods.

An *in vitro* co-immunoprecipitation (co-IP) assay was employed to examine the interaction of LIX1 with seven preys, C11ORF17, DAZAP2, DCHS1, ETFA, MRPS6, NDRG4, and SF3A3. Although not implicated by yeast two-hybrid, an interaction between LIX1 and SMN1 was also investigated by *in vitro* co-IP. A representative autoradiogram from the *in vitro* co-IPs is shown in Figure 4.1A. DCHS1 was the only protein to reciprocally immunoprecipitate with LIX1 (Figure 4.1A lanes 7 and 8). The co-IP results were confirmed by band shift assays on

Figure 4.1. Representative autoradiograms of *in vitro* co-IP band shift assays. (A) *in vitro* co-IP of LIX1 with DCHS1 and NRDG4 demonstrates that LIX1 co-immunoprecipitates with DCHS1 but not NDRG4. Lane 1: LIX1 10% input; Lane 2: LIX1 + anti c-myc; Lane 3: LIX1 + anti HA-Tag; Lane 4: DCHS1 10% input; Lane 5: DCHS1 + anti c-myc; Lane 6: DCHS1 + anti HA-Tag; Lane 7: LIX1 + DCHS1 + anti c-myc; Lane 8: LIX1 + DCHS1 + anti HA-Tag; Lane 9: NDRG4 10% input; Lane 10: NDRG4 + anti c-myc; Lane 11: NDRG4 + anti HA-Tag; Lane 12: LIX1 + NDRG4 + anti c-myc; Lane 13: LIX1 + NDRG4 + anti HA-Tag. (B) Band shift assay (pH 6.8) of LIX1 with DCHS1 and SF3A3. Lane 1: LIX1; Lane 2: DCHS1; Lane 3: LIX1 + DCHS1; Lane 4: LIX1; Lane 5: SF3A3; Lane 6: LIX1 + SF3A3. (C) Band shift assay (pH 8.8) of LIX1 and DCHS1. Lane 1: LIX1; Lane 2: DCHS1; Lane 3: LIX1 + DCHS1.

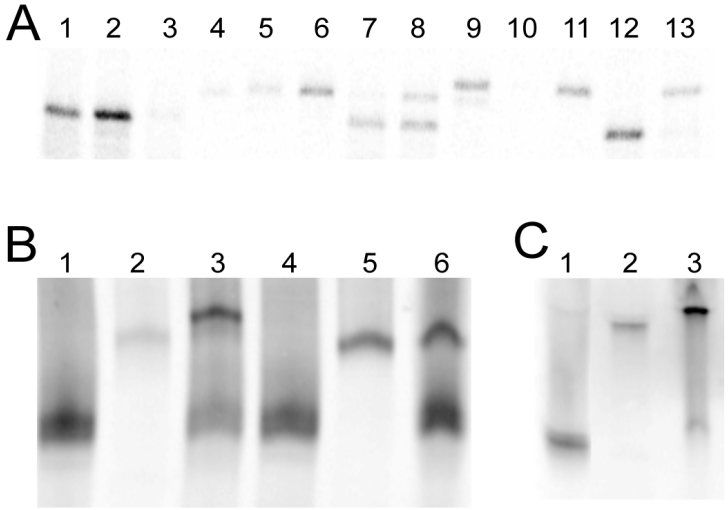

Figure 4.2. Representative confocal laser scanning microscopy images of GFP-Lix1 and GFP-Lix1alt transfected Cos7 cells. (A-F) GFP-Lix1 transfected cells. (G-L) GFP-Lix1alt transfected cells. (A, D, G, J) DAPI (blue) fluorescence. (B, E, H, K) GFP (green) fluorescence. (C, F, I, L) Blue- green merged images. In A-F and J-L, bars = 20 μm. In G-I, bars = 50 μm.

Figure 4.2 continued.

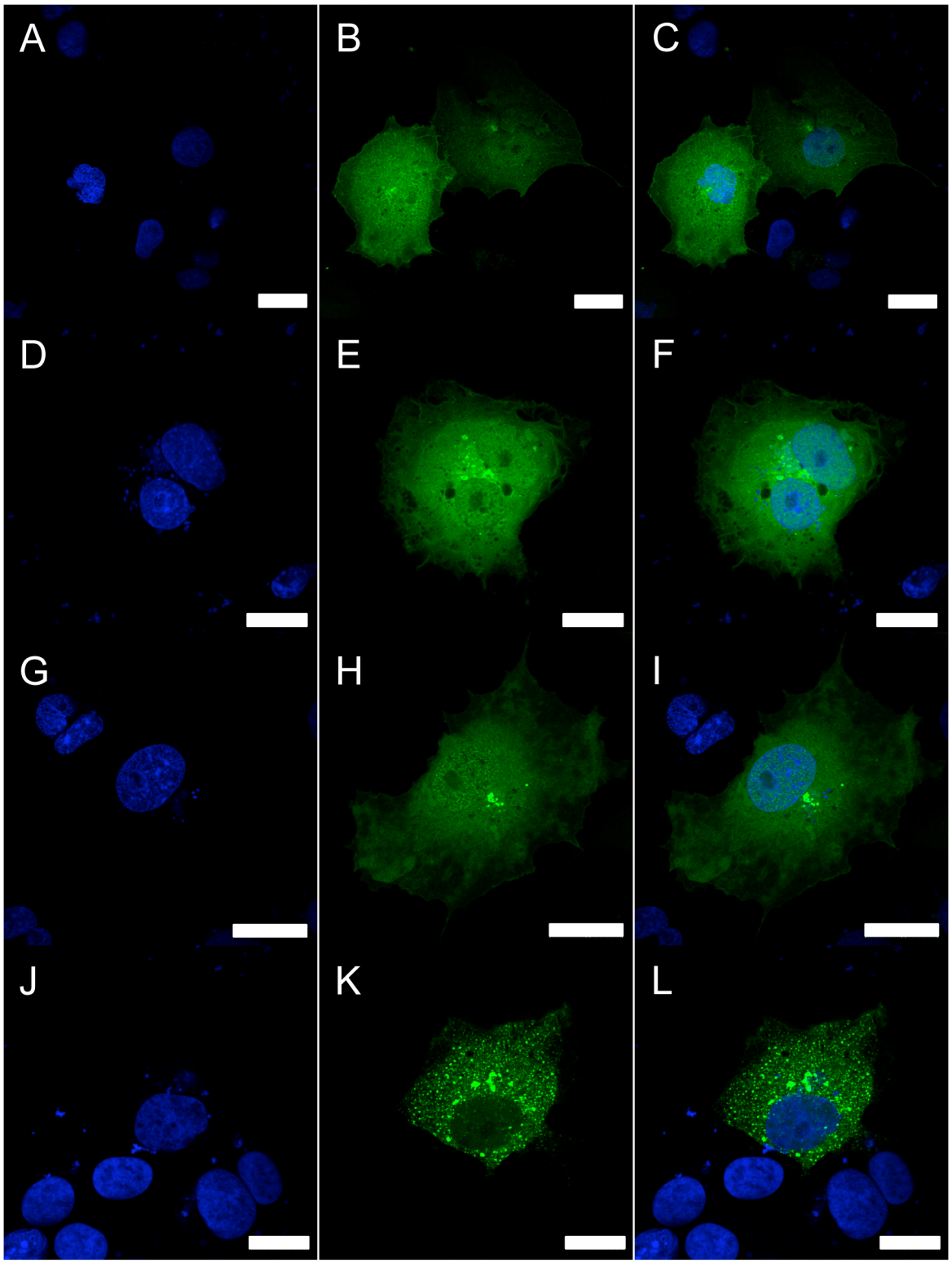

native polyacrylamide gels, pH 6.8 (Figure 4.1B) and pH 8.8 (Figure 4.1C), A shift in gel mobility was seen when LIX1 and DCHS1 were incubated together. No such shift was seen with LIX1 and SF3A3. In agreement with the co-IP results, a mobility shift was not detected with LIX1 and any of the other proteins examined (results not shown). Therefore, of the proteins identified in the yeast two-hybrid, only LIX1 and DCHS1 interact *in vitro.*

Next the co-localization of Lix1 or Lix1alt (see Chapter 3) with Dchs1 was examined in transfected Cos7 cells. When transfected alone, GFP-Lix1 localizes to the nucleus and cytoplasm of Cos7 cells (Figure 4.2A-F). A similar expression pattern is seen with GFP-Lix1alt (Figure 4.2G-L). In some cells, there were granules of GFP-Lix1alt (Figure 4.2J-L), however, this may have been an artifact of over-expression. Due to the large size of Dchs1 (>3000 amino acids), a Dchs1 deletion construct with C terminal DsRed tag was cloned. This deletion construct, called pDsRed-Monomer-N1-Dchs1ΔECD, contained the sequences coding for the endogenous Dchs1 signal peptide, the first extracellular cadherin domain, the transmembrane domain, and cytoplasmic domain. As Lix1 is an intracellular protein, the cytoplasmic domain of Dchs1 is the only domain that could interact with Lix1. Furthermore, the cytoplasmic domain of DCHS1 was sufficient to interact with LIX1 *in vitro*. Therefore, if Lix1 and Dchs1 interact *in vivo*, the Dch1ΔECD-DsRed protein should contain the required residues for that interaction. When transfected together, GFP-Lix1 no longer localized to the nucleus (Figure 4.3A-F). Expression of GFP-Lix1 was entirely cytoplasmic and co-localized strongly with Dchs1ΔECD-DsRED. GFP-Lix1alt also co-localized with Dchs1ΔECD-DsRED, however, GFP-Lix1alt was not excluded from the nucleus like GFP-Lix1. The co-localization of GFP-Lix1 and GFP-Lix1alt with Dchs1ΔECD-DsRed is consistent with an interaction between these proteins. Based on these results, the co-localization of Lix1 or Lix1alt with Dchs1 was examined in NSC34 cells.

The NSC34 cell line is a hybrid cell line created by the fusion of mouse neuroblastoma cells with motor neuron-enriched embryonic day 12-14 spinal cord cells (9). The resulting hybrid

Figure 4.3. Representative laser scanning confocal microscopy images of co-transfected Cos7 cells. (A-F) Cos7 cells co-transfected with GFP-Lix1 and Dchs1ΔECD-DsRed. (G-L) Cos7 cells co-transfected with GFP-Lixalt and Dchs1ΔECD-DsRed. (A, D, G, J) GFP (green) fluorescence. (B, E, H, K) DsRed (red) fluorescence. (C, F, I, L) Red-green merged images. In A-C, bars = 20 μm. In D-F and J-L, bars = 50 μm. In G-I, bars = 50 μm.

Figure 4.3 continued.

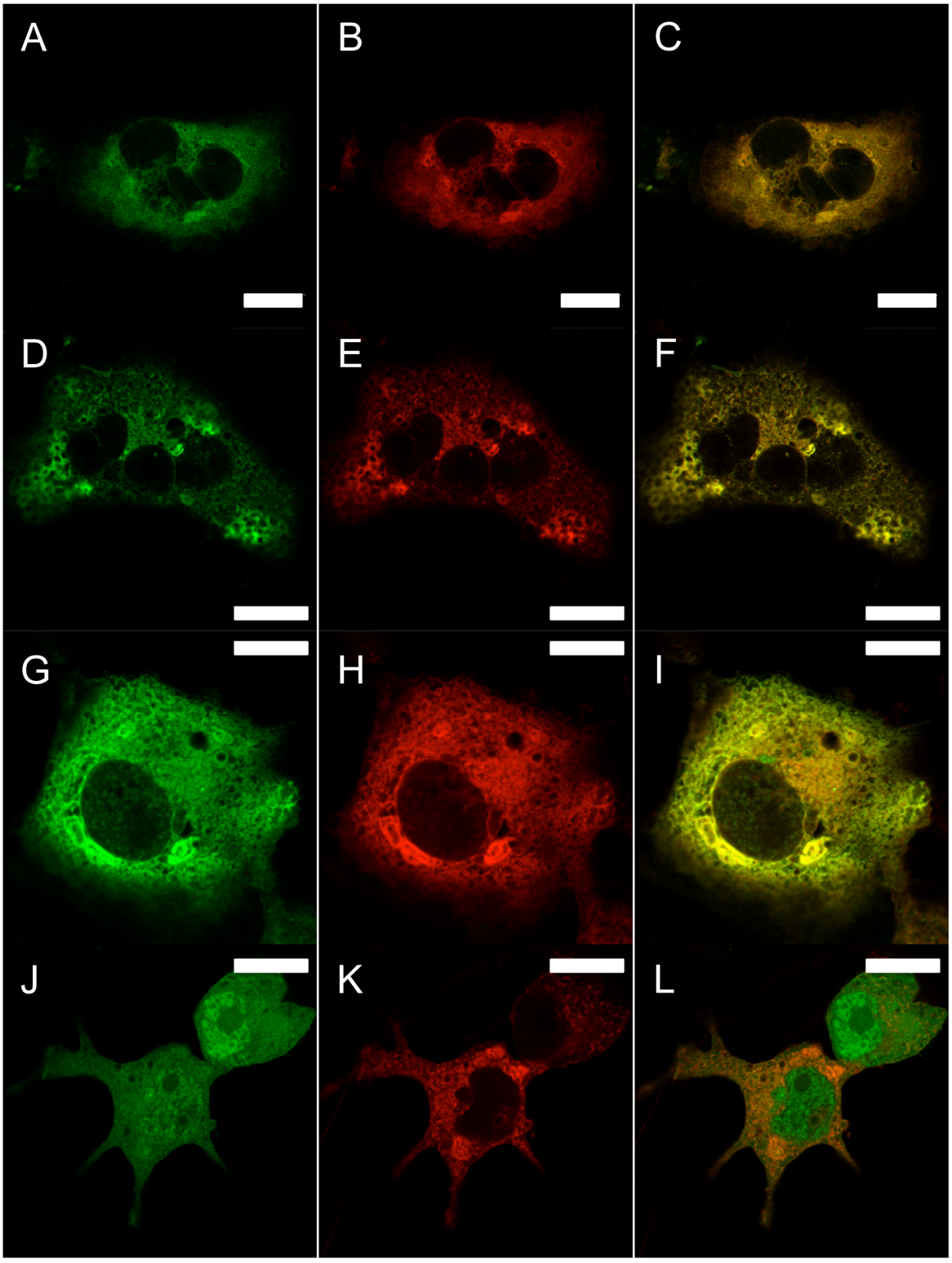

cell line is immortal and possesses several motor neuron characteristics. NSC34 cells synthesize and accumulate acetylcholine, extend neurites with well-defined growth cones and express the neurofilament triplet proteins. Furthermore, RT-PCR analysis of this cell line indicated endogenously expresses *Lix1*, *Lix1alt* and *Dchs1* (Figure 4.4). *Dchs1* was expressed in undifferentiated and differentiated cells, whereas, *Lix1* and *Lix1alt* were only expressed in differentiated cells. I was unable to examine endogenous Lix1 and Lix1alt localization because production of a custom LIX1 antibody was unsuccessful. Generation of a rabbit anti-Dchs1 peptide antibody was successful. This rabbit polyclonal antibody was suitable for both western blots (Figure 4.5) and immunocytochemistry (Figure 4.6). However, I was unable to immunoprecipitate either endogenous Dchs1 or Dchs1ΔECD-DsRed (data not shown). Endogenous Dchs1 in NSC34 cells localized to the periphery of the cell body and was found along neurites and within growth cones (Figure 4.6B and G). The expression pattern of Dchs1ΔECD-DsRed in NSC34 cells was very similar to endogenous Dchs1, thus it appear that the extra-cellular domain deletion does not impact the protein localization (Figure 4.6G-I).

As was seen in Cos7 cells, GFP-tagged Lix1 co-localized with Dchs1ΔECD-DsRed in NSC34 cells (Figure 4.7). Lix1 was located throughout the cell body, neurites and growth cones. The position of the tag either C-terminal (Figure 4.7A-D) or N-terminal (Figure 4.7E-H) did not affect the cellular distribution of Lix1 or its ability to co-localize with Dchs1ΔECD-DsRed. GFP-tagged Lix1alt also co-localized with Dchs1ΔECD-DsRed in the cell body, neurites and growth cones of NSC34 cells (Figure 4.8). Similar to results in Cos7 cells, GFP-tagged Lix1alt localized to the nucleus whereas GFP-tagged Lix1 did not. The co-localization of GFP-tagged Lix1 and GFP-tagged-Lix1alt with Dchs1ΔECD-DsRed is consistent with an interaction between these proteins.

Recently, Mao *et al*. (2009) demonstrated that LIX1 co-immunoprecipitated from Drosophila S2 cells with the intracellular domains of DACHSOUS (Ds) and a related planar cell

polarity protein, FAT (10). The last 100 amino acids of FAT and Ds are similar and were found to be important for the association of FAT and LIX1. Based on these results, I constructed another DsRed tagged Dchs1 expression construct that not only lacked the extracellular domain, but also the last 100 amino acids of the cytoplasmic domain. Since the C terminal deletion removes the peptide recognized by our custom Dchs1 antibody (Figure 4.5B), I also included a FLAG tag for future immunoprecipitations and western blots. When NSC34 cells were transfected with pDsRed-Monomer-N1-Dchs1ΔECDΔC-FLAG, localization of Dchs1ΔECDΔC-FLAG-DsRed was similar to Dchs1ΔECD-DsRed. However, the DsRed fluorescence intensity was always lower in cell expressing Dchs1ΔECDΔC-FLAG-DsRed than in cells expressing Dchs1ΔECD-DsRed. GFP tagged Lix1 and Lix1alt did co-localize with Dchs1ΔECDΔC-FLAG-DsRed (Figure 4.9); however, the apparent co-localization was strongly reduced when compared with Dchs1ΔECD-DsRed.

Since intracellular co-localization is consistent with but does not prove a physical interaction, I immunoprecipitated GFP-tagged Lix1 from transfected Cos7 and NSC34 cells and analyzed the precipitated complexes for the presence of Dchs1ΔECD-DsRed by western blots (Figure 4.10). I was unable to detect any Dchs1ΔECD-DsRed or Dchs1ΔECDΔC-FLAG-DsRed in any of the GFP immunoprecipitates from either Cos7 (Figure 4.10A) or NSC34 cells (Figure 4.10B). The reciprocal co-immunoprecipitations could not be performed because neither commercially available anti-DsRed antibodies nor our custom anti-Dchs1 antibody are suitable for immunoprecipitations. Therefore, these data do not support an interaction between Dchs1 and Lix1 under the conditions tested, but remain inconclusive.

Figure 4.4. RT-PCR analysis of NSC34 cells. Lane 1: 100 bp DNA ladder (New England Biolabs); Lane 2: mouse spinal cord with reverse transcriptase (RT); Lane 3: mouse spinal cord no RT control; Lane 4: undifferentiated NSC34 cells with RT; Lane 5: undifferentiated NSC34 cells no RT control; Lanes 6, 8, and 10: NSC34 cells differentiated for 24, 48 and 72 hours, respectively; Lanes 7, 9 and 11: no RT controls for lanes 6, 8 and 10; Lane 12: H_2O negative control.

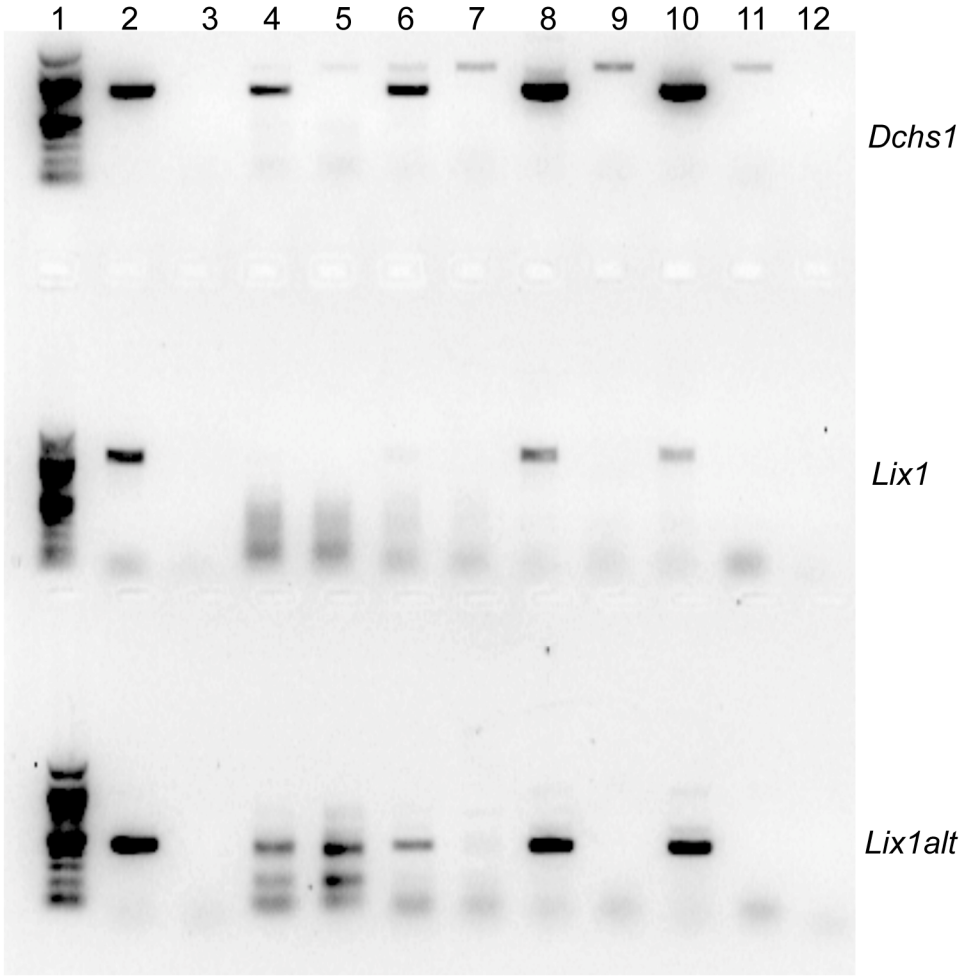

Figure 4.5. Representative results from western blots with our custom rabbit anti-Dchs1 antibody. (A) Immunoblot of mock transfected (Lane 1) and pDsRed-Monomer-N1-Dchs1ΔECD transfected (Lane 2) Cos7 cell lysate. Ten µg of protein were loaded into each well. (B) Immunoblot of pDsRed-Monomer-N1-Dchs1ΔECD (lane 1) or pDsRed-Monomer-N1-Dchs1ΔECDΔC-FLAG (lane 2) transfected NSC34 cell lysate. Fifteen µg of protein were loaded into each well.

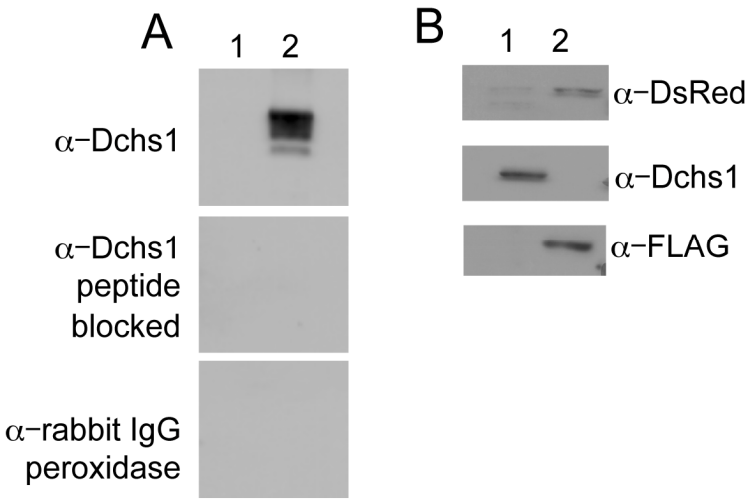

Figure 4.6. Confocal laser scanning microscopy of NSC34 cells immunolabeled with rabbit anti-Dchs1. (A, C, and E) Fluorescence of goat anti-mouse Alexa Fluor® 350 immunolabeled NF-H (blue). (B, D, and F) Fluoresence of goat anti-rabbit Alexa Fluor® 546 immunolabeled Dchs1 (red). (A and B) Untransfected NSC34 cells immunolabeled with mouse anti-NFH and rabbit anti-Dchs1. (C and D) Untransfected NSC34 cells immunolabeled with mouse anti-NFH and immunizing peptide blocked rabbit anti-Dchs1. (E and F) Untransfected NSC4 cells immunolabeled with mouse anti-NFH and goat anti-rabbit Alexa Fluor® 546. (G-I) NSC34 transfected with Dchs1ΔECD-DsRed and immunolabeled with rabbit anti-Dchs1. (G) Fluorescence of goat anti-rabbit Alexa Fluor® 488 immunolabeled Dchs1 (green). (H) Fluorescence of Dchs1ΔECD-DsRed (red). (I) Red-green merged image. In A and B the bars = 20 μm. In C-F the bars = 50 μm. In G-I the bars = 10 μm.

Figure 4.6 continued.

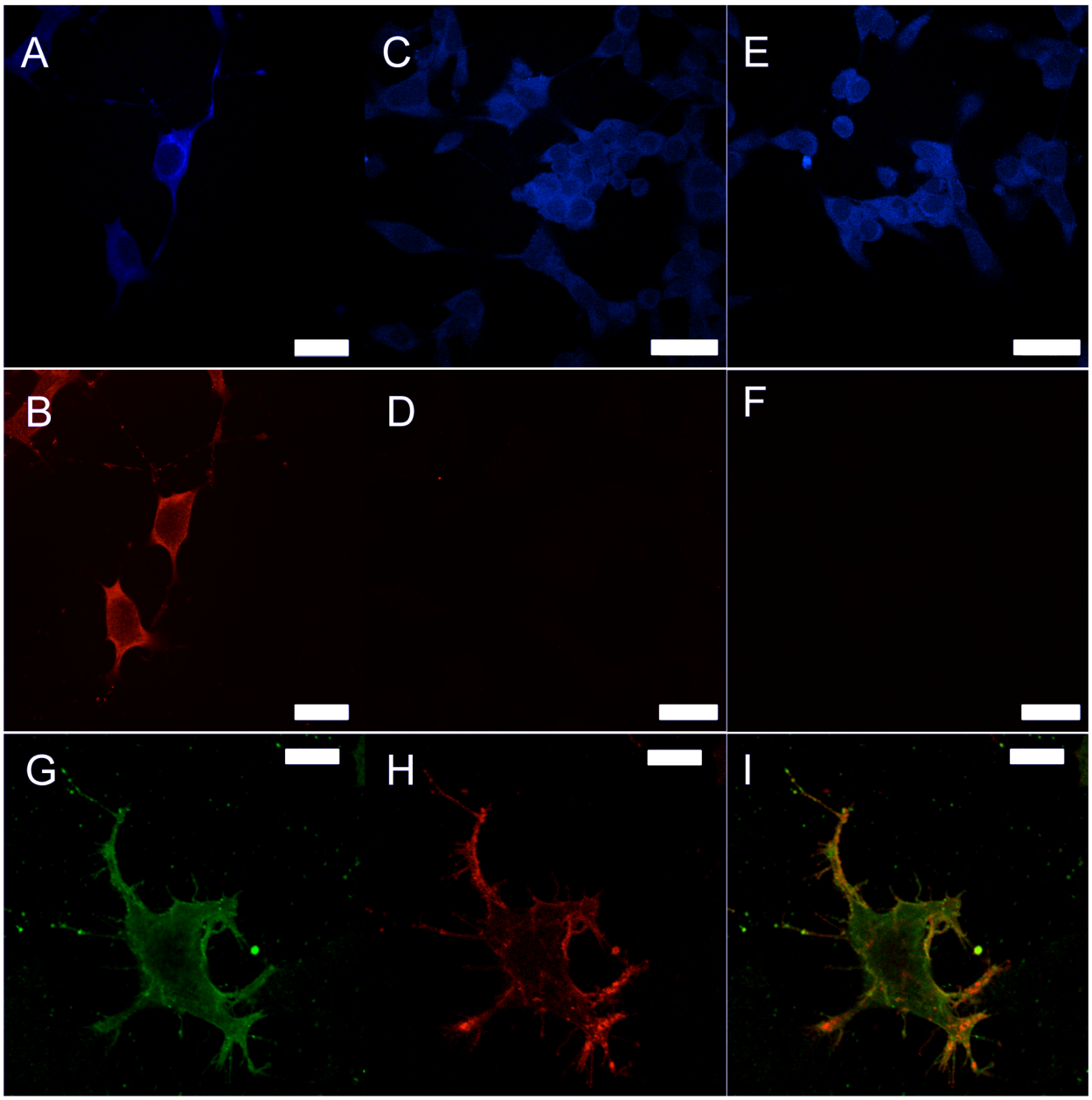

Figure 4.7. Representative confocal laser scanning microscopy image of NSC34 cells co-transfected with GFP tagged Lix1 and Dchs1ΔECD-DsRed. (A-D) NSC34 cell expressing C-terminally tagged Lix1-GFP and Dchs1ΔECD-DsRed. (E-H) NSC34 cell expressing N-terminally tagged GFP-Lix1 and Dchs1ΔECD-DsRed. (A and E) Fluorescence of goat anti-mouse Alexa Fluor® 350 immunolabeled NF-H (blue). (B and F) GFP fluorescence (green). (C and G) DsRed fluorescence (red). (D and H) Red-green merged images. Bars = 20 μm.

Figure 4.7 continued.

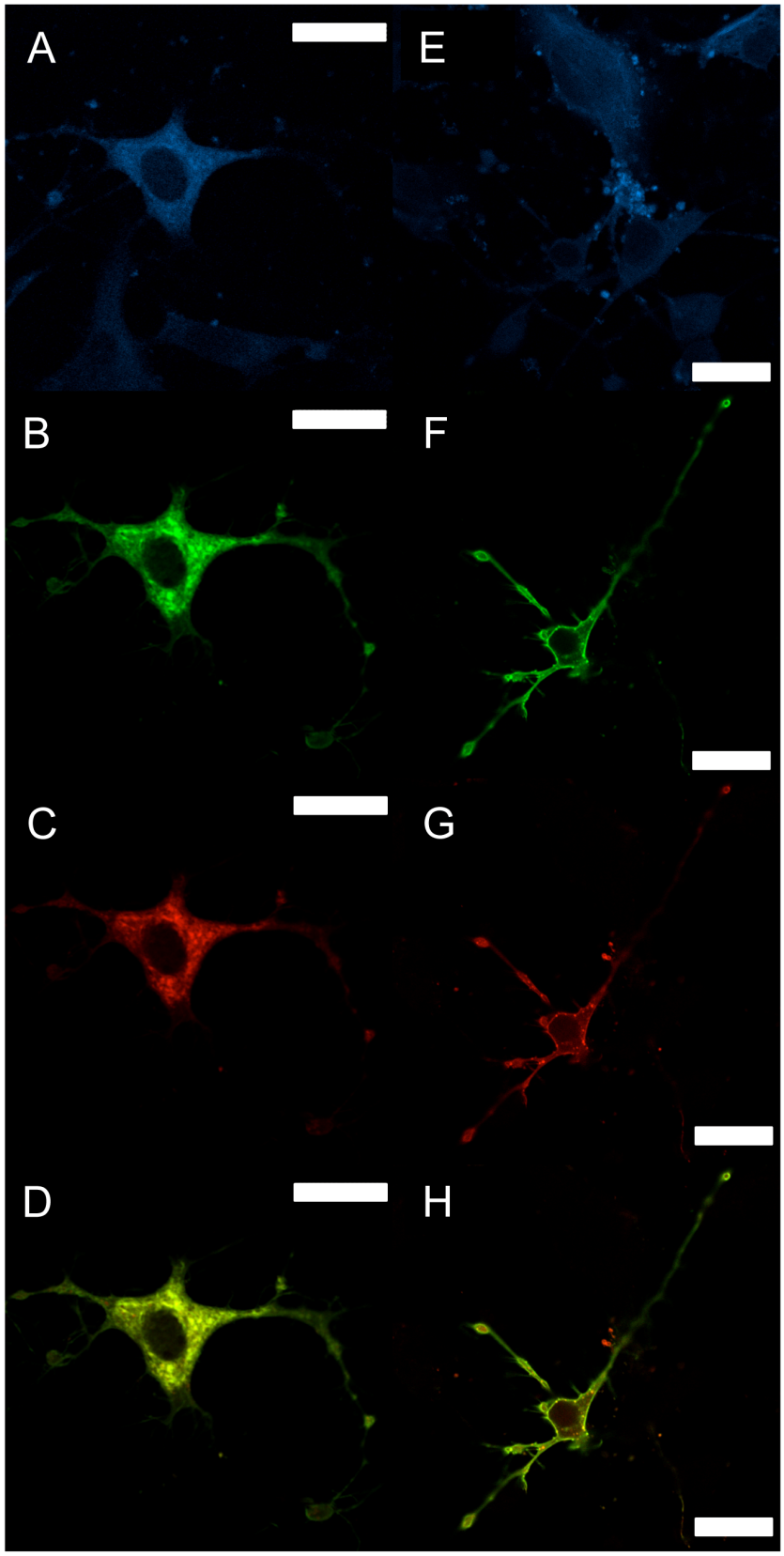

Figure 4.8. Representative confocal laser scanning microscopy image of NSC34 cells co-transfected with GFP tagged Lix1alt and Dchs1ΔECD-DsRed. (A-D) NSC34 cells expressing C-terminally tagged Lix1alt-GFP and Dchs1ΔECD-DsRed. (E-H) NSC34 cells expressing N-terminally tagged GFP-Lix1alt and Dchs1ΔECD-DsRed. (A and E) Fluorescence of goat anti-mouse Alexa Fluor® 350 immunolabeled NF-H (blue). (B and F) GFP fluorescence (green). (C and G) DsRed fluorescence (red). (D and H) Red-green merged images. Bars = 20 μm.

Figure 4.8 continued.

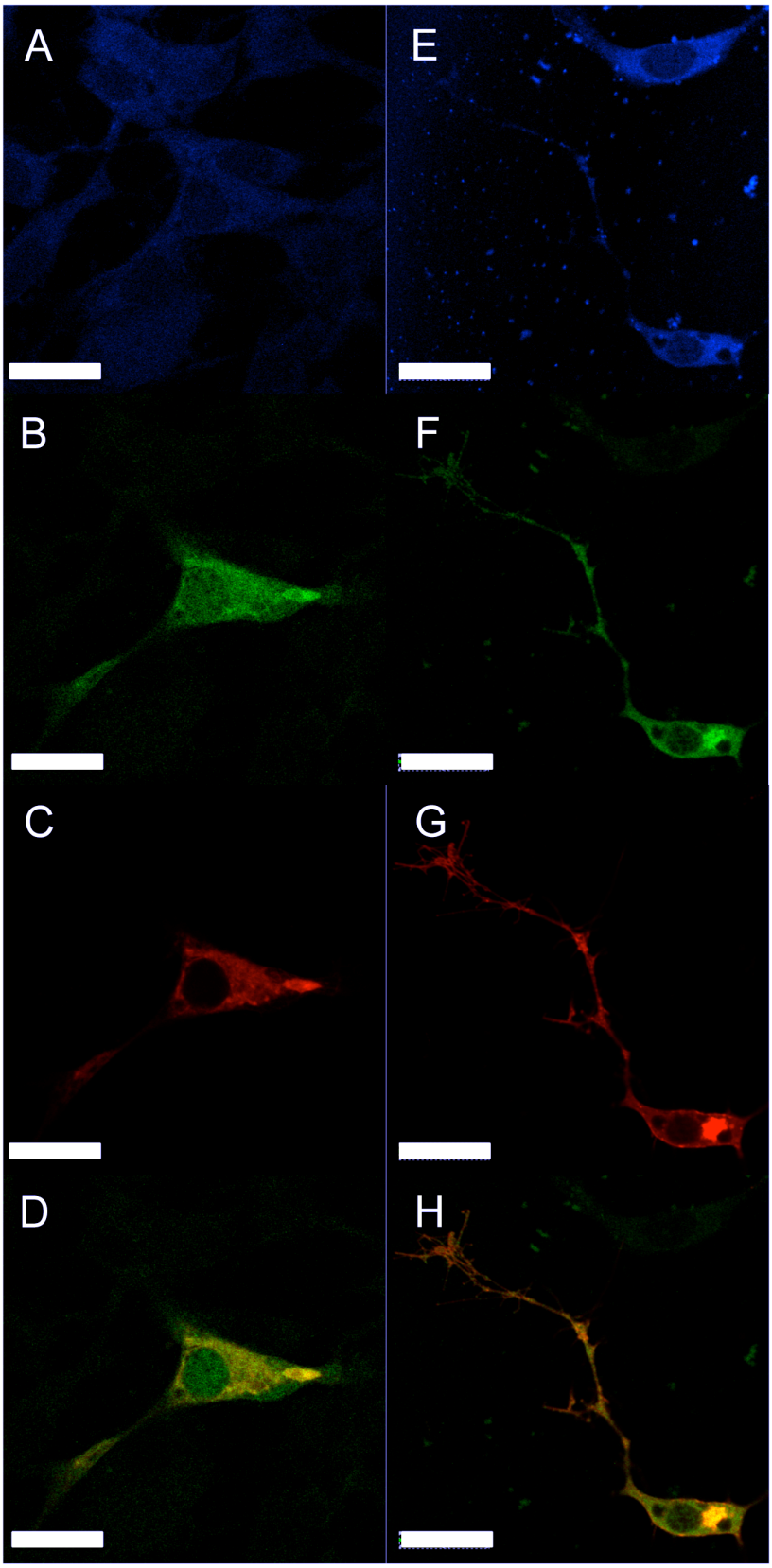

Figure 4.9. Representative confocal laser scanning microscopy image of NSC34 cells co-transfected with GFP tagged Lix1 or Lix1alt and Dchs1ΔECDΔC-FLAG-DsRed. (A-D) NSC34 cells expressing C-terminally tagged Lix1-GFP and Dchs1ΔECDΔC-FLAG-DsRed. (E-H) NSC34 cells expressing N terminally tagged GFP-Lix1 and Dchs1ΔECDΔC-FLAG-DsRed. (I-L) NSC34 cells expressing N-terminally tagged GFP-Lix1alt and Dchs1ΔECDΔC-FLAG-DsRed. (A, E and I) Fluorescence of goat anti-mouse Alexa Fluor® 350 immunolabeled NF-H (blue). (B, F and J) GFP fluorescence (green). (C, G and K) DsRed fluorescence (red). (D, H and K) Red-green merged images. In A-D, bars = 20 μm. In E-K, bars = 10 μm.

Figure 4.9 oontinued.

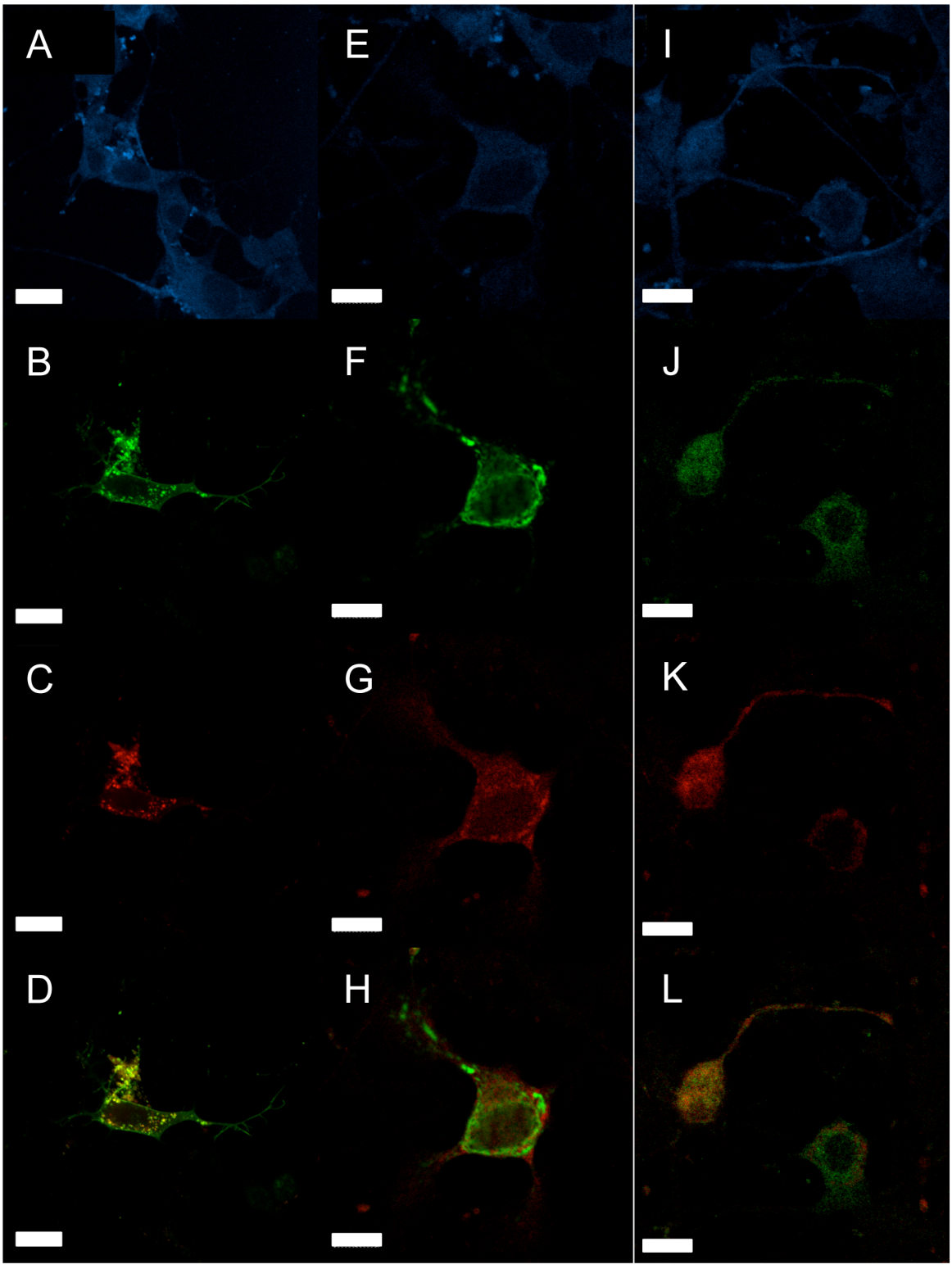

Figure 4.10. Representative western blots showing the results of co-immunoprecipitation experiments. (A) Western blots of Cos7 lysate 5% input and anti-GFP sepharose immunoprecipitates. Lane 1: Cos7 mock transfected lysate; Lane 2: Cos7 cells transfected with Lix1-GFP and Dchs1ΔECD-DsRed; Lane 3: Cos7 cells transfected with GFP-Lix1 and Dchs1ΔECD-DsRed; Lane 4: Cos7 cells transfected with Lix1-GFP and Dchs1ΔECDΔC-FLAG-DsRed; Lane 5: Cos7 cells tranfected with GFP-Lix1 and Dchs1ΔECDΔC-FLAG-DsRed. (B) Western blots of NSC34 lysate 6.67% input and anti-GFP sepharose immunoprecipitates. Lane 1: NSC34 cells transfected with GFP-Lix1 and Dchs1ΔECD-DsRed, Lane 2: NSC34 cells

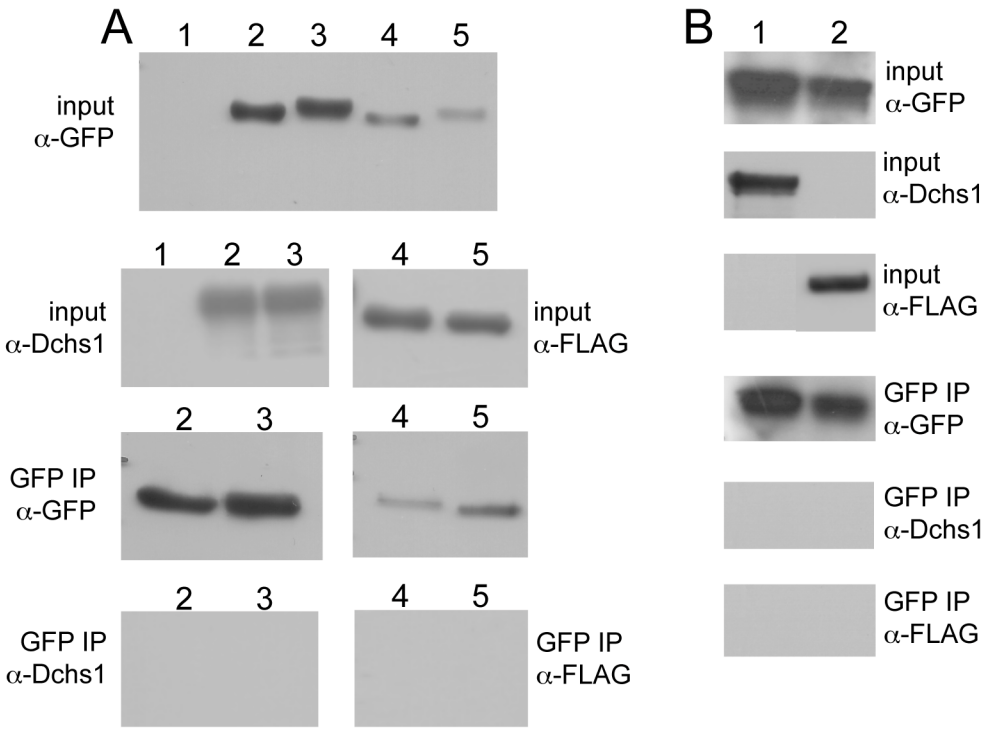

transfected with GFP-Lix1 and Dchs1ΔECDΔC-FLAG-DsRed.

Discussion

The cytoplasmic domain of *Dachsous1* (DCHS1) was identified 20 times in this yeast two-hybrid screen. An interaction between the cytoplasmic domains of DCHS1 and LIX1 was confirmed *in vitro* by co-immunoprecipitation and band shift assay. Furthermore, an interaction in cultured Cos7 and NSC34 was suggested by the co-localization of GFP-tagged Lix1 and Lix1alt with Dchs1ΔECD-DsRed. However, a physical interaction in cells could not be confirmed by co-immunoprecipitation experiments. LIX1 did co-immunoprecipitate with DACHSOUS and FAT in immunoprecipitation experiments reported previously in *D. melanogaster* S2 cells (10). However, these experiments used much smaller epitope tags to label LIX1, DACHSOUS and FAT. Therefore, it is possible that the large GFP and DsRed tags used in my experiments are interfering with the ability of Lix1 and Dchs1 to associate. I was also unable to use the same lysis and wash buffer conditions for my experiments, because the RIPA buffer (50 mM Tris-HCL pH 8.0, 150 mM NaCl, 1% NP-40, 0.5% sodium deoxycholate, 0.1% SDS) utilized by Mao et al, disrupted the interaction between the anti-GFP sepharose beads and GFP tagged Lix1 (data not shown).

Dachsous (*Ds*) is a unique member of the cadherin superfamily that was first discovered in *D. melanogaster* (11). This large type I transmembrane protein possesses 27 extracellular cadherin (EC) domains in contrast to the 4 EC domains found in classical vertebrate cadherins. The large intracellular domain shares sequence similarity to the β̃catenin binding sites of vertebrate cadherins; however, the sequence is interrupted by a stretch of amino acids, and binding of β-catenin has yet to be demonstrated (12). *Ds* mutants have shortened wings and legs and the photoreceptor cells of the eyes are disorganized (13). Flies with severe mutations in *ds* emerge from the pupa with a reduced frequency and adults cannot fly, jump or reproduce (11).

Ds is involved in planar cell polarity (PCP), a process by which epithelia become polarized along the axis perpendicular to the apical-basal axis (11). PCP is necessary for the proper organization of the wing hairs and body bristles of *D. melanogaster* and the stereocilia of the vertebrate inner ear (14). In *D. melanogaster*, Ds was found to play a role in the proximal-distal patterning of the wings, legs and abdominal denticle belts as well as the equatorial-polar patterning of the eye (15, 16). Ds expression is graded with the highest expression in the proximal portion of the wing and polar region of the eye and lower expression in the distal wing and equatorial region of the eye. This gradient is complemented by opposing expression of Four-jointed (Fj), a Golgi-associated kinase that modulates the PCP activity of Ds (17, 18). Together, Ds and Fj regulate the activity of Fat (Ft) another unique cadherin (13). Ds and Ft bind in a heterophilic manner and stabilize each other in the plasma membrane, and this interaction directs planar cell polarity (19). It was originally thought that Ft exerted its effects by activating Frizzled (Fz), a member of the *wingless* signaling pathway, to polarize Starry Night (Stan) and a set of other core PCP proteins (20, 21). However, recent evidence suggests that planar cell polarity is conferred by two separate pathways, the Ds system and the Fz/Stan system (22).

Mice and humans have two Ds homologs; murine Dchs1/Dchs2 are 26% and 28% similar to *D. melanogaster* Ds (23). The human proteins are 98% and 79% similar to the respective mouse proteins. During murine embryogenesis, *Dchs1* is expressed in the brain and the mantle layer of the neural tube, which later develops into the spinal cord gray matter. Dchs1 is also expressed in the adult brain, heart, kidney, muscle and spleen. Although the function of Dchs1 in vertebrates has yet to be determined, the strong conservation of protein sequences and overlapping expression patterns with other PCP genes implies that Dchs1 may play a similarly important role as in *D. melanogaster*. Knockout of the mouse *Fat* homolog, *Fat4* resulted in death at birth, polycystic kidneys and disorientation of cochlear stereocilia (24). More

relevant to my work was the observation that the spinal cords of *Fat4*$^{-/-}$ mice were significantly wider than normal controls. However, this observation was not further investigated.

The only known binding partner for the intracellular domain of DACHSOUS, is LIX1(10, 25). The intracellular domain of Ds is not necessary to determine PCP in the *D. melanogaster* wing, suggesting that it may have another function (26, 27). Loss of Ds function results in aberrant outgrowth of scaffold axons in the *D. melanogaster* eye (28). Defects in axon growth and guidance are also seen in *Fz3* or *Celsr3* null mice, which are homologs of core *D. melanogaster* PCP genes (29). Thus, DCHS1 and LIX1 may function to direct axonal outgrowth. However, axonal outgrowth defects were not observed our SMA affected cats. Therefore, it remains to be seen whether the LIX1 and DCHS1 interaction is critical for feline SMA pathogenesis or completely unrelated to it.

REFERENCES

References

1. Swindell E, Moeller C, Thaller C, et al. Cloning and expression analysis of chicken Lix1, a founding member of a novel gene family. Mech Dev 2001;109:405-408.

2. Moeller C, Yaylaoglu MB, Alverez-Bolado G, et al. Murine Lix1, a novel marker for substantia nigra, cortical layer 5, and hindbrain structures. Brain Res Gene Expr Patt 2002;1:199-203.

3. Fyfe JC, Menotti-Raymond M, David VA, et al. An ~ 140-kb deletion associated with feline spinal muscular atrophy implies an essential LIX1 function for motor neuron survival. Genome Res 2006;16:1084-1090.

4. Tepass U. Genetic analysis of cadherin function in animal morphogenesis. Curr Opin Cell Biol 1999;11(5):540-548.

5. Schiff M, Froissart R, Olsen R, et al. Electron transfer flavoprotein deficiency: Functional and molecular aspects. Mol Genet Metab 2006;88:153-158.

6. Koc E, Burkhart W, Blackburn K, et al. The small subunit of the mammalian mitchondrial ribosome: identification of the full complement of ribosomal proteins present. J Biol Chem 2001;275(22):19363-19374.

7. Kramer A, Ferfoglia F, Huang C, et al. Structure-function analysis of the U2 snRNP-associated spicing factor SF3a. Biochem Soc Trans 2005;33(3):439-442.

8. Ohki T, Hongo S, Nakada N, et al. Inhibition of neurite outgrowth by reduced levels of NDRG4 protein in antisense transfected PC12 cells. Dev Brain Res 2002;13:555-563.

9. Cashman N, Durham H, Blusztain J, et al. Neuroblastoma x spinal cord (NSC) hybrid cell lines resemble developing motor neurons. Dev Dyn 1992;194:209-221.

10. Mao Y, Kucuk B, Irvine KD. Drosophila lowfat, a novel modulator of Fat signaling. Development 2009;136:3223-3233.

11. Clark H, Brentrup D, Schneitz K, et al. Dachsous encodes a member of the cadherin superfamily that controls imaginal disc morphogenesis in Drosophila. Genes Dev 1995;9:1530-1542.

12. Halbeib JM, Nelson WJ. Cadherins in development: cell adhesion, sorting, and tissue morphogenesis. Genes Dev 2006;20:3199-3214.

13. Simon MA. Planar cell polarity in the Drosophila eye is directed by graded Four-jointed and Dachsous expression. Development 2004;131:6175-6184.

14. Zallen J. Planar polarity and tissue morphogenesis. Cell 2007;129:1051-1063.

15. Fanto M, McNeill H. Planar polarity from flies to vertebrates. J Cell Sci 2004;117:527-533.

16. Repiso A, Saavedra P, Casal J, et al. Planar cell polarity: the orientation of larval denticles in Drosophila appears to depend on gradients of Dachsous and Fat. Development 2010;137:3411-3415.

17. Brittle AL, Repiso A, Lawrence PA, et al. Four-Jointed modulates growth and planar polarity by reducing the affinity of Dachsous for Fat. Curr Biol 2010;20(9):803-810.

18. Ishikawa HO, Takeuchi H, Haltiwanger RS, et al. Four-jointed is a golgi kinase that phosphorylates a subset of cadherin domains. Science 2008;401(321):401-404.

19. Matakatsu H, Blair SS. Interactions between Fat and Dachsous and the regulation of planar cell polarity in the Drosophila wing. Development 2004;131:3785-3794.

20. Cho E, Irvine KD. Action of fat, four-jointed, dachsous, and dachs in distal-to-proximal wing signaling. Development 2004;131:4489-4500.

21. Rodrıguez I. The dachsous gene, a member of the cadherin family, is required for Wg-dependent pattern formation in the Drosophila wing disc. Development 2004;131:3195-3206.

22. Casal J, Lawrence PA, Struhl G. Two separate molecular systems, Dachsous/Fat and Starry night/Frizzled, act independently to confer planar cell polarity. Development 2006;133:4561-4572.

23. Rock R, Schrauth S, Gessler M. Expression of mouse dchs1, fjx1, and fat-j suggests conservation of the planar cell polarity pathway identified in Drosophila. Dev Dyn 2005;234:747-755.

24. Saburi S, Hester I, Fischer E, et al. Loss of Fat4 disrupts PCP signaling and oriented cell division and leads to cystic kidney disease. Nat Genet 2008;40(8):1010-1015.

25. Giot L, Bader J, Brouwer C, et al. A protein interaction map of Drosophila melanogaster. Science 2003;302(5651):1727-1736.

26. Lawrence PA, Struhl G, Casal J. Planar cell polarity: one or two pathways? Nat Rev Genet 2007;8:555-563.

27. Matakatsu H, Blair SS. Separating the adhesive and signaling functions of the Fat and Dachsous protocadherins. Development 2006;133:2315-2324.

28. Dearborn R, Kunes S. An axon scaffold induced by retinal axons directs glia to destinations in the Drosophila optic lobe. Development 2004;131:2291-2303.

29. Wang Y, Nathans J. Tissue/planar cell polarity in vertebrates: new insights and new questions. Development 2007;134:647-658.

Chapter 5: LIX1 and its putative RNA binding activity

Abstract

The putative feline SMA disease gene, *LIX1*, is poorly annotated. Computational secondary structure analysis predicted the N-terminus of LIX1 to fold into a double-stranded RNA binding domain. To test this prediction I conducted *in vitro* gel mobility shift assays with purified recombinant LIX1 and ^{32}P 5' end labeled RNAs of varying secondary structure. No interaction was seen between LIX1 and any of the RNA species in any reaction condition tested. Furthermore, GFP tagged Lix1 and its alternative transcript Lix1alt failed to co-localize with an mRNA granule marker, Poly A-binding protein (Pabp1) in cultured motor neuron like cells. GFP tagged Lix1 and Lix1alt also failed to co-localize with Smn, the protein depleted in human SMA, in NSC34 cell cultures. These results are inconsistent with the predicted RNA binding ability of LIX1.

Introduction

The vast majority of human SMA cases are caused by mutations in a ubiquitously expressed gene, *SMN1*. The first identified function of SMN was its role in snRNP biogenesis, where it loads the Sm proteins onto U snRNAs (1, 2). SMN has also been found to bind poly-G RNA *in vitro* and to co-localize with mRNA granules in axons of cultured neurons (3, 4). Most recently, SMN has been found to co-immunoprecipitate with β-actin mRNA in a human neuroblastoma cell line (5). *Immunoglobulin μ binding protein 2* (*IGHMBP2*) the gene mutated in a similar motor neuron disease, SMA with respiratory distress, is predicted to have a DEAD/H box domain, often found in RNA helicases and a single stranded nucleic acid binding domain (6; 7). IGHMBP2 has recently been shown to unwind RNA duplexes 5' to 3' *in vitro* in an ATP dependent manner (8). Furthermore, IGHMBP2 co-localized with ribosomes in the axons and growth cones of cultured primary motor neurons. Taken together, these data suggest a critical role for axonal ribonucleoprotein complexes (RNP) in the maintenance of lower motor neurons.

The feline SMA candidate disease gene, *LIX1*, has no identified function. However, secondary structure prediction software identified a putative double stranded RNA binding domain in its N-terminus (9). This potential function provides a link between the clinically similar but molecularly distinct human and feline disease. To test this computational prediction, I conducted *in vitro* gel mobility shift assays with purified recombinant LIX1 and RNA with varying degrees of secondary structure. Furthermore, I assessed transfected NSC34 cells for co-localization of GFP tagged LIX1 with markers of axonal RNPs, Poly-A Binding Protein (Pabp1) and Smn.

Materials and Methods

Cloning of human LIX1

The open reading frame of human *LIX1* was PCR amplified from a full-length cDNA IMAGE clone (ID #: 5264055) in a 50 μl reaction containing a final concentration of 250 μM dNTPs (Invitrogen, Carlsbad, CA), 0.05 U/μl Choice-Taq™ DNA polymerase and 10 mM Tris-HCl, pH 9.0, 10 mM KCl, 1.5 mM $MgSO_4$, 8 mM $(NH_4)_2SO_4$, 1.5 mM $MgCl_2$, and 0.05% NP-40 (Denville Scientific, South Plainfield, NJ) with 250 nM of primers 5'-TTTTGTCGACATGGACATAACCTTGGAATCTC-3' and 5'-TTTTAAGCTTCTAGTGATAGCCACACAGCT-3' (Integrated DNA Technologies, Coralville, IA), to introduce SalI and HindIII restriction sites. Thermocycling conditions were as follows: 2 minutes 95°C initial denaturation, 35 cycles at 94°C for 30 seconds (s), 57°C for 30 s, and 72°C for 1 minute and a final extension at 72°C for 10 minutes. The PCR product and pMalC4x vector (New England Biolabs, Ipswich, MA) were sequentially digested with SalI and HindIII (New England Biolabs) restriction enzymes according to manufacturer's recommendations. The digested vector and insert were ligated with T4 DNA ligase (Promega, Madison, WI) according to manufacturer's specifications and transformed into chemically competent *Escherichia coli* (*E. coli*) DH5α by heat shock. The pMalC4x-hLIX1 vector was purified from overnight liquid cultures with the PureYield™ Mini-prep System (Promega), and the insert was sequenced at the University of Michigan DNA sequencing core with the following primers: 5'-GGTCGTCAGACTGTCGATGAAGCC-3' and 5'-CAAGGCTAAGTTGGGTAAC-3'.

Expression and purification of recombinant Maltose Binding Protein 2-hLIX1 (MBP2-hLIX1)

Recombinant MBP2-hLIX1 was expressed and purified with the pMal™ Protein Fusion and Purification System (New England Biolabs) according to manufacturer's instructions. Sequence confirmed pMalC4x-hLIX1 vector was transformed by heat shock into chemically competent *E. coli* TB1 cells (New England Biolabs). A single, transformed colony was used to inoculate 25 mls of Luria broth (LB) with 100 μg/ml of ampicillin. Ten mls of this overnight culture

were used to inoculate 1 liter of LB with 100 μg/ml of ampicillin and 0.2% d-glucose. The 1 liter culture was incubated at 37°C with shaking until OD_{600}=0.5. Expression of MBP2-hLIX1 was induced with 0.3 mM isopropyl β-D-1-thiogalactopyranoside (IPTG), and the culture was incubated at 15°C for 18 hours. Cells were harvested by centrifugation at 4,000 x g for 20 minutes at 4°C, and the pellet was resuspended in column buffer (20 mM Tris-HCl, pH 7.4, 200 mM NaCl, 1 mM EDTA). Cells were lysed by sonication for 2 minutes of 15 s pulses, and the lysate was cleared at 9,000 x g for 30 minutes at 4°C. The supernatant was diluted 1:5 in column buffer and loaded onto a 15 ml amylose resin column at a rate of 1 ml/minute. The column was washed with 12 column volumes of column buffer and bound protein was eluted with column buffer plus 10 mM maltose. The elutant was collected in 3 ml fractions and MBP2-hLIX1 was detected in the fractions by UV absorbance at 280 nm and sodium dodecyl sulfate-polyacrylamide gel electrophoresis (SDS-PAGE) (Figure 5.1). Fractions containing the recombinant protein were pooled and protein was quantitated by a Bradford assay (Bio-Rad Laboratories, Hercules, CA).

Labeling and purification of RNA

In vitro transcribed A6U (*ATPase subunit 6*) or CYbU (*cytochrome b*) RNA (Figure 5.2), provided by Dr. Donna Koslowsky, was 5' end labeled with [γ-^{32}P] ATP (3,000 Ci/mmol) (Perkin Elmer, Waltham, MA) by incubation at 37°C for 45 minutes with 20 U of T4 polynucleotide kinase (New England Biolabs) in 70 mM Tris-HCl, pH 7.6, 10 mM $MgCl_2$, 5 mM DTT, and 1.6 μM ATP. Labeled RNA was purified on 10%, 7 M urea acrylamide gels and extracted overnight at 4°C in 600 μl of 10mM Tris, pH 7.8, 0.1% SDS, 2 mM EDTA, 120 mM NaOAc and 400 μl of phenol. RNA was then ethanol precipitated from the aqueous phase and resuspended in

nuclease free water. Concentration of the purified ^{32}P-labeled RNA was determined by isotope incorporation.

Figure 5.1. Purification of recombinant MBP2-hLIX1. (A) Absorbance at 280 nm of fractions collected during the elution of sMBP2-hLIX1 from an amylose resin column. (B) Image of Coomassie stained gels from SDS-PAGE analysis of MBP2-hLIX1 purification. Lane 1: molecular weight marker; Lane 2: lysate from uninduced TB1 cells transformed with pMalC4x-hLIX1; Lane 3: lysate from IPTG-induced TB1 cells transformed with pMalC4x-hLIX1; Lane 4: soluble fraction of cell lysate; Lane 5; insoluble fraction of cell lysate; Lanes 6-14: fractions 1-9 of MBP2-hLIX1 elution from amylose resin column. Fractions 4 through 8 were pooled for gel mobility shift assays.

Figure 5.1 continued.

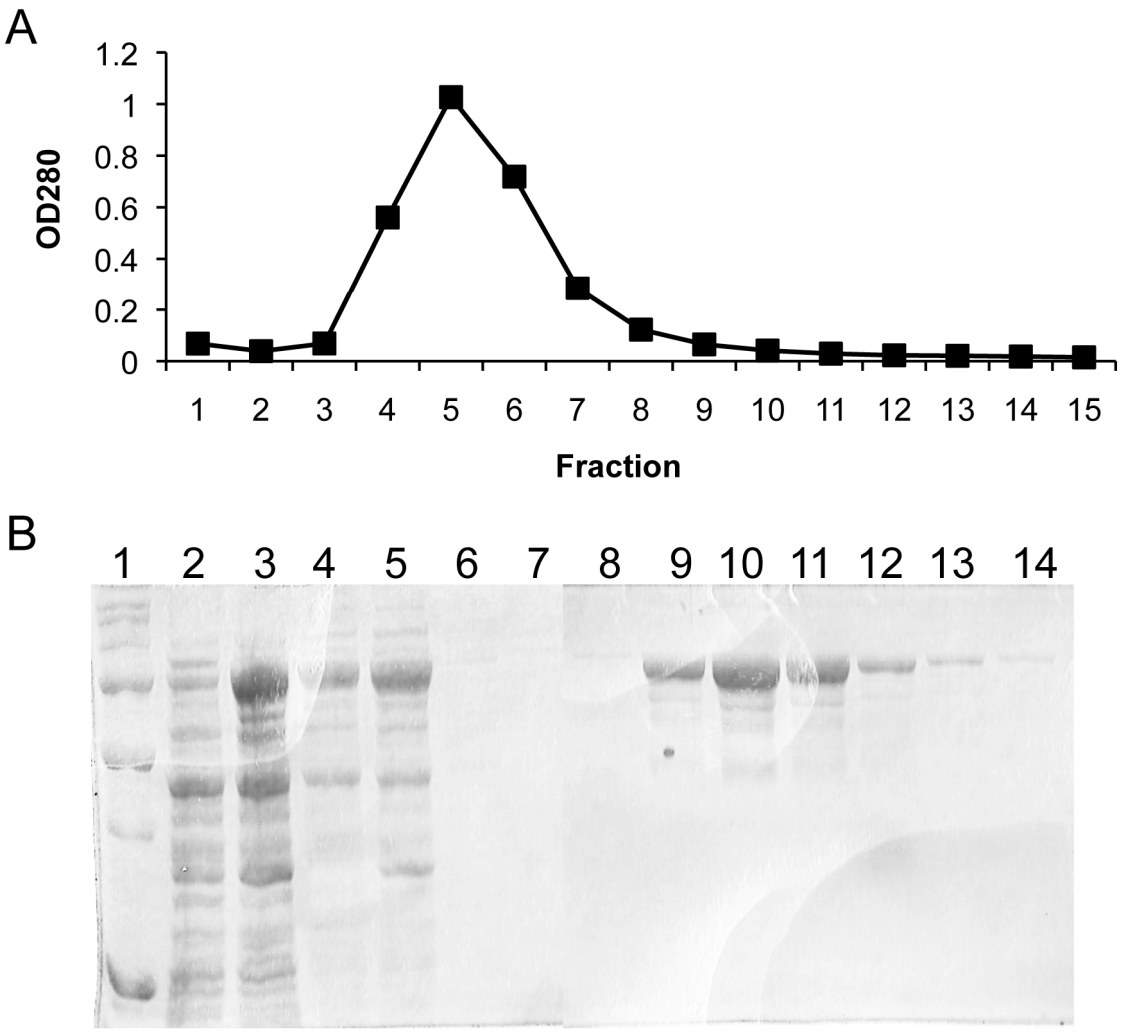

Figure 5.2. Secondary structure of A6U and CYbU RNAs. CYbU forms a very stable stem loop and its almost entirely double stranded. Figure courtesy of Dr. Donna Koslowsky (10).

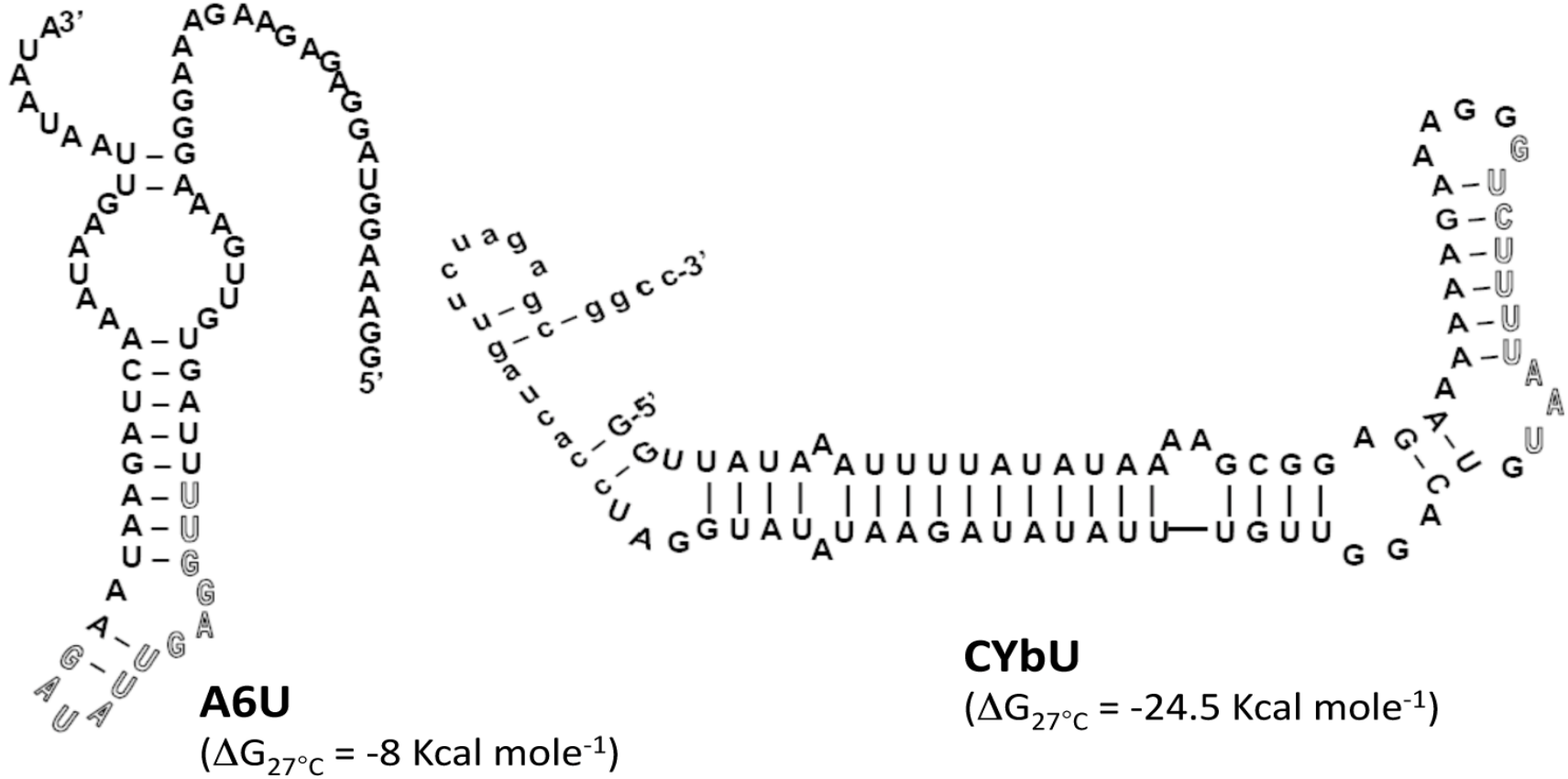

Gel mobility shift assays

Prior to gel mobility shift assays, MBP2 (New England Biolabs) and MBP2-hLIX1 proteins were exchanged into binding buffer (10mM Tris-HCl, pH 7.5, 50 mM KCl, 0.1 mM DTT, 1 mM EDTA, 10 mM $MgCl_2$ or MgOAc, 5% glycerol, 1 mM phenylmethylsulfonyl fluoride and 1 mM N-ethylmaleimide) and concentrated to 100 μM in 30,000 NMWL Ultrafree-MC filter units (Millipore, Billerica, MA). CybUT and A6U RNAs were denatured at 70°C for 5 minutes and then cooled 2°C per minute to 4℃ to allow RNA to refold. For the 20 μl binding reactions, 5 nM of CybUT or A6U RNA (10,000 cpm of ^{32}P labeled RNA) was incubated with 0 to 50 μM of protein for 30 minutes at room temperature in binding buffer with 25 to 200 mM KCl and 2 U of RNasin (Promega). Reactions were loaded onto 5% native polyacrylamide (37.5:1) gels (50 mM Tris-glycine, pH 8.8, 10 mM MgOAc) with 6x loading dye (10 mM Tris-HCl, pH 7.5, 50 mM EDTA, 15% Ficoll® 400, 0.03% bromophenol blue and 0.03% xylene cyanol FF) and run at 4°C 160 volts until the xylene cyanol band was 2 inches from the bottom of the 0.1 cm x 20 cm 20 cm gel. Gels were fixed for 20 minutes in 7% acetic acid, 7% methanol and vacuum dried. Gels were exposed to phosphor screens overnight and visualized by autoradiography.

Immunocytochemistry

NSC34 cells were cultured and transfected with *Lix1* or *Lix1alt* expression vectors on sterile glass coverslips as described in Chapter 4. After 24 hours in Ham's F12 medium with 1% fetal bovine serum, cells were rinsed with phosphate buffered saline (PBS), pH 7.4, and fixed for 30 minutes in 4% paraformaldehyde in PBS, pH 7.4. Cells were then permeabliized with ice-cold acetone for 5 minutes. After 3 washes with PBS, cells were blocked with 10% normal goat serum in PBS with 0.1% Tween 20 (PBST). Cells were then incubated overnight at 4°C in rabbit anti-PABP1 polyclonal antibody (1:50 dilution; Cell Signaling Technology, Danvers, MA) and mouse anti-neurofilament heavy subunit (NF-H) monoclonal antibody (1:500 dilution of SMI-32;

AbCam, Cambridge, MA) or mouse anti-SMN monoclonal antibody (1:100 dilution; BD Biosciences, Franklin Lake, NJ). Cells were washed 3 times with PBS prior to a 2 hour incubation at room temperature in goat anti-rabbit IgG Alexa Flour® 546 (1:250) and goat anti-mouse IgG Alexa Flour® 350 (1:500) or goat anti-mouse IgG Alexa Flour® 546 (1:250) (Invitrogen, Carlsbad, CA). After washing with PBS, coverslips were mounted onto glass slides with Prolong Gold antiFade (Invitrogen) and sealed with nail polish.

Confocal laser scanning microscopy

Immunolabeled cells were imaged for fluorescence on an Olympus Fluoview 1000 laser-scanning microscope (Center Valley, PA) equipped with a 60x oil immersion objective NA=1.42. Fluorescence of Alexa Fluor® 350-labeled NF-H (blue) was excited at 405 nm and emission was detected through a BP 430-470 nm filter. Fluorescence of GFP-tagged Lix1 or Lix1alt (green) was excited at 488 nm and emission detected through a BP 505-525 nm filter. Fluorescence of Alexa Fluor® 546-labeled Smn or Pabp1 was excited at 543 and emission was detected through a LP 560 nm filter. Co-localization of Lix1 or Lix1alt with Pabp1 and Smn was determined in red-green merged images that were optimized for brightness and contrast with Fluoview v5 software.

Results

Recombinant MBP2-hLIX1 did not bind either A6U or CYbU RNA *in vitro* in any of the reaction conditions tested (salt and protein titrations, binding reactions from 1 to 60 minutes). The result of a single representative gel mobility shift assay is shown in Figure 5.3. Furthermore, dialysis into and then out of 7M urea, to denature MBP2-hLIX1 and MBP2 and refold the proteins, did not improve results. Thus, the predicted RNA binding activity of LIX1 was not confirmed *in vitro* with the RNA species tested.

To assess the ability of LIX1 to bind RNA *in vivo*, transfected NSC34 cells were examined by confocal microscopy for co-localization of GFP tagged Lix1 and a marker of RNPs,

Figure 5.3. CYbU and recombinant LIX1 gel mobility shift assay. (A) Representative autoradiogram from gel shift assay of MBP2-hLIX1 with 5’ end-labeled CYbU RNA. (B) Representative autoradiogram from gel shift assay of MBP2 with 5’ end-labeled CYbU RNA. Protein concentrations ranged from 0 to 50 μM (0 to 10x RNA concentration).

Figure 5.3 continued.

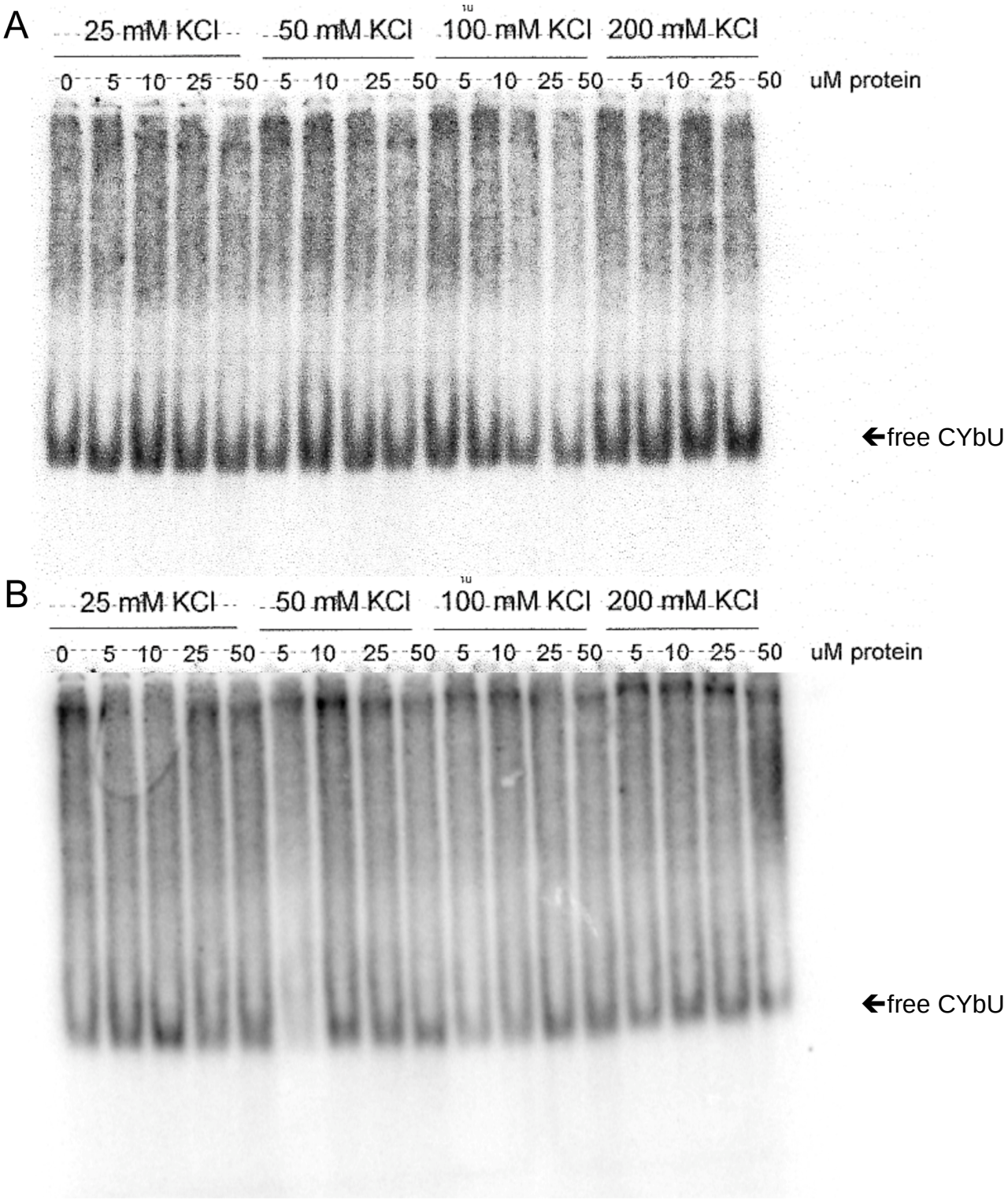

Pabp1. Lix1 only co-localized with Pabp1 very infrequently (Figure 5.4). The position of the GFP tag did not affect the level of co-localization (N terminal 4.85 ± 2.7% co-localization; C terminal 8.17 ± 1.98% co-localization in 9 images each) (Figure 5.4D and H). Furthermore, the Lix1 alternative transcript (Lix1alt), which does not contain the Lix1 putative RNA binding domain, co-localized with Pabp1 to the same extent as full-length Lix1 (9.79 ± 3.75% co-localization in 4 images; Figure 5.4L). Therefore, Lix1 does not interact with Pabp1 in cultured NSC34 cells.

Finally, transfected NSC34 cells were examined by confocal microscopy to determine whether Lix1 is associated with Smn-containing granules (Figure 5.5). Lix1 and Lix1alt failed to co-localize with Smn despite all three proteins being expressed in the same cellular compartments. Placement of GFP tag did not affect the level of co-localization (N terminal 10.51 ± 13.46% co-localization; C terminal 8.9 ± 6.64% co-localization in 18 and 14 images, respectively). In contrast, Smn and Pabp1 co-localized 65.9 ± 20.9% of the time (10 images). Therefore, Lix1 and Smn do not associate in cultured neuronal cells.

Discussion

Amino acids 22-99 of LIX1 were predicted to form a double stranded RNA binding domain by computational analyses. I tested this prediction by *in vitro* gel mobility shift assays with purified recombinant LIX1 and two different RNAs, A6U and CYbU. These RNA species are encoded by mitochondrial DNA of the African sleeping sickness causing parasite, *Trypanosome brucei* (10). In nature LIX1 would never encounter either of these RNAs, but I used these particular RNAs for my *in vitro* assays because of their well-characterized secondary structure. CYbU RNA forms a very stable stem-loop compared to the less stable secondary structure of A6U RNA. Therefore, I hypothesized that LIX1 would have a higher affinity for CYbU than A6U. However, no interaction was seen between LIX1 and either RNA in any of the reaction conditions tested. These data contradict the proposed RNA binding ability of LIX1.

Figure 5.4. Co-localization of Lix1 or Lix1alt with Pabp1. (A-D) Representative confocal images of C terminally tagged Lix1-GFP transfected NSC34 cells immunolabelled with anti-neurofilament and anti-Pabp antibodies. (E-H) Representative confocal images of N terminally tagged GFP-Lix1 transfected NSC34 cells immunolabelled with anti-neurofilament and anti-Pabp antibodies. (I-L) Representative confocal images of N terminally tagged GFP-Lix1alt transfected NSC34 cells immunolabelled with anti-neurofilament and anti-Pabp antibodies. (A, E, I) anti-NFH immunofluoresence. (B, F, J) GFP fluorescence. (C, G, K) anti-Pabp immunofluorescence. (D, H, L) Red-green merged images used for co-localization analysis. Size bars = 10 μm.

Figure 5.4 continued.

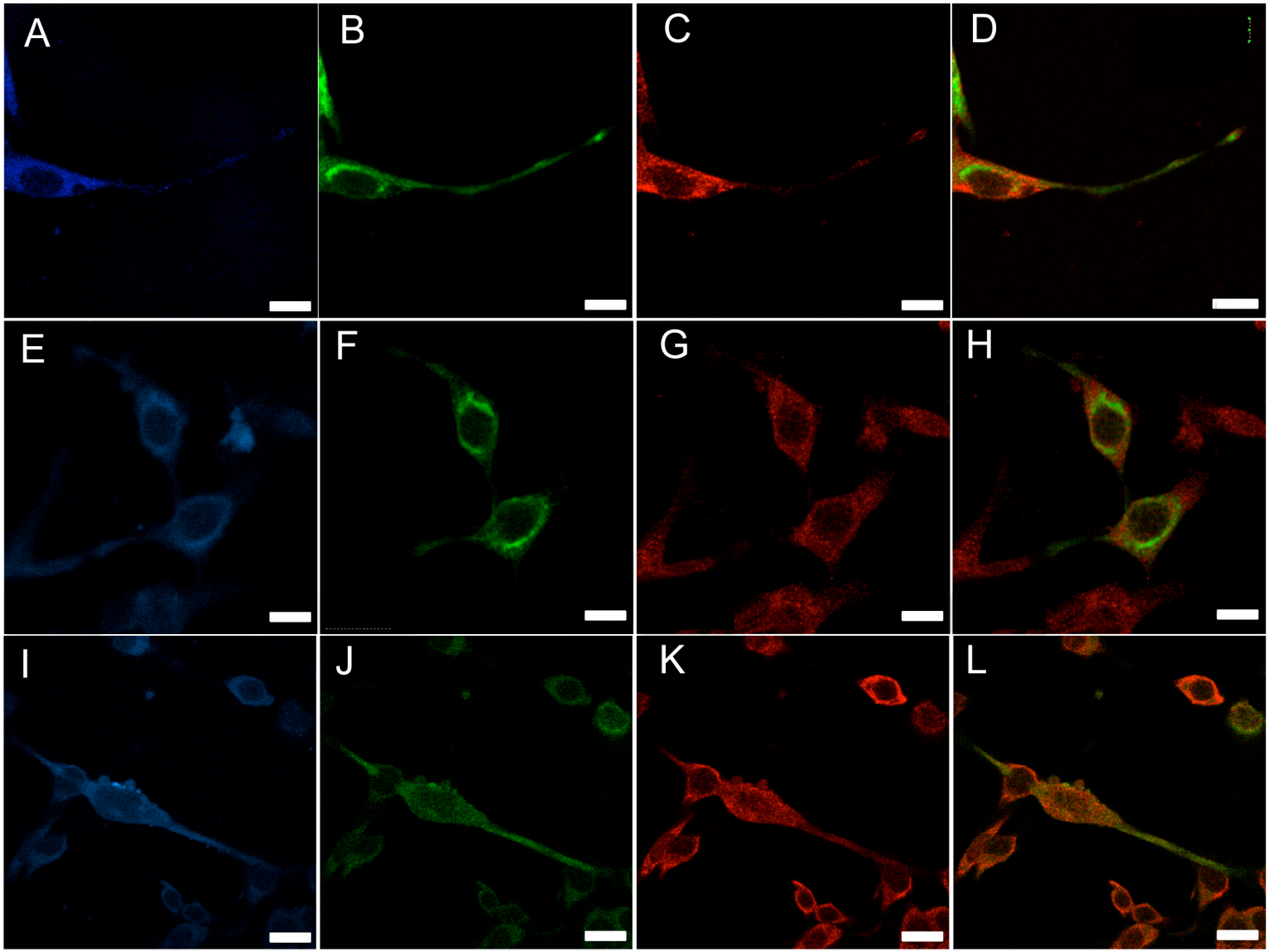

Figure 5.5. Co-localization of Lix1, Lix1alt or Pabp1 with Smn. (A-C) Representative confocal images of Lix1-GFP transfected NSC34 cells immunolabelled with anti-Smn antibody. (D-F) Representative confocal images of GFP-Lix1 transfected NSC34 cells immunolabelled with anti-Smn antibody. (G-I) Representative confocal images of GFP-Lix1alt transfected NSC34 cells immunolabelled with anti-Smn antibody. (J-L) Representative confocal images of NSC34 cells immunolabelled with anti-Smn and anti-Pabp1 antibodies (A, D, G) GFP fluorescence. (B, E, H, K) anti-Smn immunofluorescence. (C, F, I, L) Red-green merged images used for co-localization analysis. (J) anti-Pabp1 immunofluorescence. (A-F) Size bars = 10 μm. (G-I) Size bars = 25 μm. (J-L) Size bars = 20 μm.

Figure 5.5 continued.

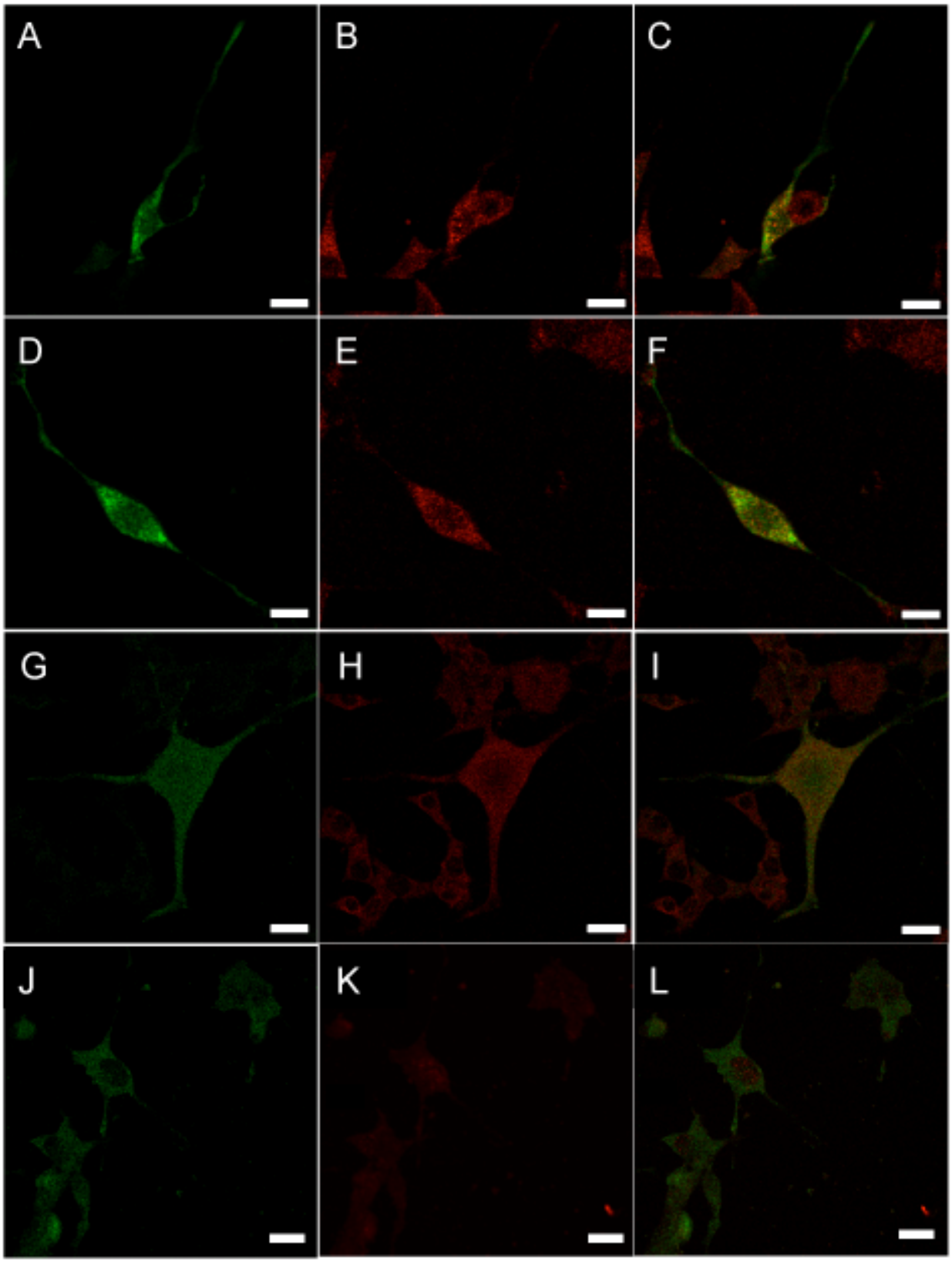

To test the ability of LIX1 to interact with RNA in a cellular environment, I examined NSC34 cells for co-localization of GFP-tagged Lix1 or Lix1alt with a marker of RNPs, Pabp1. SMN, the protein diminished in human SMA, has been found to co-localize with PABP1 containing mRNA granules in cultured neurons (4). However, Lix1 and Lix1alt did not co-localize frequently with Pabp1 in these experiments. Furthermore, Lix1 and Lix1alt rarely co-localized with endogenous Smn. Therefore, these experiments do not support the predicted RNA binding activity for LIX1. These data support two distinct pathogenic mechanisms for human and feline SMA.

REFERENCES

References

1. Pellizzoni L, Kataoka N, Charroux B DG. A novel function for SMN, the spinal muscular atrophy disease gene product, in pre-mRNA splicing. Cell 1998;95(5):615-624.

2. Pellizzoni L, Paushkin S, Mattaj IW, et al. The SMN complex is associated with snRNPs throughout their cytoplasmic assembly pathway. Mol Cell Biol 2002;22(18):6533-6541.

3. Lorson CL, Androphy EJ. The domain encoded by exon 2 of the survival motor neuron protein mediates nucleic acid binding. Hum Mol Genet 1998;7(8):1269-1275.

4. Zhang H, Xing L, Singer RH, et al. QNQKE targeting motif for the SMN-Gemin multiprotein complex in neurons. J Neurosci Res 2007;85:2657-2667.

5. Todd AG, Morse R, Shaw DJ, et al. SMN, Gemin2 and Gemin3 associate with beta-actin mRNA in the cytoplasm of neuronal cells in vitro. J Mol Biol 2010;401(5):681-689.

6. Grohmann K, Rossoll W, Kobsar I, et al. Characterization of Ighmbp2 in motor neurons and implications for the pathomechanism in a mouse model of human spinal muscular atrophy with respiratory distress type 1 (SMARD1). Hum Mol Genet 2004;13(18):2031-2042.

7. Grohmann K, Schuelke M, Diers A, et al. Mutations in the gene encoding immunoglobulin μ- binding protein 2 cause spinal muscular atrophy with respiratory distress type 1. Nat Genet 2001;29:75-77.

8. Guenther UP, Handoko L, Laggerbauer B, et al. IGHMBP2 is a ribosome-associated helicase inactive in the neuromuscular disorder distal SMA type 1 (DSMA1). Hum Mol Genet 2009;18(7):1288-1300.

9. Fyfe JC, Menotti-Raymond M, David VA, et al. An ~ 140-kb deletion associated with feline spinal muscular atrophy implies an essential LIX1 function for motor neuron survival. Genome Res. 2006;16:1084-1090.

10. Reifur L, Yu LE, Cruz-Reyes J, et al. The impact of mRNA structure on guide RNA targeting in kinetoplastid RNA editing. PLoS ONE. 2010;5(8):e12235.

CHAPTER 6: Summary and Future Directions

Feline SMA is a lower motor neuron disease that resembles human SMA type 3. Affected cats demonstrate overt clinical signs (muscle weakness, gait abnormalities) around 12 weeks of age. The disease progresses rapidly until seven or eight months of age, but slows thereafter and affected cats live to at least eight years of age. Previous work in animals that had reached the chronic stage of disease revealed variable myofiber size and several angular shaped atrophic fibers of both fiber types. Histopathological examination of affected cat spinal cord revealed astrogliosis accompanying loss of motor neurons in the ventral horn gray matter and loss of axons in the ventral horn roots. A whole genome scan for linkage in the feline SMA family identified a 140 kb deletion on feline chromosome A1q that removed exons 4-6 of *LIX1* and all but exon 1 of *LNPEP* from the disease allele. The genomic alteration abrogates mRNA expression of both genes. *LIX1* expression is restricted almost entirely to the central nervous system, whereas *LNPEP* is ubiquitously expressed. Furthermore, a *Lnpep* knockout (KO) mouse demonstrated no overt neuromuscular dysfunction. Therefore, I hypothesized that *LIX1*, a gene of unknown function, is the feline SMA disease gene.

To gain understanding of feline SMA pathogenesis and potentially ascribe a function to LIX1, I undertook a systematic examination of muscle, ventral roots and spinal cord in normal and SMA cats. Motor neurodegeneration in feline SMA proceeds in a retrograde direction with significant loss of motor neuron axons occurring at 12 weeks but no cell body loss even at 21 weeks. This “dying back” of motor neurons is consistent with engineered mouse models of SMA. Retrograde degeneration is thought to indicate primary pathogenesis at cellular sites distal to the soma. However, there has yet to be a motor neuron disease identified in which the degeneration is a "dying forward" process. A potential explanation is that retrograde degeneration is a natural survival mechanism utilized by motor neurons under stress and is independent of the lesion location. During stress conditions, motor neurons retract their axons

until the insult has subsided and new axons are then extended. In cases of chronic stress, as in genetic disease, motor neurons initially retract axons but are unable to extend new projections due to continued stress. Eventually the cell undergoes apoptosis due to a lack of trophic support from target muscle cells. This model would explain the delay in cell body loss seen in our feline SMA model and other SMA mouse models. If this model is correct it suggests that therapeutic intervention does not need to be administered prior to disease onset, but just prior to motor neuron cell death. Although it is ideal to prevent the onset of SMA symptoms by therapeutic intervention, the potential expansion of the treatment window provides hope to patients already displaying SMA symptoms.

The first pathological change in SMA affected cats, detected at 8 weeks of age was the failure of motor axons to develop the characteristic bimodal distribution of axon diameter. This failure in radial growth suggests a role for LIX1 in the regulation of axon caliber. Two key factors are known to regulate axon caliber, neurofilament expression/phosphorylation and myelination. Average myelin thickness was not significantly different in L4 ventral roots of normal and SMA affected cats, thus a structural deficit in myelin can be excluded. However, the loss of *LIX1* may result in the disruption of a signaling cascade initiated by Schwann cells to increase axon caliber in motor neurons. Little is currently known about the components of this “outside in” pathway; however, the Myelin Associated Glycoprotein (MAG) is required for axon caliber increases in the peripheral nervous system (1). LIX1 could function downstream of the MAG neuronal receptor to elicit cytoskeletal changes necessary for axon caliber expansion.

Alternatively, LIX1 could function in a motor neuron autonomous pathway that regulates neurofilament expression. Therefore it is critical to determine the levels of both phosphorylated and non-phosphorylated neurofilament subunits in affected cats. There are several commercially available antibodies against neurofilaments that could be used for immunoblots of normal and affected cat ventral root homogenate. The ventral roots alone should be used to

prevent neurofilament expression in sensory neurons and interneurons from obscuring a motor neuron specific change.

One region of the motor neuron that had been neglected in this research and other SMA research are the dendrites and their synapses with sensory neurons and interneurons. Therefore, I would propose to look at the structure of the motor neuron dendrites in paraffin embedded L5 spinal cord from SMA affected and normal cats aged 4.5 weeks to 21 weeks. To examine the gross, overall structure of the dendritic arbor an anti-microtubule associated protein 2 (MAP2) antibody would be used for immunohistochemistry. To examine the synapses of sensory neurons and interneurons with L5 motor neurons, antibodies against the vesicular glutamate transporters 1 and 2 (vGLUT1, vGLUT2), respectively, would be used for immunohistochemistry (2). It is critical to our understanding of feline SMA pathogenesis to determine whether any changes occur in the dendritic synapses and if those changes occur prior to, at the same time, or after axonal changes.

The smaller muscle fiber size and reduced compound motor action potentials at 10 weeks suggests a functional disruption of neuromuscular junctions (NMJs) prior to the denervation I observed at 12 weeks. Therefore I would propose to repeat the NMJ double-labeling experiments at 8 and 10 weeks of age in teased muscle fiber preps. For these experiments, I would use fluorophore conjugated α-bungarotoxin and anti-synaptophysin or anti-syntaxin antibodies to label the NMJs. Combined with the 100x objective now available on the laser scanning confocal microscope, these labeling techniques will provide a higher resolution image of the neuromuscular junction than was possible with the experiments I conducted.

Understanding feline SMA disease progression is also critical for *LIX1* gene therapy experiments initiated by our collaborators in Nantes, France. The results presented in Chapter 2 provide a baseline from which to assess *LIX1* adeno-associated virus (AAV-LIX1) treated cats. Injections of SMA affected kittens with AAV-LIX1 began in fall 2010. If successful, these experiments will demonstrate the feasibility and efficacy of gene therapy as a treatment for CNS

disease in an animal larger than a mouse. Furthermore, these experiments could provide the first functional evidence that *LIX1* is indeed the feline SMA disease gene.

I had hoped to confirm the role of *LIX1* in feline SMA by the characterization of a *Lix1* gene trap knockout mouse. However, the mice failed to show any neuromuscular phenotype even at two years of age. I did identify that expression of a murine specific *Lix1* alternative transcript (*Lix1alt)* with an independent promoter in intron 4 persisted in knockout mice. I hypothesize that *Lix1alt* is able to compensate for loss of *Lix1* through redundant interactions with Lix1 protein partners. To test this hypothesis, a knockout mouse that disrupts both transcripts is required. I would propose to construct a gene-targeting vector to introduce LoxP sites flanking exon 5. This vector would then be injected into mouse embryonic stem cells to generate mice with a "floxed" *Lix1* allele that could then be crossed with Cre recombinase expressing mice to generate true *Lix1* knockout mice. These mice could then be examined by the same functional tests and histological techniques described in Chapter 3 to identify and follow neuromuscular dysfunction. The advantage of the Cre-Lox system over other knockout techniques is that *Lix1* disruption could be accomplished in the whole animal or in a temporally or spatially restricted manner. Alternatively, successful treatment of SMA affected cats with a *Lix1alt* adeno-associated virus would also provide strong evidence of *Lix1* and *Lix1alt* functional redundancy. However, a lack of phenotype in this proposed *Lix1* knockout mouse or the failure of *Lix1* or *Lix1alt* gene therapy to ameliorate feline SMA symptoms, would suggest that feline SMA is due to loss of both *LIX1* and *LNPEP* or a critical regulatory element located in the ~140 kb deletion.

In this research I also identified an interaction between LIX1 and DCHS1 by yeast two-hybrid. This interaction was confirmed *in vitro* by co-immunoprecipitation and band shift assays and was supported *in vivo* by co-localization of GFP tagged Lix1 and DsRed tagged Dchs1. I was unable to confirm a physical interaction i*n vivo* by co-immunoprecipitation; however, another group has recently reported the *in vivo* co-immunoprecipitation between LIX1 and the

D. melanogaster homolog of DCHS1, DACHSOUS. For future co-immunoprecipitation experiments, Lix1 and Dchs1 should be tagged with smaller epitope tags, such a FLAG and c-Myc, to prevent steric inhibition of an interaction. These small epitope tags will also allow for reciprocal co-immunoprecipitation experiments, which I was unable to conduct due to the lack of suitable antibodies. The interaction between LIX1 and DCHS1 can also be confirmed in cultured cells by fluorescence energy transfer (FRET) or bimolecular fluorescence complementation (BiFC). In BiFC, the two proteins are fused to either the N or C terminal portion of a fluorophore (YFP or CFP) and then co-transfected into cultured cells. If the two proteins interact, it will bring the two fluorophore domains in close enough proximity to fluoresce. FRET and BIFC also offer the advantage that protein interactions can be studied in live cells.

As it currently stands, DCHS1 and FAT are the only known LIX1 interacting partners. Identification of other LIX1 interacting partners will be necessary to understand LIX1 function in motor neurons and to identify candidate genes to be screened in the 3% of human SMA patients who have no identified SMN1 mutation. To identify more LIX1 interacting partners, I would propose to immunoprecipitate c-Myc-Lix1 containing complexes from transfected NSC34 cells and then to analyze those complexes by tandem mass spectrometry. A similar experiment could be conducted with GFP-Lix1alt to identify proteins that interact with Lix1 and Lix1alt. These interactions would then need to be confirmed by *in vitro* and *in vivo* co-immunoprecipitation.

It remains unclear whether DCHS1 is directly involved in feline SMA pathogenesis or if its interaction with LIX1 is completely unrelated to motor neuron disease. No function for DCHS1 in the CNS has been described; therefore, I would propose a set of yeast two-hybrid screens of the human fetal brain cDNA library used in Chapter 4. These yeast two-hybrid screens, one with the extracellular domain of DCHS1 and one with the intracellular domains of DCHS1 would identify new interacting partners that may provide insight into the function of DCHS1 in the CNS. Being that DCHS1 is a transmembrane protein with adhesive and signaling

functions, it is an excellent candidate for a MAG interacting protein. If an interaction between DCHS1 and MAG is identified by yeast-two hybrid or co-immunoprecipitation experiments, a model emerges in which LIX1 acts as an effecter of MAG to DCHS1 signaling to regulate axon caliber in motor neurons. As loss of LIX1 and MAG each result in reduced axon caliber in motor neurons only, a *Dchs1* knockout mouse would be highly interesting. However, it may be necessary to construct a neuron, or motor-neuron specific *Dchs1* knockout mouse to prevent pleiotropic effects from planar cell polarity disruption.

Alternatively, LIX1 is known to regulate Ds/Fat signaling in *Drosophila melanogaster*. The Ds/Fat signaling pathway is known to regulate planar cell polarity and tissue size, as loss of Fat results in over-growth of wing imaginal discs (3, 4). Loss of *lowfat*, the Drosophila homolog of *LIX1*, results in decreased Ds/Fat signaling and a similar, although milder phenotype to *fat* mutants (5). Whether LIX1, DCHS1 and FAT in the mammalian CNS carry out the same functions as their homologs in *D. melanogaster* remains to be seen. However, one can envision a model in which loss of LIX1 disrupts DCHS1/FAT control of motor neuron size leading to the axon caliber phenotype seen in SMA affected cats.

A *D. melanogaster* genome-wide reciprocal yeast two-hybrid screen also identified a putative interaction between Ds and the kinesin light chain (KLC), a protein involved in axonal transport (6). This interaction is putative and needs to be confirmed by co-immunoprecipitation. If DCHS1 and KLC do interact, this would suggest a role for DCHS1 and LIX1 in axonal transport. Loss of LIX1 in SMA affected cats may disrupt axonal transport, resulting in decrease transport of neurotrophic factors required for motor neuron survival. To examine axonal transport in SMA cats, I would propose to retrogradely label motor neurons by injecting horseradish-peroxidase in hindlimb muscles of normal and affected cats. Cats would then be sacrificed at different time points after injection, and the number of labeled motor neurons in lumber spinal cord would be determined by immunohistochemistry. If axonal transport is

affected in feline SMA, I predict that fewer motor neurons would be labeled in affected cats and/or that labeling would occur at later time points in these cats compared with control animals.

The data presented in this dissertation as well as the results from proposed experiments are necessary for our understanding of feline SMA pathogenesis, a naturally occurring large animal model of human SMA. Studying the molecular pathogenesis of motor neuron disease in human patients is nearly impossible because the majority of specimens available for research are from autopsies of individuals with end-stage disease. Without appropriate animal models to investigate disease pathogenesis, discovery of therapeutic treatments is substantially more difficult. Although molecularly distinct, the phenotypic similarities between the feline and human diseases make the feline disease a good model in which to identify cellular pathways required for motor neuron maintenance and survival that may be disrupted in non-5q SMA patients and individuals with other motor neuron diseases. Identification of cellular functions critical for normal motor neuron physiology will aid in the development of novel treatments for SMA and other motor neuron diseases. Finally, the feline disease provides a naturally occurring model to the research community for safety and efficacy testing of therapeutics prior to clinical trials in humans.

REFERENCES

REFERENCES

1. Yin X, Crawford TO, Griffin JW, et al. Myelin-associated glycoprotein is a myelin signal that modulates the caliber of myelinated axons. J Neurosci 1998;18(6):1953-62.

2. Oliveira ALR, Hydling F, Olsson E, et al. Cellular localization of three vesicular glutamate transporter mRNAs and proteins in rate spinal cord and dorsal root ganglia. Synapse 2003;50(2):117-29.

3. Bennett FC, Harvey KF. Fat cadherin modulates organ size in Drosophila via the Salvador/Warts/Hippo signaling pathway. Curr Biol 2006;16(21):2101-10.

4. Willecke M, Hamaratoglu F, Kango-Singh M, et al. The fat cadherin acts through the hippo tumor-suppessor pathways to regulate tissue size. Curr Biol 2006;16(21):2090-100.

5. Mao Y, Kucuk B, Irvine KD. Drosophila lowfat , a novel modulator of Fat signaling. Development 2009;136(19):3223-3233.

6. Giot L, Bader J, Brouwer C, et al. A protein interaction map of Drosophila melanogaster. Science 2003;302(5651):1727-1736.